

TIME-DEPENDENT RELIABILITY-BASED DESIGN OF
GFRP-REINFORCED BRIDGE DECKS IN NOVA SCOTIA

by

David Idemudia

Submitted in partial fulfilment of the requirements
for the degree of Master of Applied Science

at

Dalhousie University
Halifax, Nova Scotia
April 2022

Dalhousie University is located in Mi'kma'ki, the
ancestral and unceded territory of the Mi'kmaq.
We are all Treaty people.

© Copyright by David Idemudia, 2022

DEDICATION PAGE

This thesis is dedicated to my family and friends. To my loving parents Moses and Adebisi Idemudia, who I have not been able to see for the last six years but have been more than supportive to me by providing constant words of encouragement and prayers. To my brothers and sister, Sidney, Daniel, and Pamela, who have been with me and supported me throughout my master's degree, I thank you. I also dedicate this thesis to my closest friends who have been there for me and to remind me that I can achieve great things in my life and still have fun while doing so. I would also like to thank God for his love and guidance in my life, and for always guiding me.

TABLE OF CONTENTS

LIST OF TABLES	v
LIST OF FIGURES	vi
ABSTRACT	ix
NOMENCLATURE	x
ACKNOWLEDGEMENTS	xix
CHAPTER 1 INTRODUCTION	1
1.1 Background.....	1
1.2 Objectives and Scope.....	3
1.3 Thesis Structure	4
CHAPTER 2 LITERATURE REVIEW	6
2.1 Introduction.....	6
2.2 Bridge Deck Design per CSA S6:19.....	6
2.2.1 Durability	6
2.2.2 Loads	7
2.2.3 Methods of Analysis.....	8
2.2.4 Concrete Structures	9
2.2.5 Fibre-Reinforced Structures	9
2.3 Factors Influencing Bridge Deck Service Life	11
2.3.1 Load-Induced Considerations.....	12
2.3.1.1 Traffic-Induced Loads	12
2.3.1.2 System-Dependant Loads	13
2.3.2 Natural or Man-Made Hazard Considerations.....	14
2.3.2.1 Thermal Climate	14
2.3.2.2 Reactive Materials	15
2.4 Degradation Mechanism of GFRP Bars.....	16
2.4.1 Effect of Moisture on GFRP Bars	16
2.4.2 Effects of Alkalinity on GFRP Bars	17
2.5 Durability and Life Prediction Methods for GFRP Bars	18
2.5.1 Arrhenius Relation.....	18

2.5.2	FRP Strength Degradation Models.....	19
2.5.3	Tensile Strength Prediction Based on Environmental Reduction Factor (C_E).....	20
2.5.4	Life Prediction Approach Using Time-Variant Capacity of GFRP Bars Embedded in Concrete ...	23
2.5.5	Performance of GFRP-Reinforced Concrete Beams Under Sustained Load and Natural Aging ...	26
2.5.6	Creep Rupture and Long-Term Performance of GFRP bars Under Sustained Load	29
2.6	Reliability Analysis of GFRP-Reinforced Bridge Decks	32
CHAPTER 3 FRAMEWORK OF THE TIME-DEPENDENT RELIABILITY ANALYSIS		34
3.1	Introduction.....	34
3.2	Ultimate Limit State (ULS) for Bridge Decks	34
3.3	Models and Statistical Parameters of Random Variables	36
3.3.1	Load Model	37
3.3.1.1	Live load moment, $M_L(t)$	37
3.3.1.2	Model error in live load analysis, x_{LL}	49
3.3.1.3	Dynamic load allowance, DLA	49
3.3.1.4	Dead load moments, $M_{D_{sw}}$ and $M_{D_{ws}}$	50
3.3.2	Resistance Model	51
3.3.2.1	Concrete compressive strength, f'_c	51
3.3.2.2	Time-dependent GFRP tensile capacity, $f_{frp}(t)$	51
3.3.2.3	FRP modulus of elasticity, E_{frp}	55
3.3.2.4	Concrete cover thickness, d_c	55
3.3.2.5	Time-dependent concrete damage due to freeze-thaw effect, $\psi_{FT,f}(t)$	56
3.3.3	Methods of Structural Analysis	59
3.3.3.1	Model error in FE analysis of live loads, x_{FE}	59
3.3.3.2	Model error in simplified analysis of structural resistance, PF	60
3.4	Time-Dependent Reliability Analysis using MC simulation	60
3.4.1	Procedure of Time-Dependent Reliability Analysis.....	62
3.4.2	Accuracy of MC simulation	64
3.4.3	Target Reliability Index.....	66
3.5	MATLAB Code Structure.....	67
CHAPTER 4 TIME-DEPENDENT RELIABILITY-BASED ASSESSMENT OF BRIDGE DECK DESIGN OPTIONS IN NS		72
4.1	Introduction.....	72

4.2	Time-Dependent Reliability-Based Assessment of Select NS Bridge Decks (Step 1)	72
4.2.1	Description of the Select Bridge Decks	72
4.2.2	Time-Dependent Reliability Analysis Results.....	76
4.3	Time-Dependent Reliability-Based Parametric Analysis of Representative Bridge Deck Configurations (Step 2).....	80
4.3.1	Description of the Considered Bridge Deck Configurations	80
4.3.2	Time-Dependent Reliability Analysis Results.....	83
CHAPTER 5 CONCLUSIONS AND RECOMMENDATIONS		87
5.1	Summary	87
5.2	Conclusions and Design Recommendations	88
5.3	Recommended Future Research	89
BIBLIOGRAPHY.....		91
Appendix A: Detailed Design Check of Select NS Bridge Decks.....		99
Appendix B: Annual Reliability Index for Configurations in Parametric Analysis		123

LIST OF TABLES

Table 1. Flexural response of GFRP-reinforced beams before and after conditioning in Nova Scotia (Esmaeili et al., 2020).....	29
Table 2. Loading and environmental conditioning of GFRP bars tested for creep rupture by Esmaeili et al. (2021).....	31
Table 3. Input statistical properties of the random variables for the reliability analysis.....	36
Table 4. Model descriptions for finite element model sensitivity analysis.....	44
Table 5. Summary of Nova Scotia bridges in created database.....	74
Table 6. Nova Scotia bridges analysed using time-dependent reliability analysis.....	74
Table 7. Summary of section details for analysed NS bridge decks.....	75
Table 8. Bridge deck configuration details for reliability-based parametric study for proposing alternative deck design options.....	81
Table 9. Section details for feasible durable alternative GFRP-reinforced bridge deck configurations for NS validated for a range of moment resistances.....	86

LIST OF FIGURES

Figure 1. Typical cross-section of a bridge deck.	1
Figure 2. Load-induced deficiency fault tree for bridge decks (Azizinamini et al., 2013).....	12
Figure 3. Bridge deck natural or man-made hazards fault tree (Azizinamini et al., 2013).....	14
Figure 4. Relationship between the correction factor, n_H , and relative humidity for GFRP bars (Benmokrane et al., 2020).....	22
Figure 5. Illustration of the prediction method for calculating tensile-strength retention factor for GFRP bars, C_E , (Benmokrane et al., 2020).....	23
Figure 6. Failure modes of GFRP-reinforced bridge deck: (a) concrete crushing failure; and (b) GFRP bar failure (Kim et al., 2012).....	25
Figure 7. Geometric and reinforcement details of beams tested by Esmaeili et al. (2020) (dimensions are in millimeters).....	27
Figure 8. Apparatus used to apply sustained load of beams tested by Esmaeili et al. (2020) (dimensions are in millimeters).....	27
Figure 9. Photos of beams tested by Esmaeili et al. (2020): (a) beams under the sustained load and natural weather conditioning (December 2008); (b) beams under the sustained load and natural weather conditioning (October 2009); (c) number of cracks formed along the length of a conditioned beam; and (d) a close-up photo of a crack. (Images by John Newhook).....	28
Figure 10. GFRP bars used for creep-rupture tests by Esmaeili et al. (2021).	30
Figure 11. Creep-rupture curves of GFRP bars by Esmaeili et al. (2021).....	31
Figure 12. FHWA vehicle category classification (FHWA, 2014).	39
Figure 13. Histogram of gross vehicle weights (GVW) of Class 13 vehicles in NS.....	40

Figure 14. Probability density functions (PDFs) and histograms for Axle 3 of Class 13 vehicles in NS.....	40
Figure 15. Cross-section of bridge analysed using finite element (FE) extracted from bridge drawings provided by NS-PW (all dimensions in millimeters).	41
Figure 16. Isometric view of the bridge FE model.	42
Figure 17. Extruded cross-section view of the bridge FE model (all dimensions in millimeters).	42
Figure 19. Sensitivity analysis results for positive and negative transverse moments on bridge deck FE model.	45
Figure 20. Maximum positive transverse moments along the span of the bridge deck FE model.	46
Figure 21. Distribution of normalized GFRP ultimate tensile strength (UTS) against distribution of time-to-failure values.	53
Figure 22. Bias, $\lambda_{\psi_{frrp,d}}$, and coefficient of variation, $V_{\psi_{frrp,d}}$, of GFRP tensile strength with respect to time.	54
Figure 23. Histogram and probability density function (PDF) of concrete cover thickness based on GPR data from Upper and Lower Durham Bridges.....	56
Figure 24. Sensitivity analysis of the number of trails, n , considered in the MC analysis.....	66
Figure 25. Flowchart describing the main algorithm for the time-dependent reliability analysis.	69
Figure 26. Flowchart describing the moment resistance function for GFRP-reinforced bridge deck sections (M_r Function).....	71
Figure 27. Locations of NS bridges analysed using time-dependent reliability analysis.	73

Figure 28. Annual reliability index, β_A , for the positive transverse, negative transverse, and positive longitudinal moments for NS bridge decks..... 78

Figure 29. Design lifetime reliability index, β_R , for the positive transverse, negative transverse, and positive longitudinal moments for NS bridge decks. 79

Figure 30. Design lifetime reliability index, β_R , for the six analyses of the parametric study..... 85

Figure 31. General schematic of GFRP-reinforced bridge deck variables for durable alternative deck designs. 86

ABSTRACT

The use of glass-fibre reinforced polymer (GFRP) reinforcement in bridge decks has gained popularity due to its corrosion resistance. Review of design practice of bridge decks in Nova Scotia (NS) indicates that GFRP-reinforced decks have similar design specifications including concrete compressive strength, concrete cover thickness, and section depth to the steel-reinforced bridge decks, despite the differences in their durability performance.

A research program sponsored by Nova Scotia Public Works (NS-PW) was initiated with an objective to propose durable alternative GFRP-reinforced bridge deck design options for NS in accordance with CSA S6:19. A two-phase approach is implemented to deliver on the project objective: development of a time-dependent reliability analysis framework to assess bridge decks (Phase I); and application of the framework to propose alternative design options (Phase II).

The framework in Phase I consists of developing degradation models for GFRP-reinforced concrete decks in NS, quantifying the statistical parameters (distribution type, bias, and coefficient of variation) of the load and resistance variables in NS, and developing a MATLAB[®] code to conduct the reliability assessment using Monte Carlo (MC) simulation. The framework is applied in Phase II to select existing bridge decks in NS and a comprehensive parametric analysis is performed to check the feasibility of durable alternative design options.

The analysis results show that the reliability of bridge decks in NS that follow the current design practice meet the recommended target reliability index, leaving room for exploring designs options that use alternative material and geometric properties. The parametric study in Phase II yielded four recommended alternative designs which specify the minimum deck section depth, maximum concrete cover thickness, and specified concrete compressive strength for deck sections validated for a range of factored moment resistances.

NOMENCLATURE

ACI	American Concrete Institute
ASR	Alkali-Silica Reactivity
ASTM	American Society for Testing and Materials
BLL	Bottom Lower Layer
BUL	Bottom Upper Layer
CHBDC	Canadian Highway Bridge Design Code
COV	Coefficient of Variation
CSA	Canadian Standards Association
DLA	Dynamic load allowance
FE	Finite Element
FHWA	Federal Highway Administration
FLS	Fatigue Limit State
FORM	First-Order Reliability Analysis
FRP	Fibre-Reinforced Polymer
GFRP	Glass Fibre-Reinforced Polymer
GMM	Gaussian Mixture Model
GVW	Gross Vehicle Weight
HRM	Halifax Regional Municipality
MC	Monte Carlo
NEBT	New-England Bulb Tee
NS	Nova Scotia
OHBDC	Ontario Highway Bridge Design Code
PDF	Probability Density Function
SAR	Structural Assessment and Retrofit
SLS	Serviceability Limit State
TUL	Top Upper Layer
U.R.	Utilization Ratio
ULS	Ultimate Limit State
UTS	Ultimate Tensile Strength

WIM	Weigh-In-Motion
A_b	cross-sectional area of a GFRP reinforcing bar
a_c	parameter from the test type for determining E_d
A_{frp}	total cross-sectional area of GFRP reinforcement in a given section
a_i	data fitting factor
a_y	regression constant
b_c	parameter from a function of the test type for determining E_d
b_i	data fitting factor
b_w	barrier width
b_y	regression constant
$C_{BF,t}$	nominal moment capacity of the deck when the GFRP bar failure occurs at time, t
$C_{CF,t}$	nominal moment capacity of the deck when the concrete crushing failure occurs at time, t
C_E	environmental reduction factor
c_i	data fitting factor
$d_{c_{bot}}$	bottom concrete cover thickness
$d_{c_{top}}$	top concrete cover thickness
d_{bar}	bar diameter
d_c	concrete cover thickness
D_c	diffusion coefficient
d_i	data fitting factor
d_s	distance from the top of the slab to the centroid of the bottom transverse FRP bars
$D_{T,23}$	diffusion coefficient at a defined reference temperature
e_0	model error term
e_1	model error term
E_a	activation energy of the reaction causing the degradation of tensile strength of the GFRP bars
E_c	static modulus of elasticity of concrete
e_{cu}	maximum strain in concrete
E_d	dynamic modulus of elasticity of concrete

e_E	model error term
E_{FRP}	modulus of elasticity of an FRP bar
E_{frpu}	ultimate elastic modulus of FRP
$f_{allowable}$	allowable tensile stress in FRP at SLS
f_{cm}	compressive stress at the compressive strain ε_{cm}
f_{cr}	cracking stress of concrete
f_{frp}	stress in FRP
$f_{frp}(t)$	time-dependent tensile capacity of GFRP bars
f_{frpu}	ultimate tensile strength of FRP
f_{fu}^*	guaranteed tensile strength of GFRP bars
f_{fu}	design tensile strength of GFRP bars
F_i	number failure points in year i in the MC simulation
$F_{i_{ref}}$	number of failure points from year i to year t_{ref}
F_t	fragility of GFRP bridge deck at any time t
f_t	girder flange thickness
$F_{u,k}$	characteristic tensile strength
$F_{u,m}$	average ultimate tensile strength at time zero
F_u^*	guaranteed tensile strength
f_w	girder flange width
f'_c	concrete compressive strength
g_t	performance function
h_1	distance from the centroid of tension reinforcement to the neutral axis
h_2	distance from the extreme flexural tension surface to the neutral axis
$h_{t,r}$	redistributed length of P_t
h_t	length of P_t
h_{tt}	height to P_t
$h_{v,r}$	redistributed length of P_v
h_v	length of P_v
h_{ws}	asphalt (wearing surface) thickness
k_b	coefficient depending on bond between FRP and concrete

l_e	maximum length of cantilever
$M_{D_{sw,cant}}$	dead load moment due to self-weight for exterior sections of decks
$M_{D_{sw}}$	dead load moment due to self-weight
$M_{D_{ws,cant}}$	dead load moment due to wearing surface for exterior sections of decks
$M_{D_{ws}}$	dead load moment due to wearing surface
M_f	bending moment demand
m_{frp}	slope of the bias of GFRP degradation curve
M_L	factored moment demand due to live load
$M_{Lb,t}$	transverse barrier live load moment intensity
$M_{Lb,v}$	vertical barrier live load moment intensity
M_{Lb}	total barrier live load moment intensity
$M_{LL,DLA}$	longitudinal live load moment intensity
$M_{LL,DLA}$	longitudinal live load moment intensity including the effects of DLA
m_p	mixing proportion of GMM distribution
M_r	factored bending moment resistance
M_s	moments due to loads at SLS
M_{S6}	maximum transverse moment according to CSA S6:19
M_T^+	maximum positive transverse moment on a bridge deck
M_T^-	maximum negative transverse moment on a bridge deck
$M_{TL,DLA}$	transverse live load moment intensity including the effects of DLA
M_{TL}	transverse live load moment intensity
M_y	transverse cantilever live load moment intensity
N_A	annual number of freeze-thaw cycles in a specific geographical region
n_b	number of GFRP bars in a given section
n_{frp}	modular ratio between FRP and concrete
n_H	correction factor equal to the ratio of the mobile water in the concrete under different
N_{RP}	total number of trucks within a return period
N_T	number of freeze-thaw cycles
n_{yr}	number of trucks in 1-year of WIM data

P_1	factor describing the shape of the polynomial equation for the COV of GFRP degradation as a function of time
P_2	factor describing the shape of the polynomial equation for the COV of GFRP degradation as a function of time
P_3	factor describing the shape of the polynomial equation for the COV of GFRP degradation as a function of time
$P_{f,i_{ref}}$	cumulative probability failure from year i to t_{ref}
P_f	probability of failure
P_l	longitudinal barrier load
P_t	transverse barrier load
P_v	vertical barrier load
P_W	truck wheel load
R_g	universal gas constant
r_o	initial radius of an FRP bar
r_t	ratio of smallest slab thickness to the largest slab thickness of the bridge deck
s_0	standard deviation of model error term e_0
s_1	standard deviation of model error term e_1
S_e	effective transverse length for interior spans of decks
S_e	equivalent transverse span
s_E	standard deviation of model error term e_E
S_i	number of survival points in year i in the MC simulation
S_p	effective transverse length for exterior spans of decks
t_1	experimental exposure time
T_1	first temperature for conducting accelerated aging experiment
T_2	second temperature for conducting accelerated aging experiment
T_{23}	reference temperature
t_D	design life
T_g	glass transition temperature of FRP
t_{ref}	reference year
u_N	most probable value for a Gumbel distribution

$V_{\psi_{frp,d}}$	time-dependent coefficient of variation of GFRP tensile capacity
w_{cr}	concrete crack width
w_d	deck width
w_{sw}	uniform load due to self-weight
w_t	girder web thickness
w_{ws}	uniform load due to wearing surface
x_b	vector of basic variables
x_d	vector of design and mechanical properties of a deck
$x_{FT,Ec}$	random variable to account for the uncertainty in predicting elastic static concrete modulus of elasticity
$x_{FT,f}$	random variable to account for model uncertainty in predicting $\psi_{FT,f}$
$x_{FT,N}$	random variable to account for model uncertainty in predicting N_T
$x_{FT,NA}$	random variable to account for the variance in field measured N_T
x_{LL}	model error in live load analysis
\bar{y}	distance from the neutral axis to the location of the resultant compression force
$\alpha_{D_{sw}}$	dead load factor for self-weight
$\alpha_{D_{ws}}$	dead load factor for wearing surface
α_1	rectangular stress block stress factor
α_L	live load factor
α_N	dispersion coefficient for a Gumbel distribution
β_1	rectangular stress block depth factor
β_A	annual reliability index
β_R	design lifetime reliability index
β_T	target reliability index
γ_c	concrete unit weight
γ_N	conversion factor for freeze-thaw effect
γ_{ws}	asphalt unit weight
Δ_1	value obtained by accelerated aging data through linear regression; Tensile-strength reduction after t_1 experimental exposure at T_1

Δ_2	tensile-strength reduction between t_1 experimental exposure and design life t_D at T_1
Δ_3	additional tensile-strength reduction due to effects of elevated temperature at T under design lifetime exposure
ε_{cc}	peak strain in concrete
ε_{cm}	compressive strain
ε_{cu}	maximum allowable compressive strain in concrete
ε_f	strain in the GFRP reinforcement when the concrete strain reaches crushing failure
ε_{frp}	strain in FRP reinforcement
ε_{frpu}	ultimate strain in FRP in tension
θ_1	data fitting parameter
θ_2	data fitting parameter
θ_3	data fitting parameter
Θ_E	vector of unknown parameters to fit the data
Θ_σ	vector of unknown parameters
$\lambda_{\psi_{frp,d}}$	time-dependent bias of GFRP tensile capacity
λ_1	data fitting parameter
λ_{fc}	bias of concrete compressive strength
μ_e	mean of GMM distribution
μ_{max}	mean maximum load effect
μ_{σ_0}	mean of error term s_0
ρ_{bal}	balanced reinforcing ratio
ρ_{frp}	ratio of the cross-sectional area of longitudinal FRP reinforcement to the effective cross-sectional area of a beam
σ_e	standard deviation of GMM distribution
σ_t	parameter to predict the capacity of GFRP bars embedded in concrete at a given time
σ_{max}	standard deviation of maximum load effect
ϕ_c	material resistance factor for concrete
ϕ_{frp}	material resistance factor for FRP

$\psi_{frp,d}$	time-dependent GFRP tensile capacity damage parameter
$\psi_{FT,Ec}$	static elastic modulus of concrete
$\psi_{FT,Ed}$	dynamic elastic modulus of concrete
$\psi_{FT,f}$	concrete compressive strength damage factor
A	constant relative to the material and degradation process in Arrhenius Relation
B	constant determined using the time shift of two known curves
b	width of the concrete section
c	distance measured from the top extreme fibre to the neutral axis of a given section
C	normalized or relative term describing the alkaline or chloride concentration
D	moment demand
d	distance measured from the extreme compression fibre to the centroid of tension reinforcement
D/L	dead-to-live load ratio for self-weight or wearing surface
DLA	dynamic load allowance variable
G	performance function
h	depth of the section
I	dynamic amplification factor
i	year of evaluation in reliability analysis
k	degradation rate in Arrhenius Relation;
l	girder spacing
L	span length
n	number of trials
P	maximum wheel load of the CL-625 Truck
PF	professional factor
r	radius of an FRP bar
R	vector of resistances
RH	relative humidity
RP	return period
s	spacing of tensile reinforcement
S	vector of loads

T	temperature
t	time
TSF	time shift factor
$U.R.$	utilization ratio
V	coefficient of variation
W	gross vehicle weight
w	unit weight of concrete
X	vector of random variables
Y	strength retention
α	data fitting parameter where the value is obtained by accelerated aging data through linear regression
λ	bias
τ	fitted coefficient using least squares method

ACKNOWLEDGEMENTS

First and foremost, I am deeply grateful to my supervisors, Dr. Fadi Oudah and Dr. John Newhook for their invaluable support, patience, and advice, and for their trust in me to be able to take on this project. I would also like to thank Dalhousie University and Nova Scotia Public Works (NS-PW) for sponsoring and making this project possible. I would also like to thank the members of the Structural Assessment and Retrofit (SAR) research group, particularly Connor, Elizabeth, and Koosha, for their support and assistance during my master's degree.

CHAPTER 1 INTRODUCTION

1.1 BACKGROUND

Nova Scotia (NS) has more than 4,100 bridges under the provincial government's purview. Approximately 10% percent of the \$300 million 2019-2020 Nova Scotia Public Works (NS-PW) budget is allocated for bridge rehabilitation projects, which typically involve bridge deck maintenance or replacement (Andrea, 2019). A bridge deck is the portion of a bridge that carries and distributes loads to supporting girders and serves as the roadway for vehicular and pedestrian traffic usually with a wearing surface overlay as shown in Figure 1. The types of bridge decks include reinforced concrete decks (composite or non-composite), steel orthotropic decks, and wooden decks.

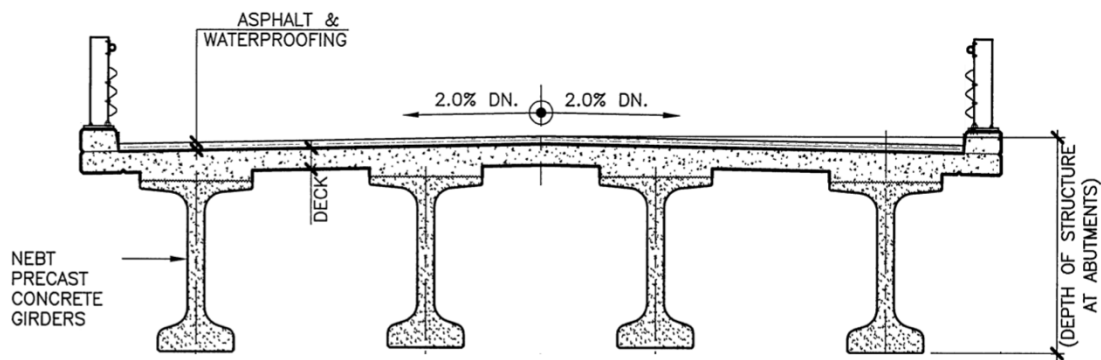


Figure 1. Typical cross-section of a bridge deck.

The durability of bridge decks largely influences the lifespan of bridge structures. Environmental factors such as high pH, saltwater, de-icing salts, high temperature, freeze-thaw cycles, and wet/dry cycles cause long-term durability issues in concrete bridge decks leading to a reduced lifespan (Kim et al., 2012). Advanced composite materials such as fibre-reinforced polymers (FRP) have been used as reinforcing material for bridge decks to tackle the effects of

CHAPTER 1: INTRODUCTION

adverse environmental conditions (Benmokrane et al., 2020). Glass fibre-reinforced polymers (GFRP) bars are the most frequently used type of FRP bars in bridge construction mostly because they are high strength, lightweight, non-corrosive, and economical, making them ideal for use in bridge environments (ISIS, 2007).

The Canadian Highway Bridge Design Code (CHBDC), CSA S6:19 (2019), permits the use of FRP bars, and practicing engineers have been designing with FRP as the primary concrete deck reinforcing material for the last three decades. Despite the significant benefits of FRP bars, there is some uncertainty concerning the long-term performance of the material when embedded in concrete, which resulted in having most codes include an ‘environmental factor’ in the calculation of the capacity of FRP reinforced members. The durability of FRP bars used in concrete decks still needs to rely heavily on lab testing and statistical analysis for any quantitative data on performance as the FRP bars have only been used in field structures since the mid-1990s.

Review of industry practice of GFRP-reinforced bridge decks in NS indicates that design specifications including concrete strength, concrete cover thickness (top and bottom), and section depth are based on older designs that used steel reinforcing bars as opposed to GFRP (Idemudia et al., 2021). Design specifications are typically set to meet minimum acceptable structural and durability requirements, where the structural requirements relate to the response at the ultimate limit state (ULS) while the durability requirements relate to the service life of the bridge deck. Adapting design specifications of steel-reinforced bridge decks for the design of GFRP-reinforced bridge decks, as is the case in NS, is likely not to yield optimized designs since the durability performance of GFRP-reinforced structures are proven to differ than steel-reinforced counterparts (Mufti et al., 2005).

CHAPTER 1: INTRODUCTION

Predicting the structural safety for a target service life is a time-dependent problem since the response at ULS is affected by the durability performance of the bridge deck when exposed to harsh environment. This coupled ULS-durability performance of bridge decks requires the use of time-dependent reliability analysis to assess structural safety since it accounts for the degradation in the capacity as a function of time. A research programme at Dalhousie University, sponsored by Nova Scotia Public Works (NS-PW), was initiated to propose durable alternative GFRP-reinforced bridge deck design options with alternative material and geometric properties that meet the structural and durability requirements of CSA S6:19 for the specific environmental exposure and traffic loading in NS.

1.2 OBJECTIVES AND SCOPE

The objective of this project is to propose durable GFRP-reinforced concrete bridge deck design options in accordance with CSA S6:19 requirements for NS-PW using a time-dependent reliability-based design approach. The scope of work to achieve the project objectives include:

- Development of a time-dependent reliability-based framework of analysis to evaluate the structural safety of GFRP reinforced concrete bridge decks at ULS.
- Application of the developed framework to assess select GFRP reinforced concrete bridge decks in NS to evaluate typical design practice and recognize areas for further design refinement.
- Recommendation of design specifications for alternative design options of GFRP reinforced concrete bridge decks in NS, following a parametric analysis conducted using the developed framework.

CHAPTER 1: INTRODUCTION

The project was undertaken in two phases which were executed sequentially: development of a time-dependent reliability analysis framework (Phase I); and application of the reliability analysis framework (Phase II). Phase I consisted of developing a framework for conducting time-dependent reliability analysis of bridge decks reinforced using GFRP using Monte Carlo (MC) simulation. It included proposing a degradation model for GFRP reinforcement, degradation model of concrete damage due to freeze-thaw effect, and a live load model for bridge decks. The statistical parameters (distribution type, bias, and coefficient of variation) of the random variables considered in the analysis (loads, resistance, and methods of structural analysis) were developed to reflect conditions in NS. The time-dependent reliability based analysis was coded in MATLAB[®].

Phase II consisted of applying the framework to select existing bridge decks in NS to evaluate the current design practice and identify room for further design refinement. A parametric analysis was conducted to propose durable alternative bridge deck configurations for bridge decks in NS that meet a predefined target safety level. The performance objectives for proposing the alternative bridge deck designs are to minimize the specified concrete compressive strength, concrete cover thickness, and overall section depth while satisfying the ULS and reliability requirements.

1.3 THESIS STRUCTURE

This thesis consists of five chapters, a bibliography, and appendices. The content and description of the comprising chapters are given below:

Chapter 1. *Introduction.* It provides a general introduction into the research topic and describes the need for the project. It also details the objectives and the scope of work.

Chapter 2. *Literature Review.* It provides a general background into the main aspects of the research and discusses the available literature relevant to the research topic such as

CHAPTER 1: INTRODUCTION

bridge deck design in Canada, the degradation of GFRP bars, durability, and reliability of bridge decks.

Chapter 3. *Framework of the Time-Dependent Reliability Analysis.* It presents the limit state function used in the time-dependent reliability analysis and the models and statistical parameters of random variables. This chapter also describes the solution method for the time-dependent reliability analysis and the MATLAB[®] code structure.

Chapter 4. *Time-Dependent Reliability-Based Assessment of Bridge Deck Design Options in NS.* It presents the results of the reliability analysis of select existing GFRP-reinforced bridge decks in NS. This chapter also presents the results of a parametric study to propose durable alternative GFRP-reinforced bridge deck sections.

Chapter 5. *Conclusions and Recommendations.* It summarises the steps taken to deliver on the project objectives, presents the significant results from the performed reliability analyses. This chapter presents the final conclusions and design recommendations regarding the project and recommended future research.

CHAPTER 2 LITERATURE REVIEW

2.1 INTRODUCTION

This Chapter provides a general review of the literature relevant to aspects of the research topic including bridge deck design procedure per CSA S6:19, factors influencing bridge deck design service life, degradation mechanisms of GFRP bars, durability and life prediction methods for GFRP bars, and prior reliability-based analysis of GFRP-reinforced bridge decks. The literature reviewed in this Chapter is specific to the topics discussed within the subheadings, whereas the literature for the statistical parameters used in the time-dependent reliability analysis is presented in the respective sections of Chapter 3.

2.2 BRIDGE DECK DESIGN PER CSA S6:19

Bridges in Canada are designed in accordance with CSA S6:19 and provincial design specifications. CSA S6:19 applies to the design, evaluation, and structural rehabilitation of fixed and movable highway bridges in Canada. The following subsections discuss the bridge deck design requirements and procedures as per CSA S6:19.

2.2.1 Durability

Section 2 of CSA S6:19 specifies the requirements for durability that need to be considered during the design process in addition to the code's requirements for strength and serviceability. These requirements apply to the design of new bridges as well as rehabilitation and replacement work.

According to Clause 2.3.1 of CSA S6:19 (2019), the design of bridges shall ensure that the structure will be able to maintain its level of serviceability during its design life. Designers are

CHAPTER 2: LITERATURE REVIEW

required to consider the environmental conditions that exist at the site or are likely to exist during the design life of the structure and shall assess their significance in relation to the possible mechanisms of deterioration in the structure (CSA S6:19, 2019).

The durability requirements specified in CSA S6:19 include structural form, materials, and details which shall be suitable for the design loads and environmental conditions that will be experienced during the design life of the structure (75 years for new structures according to Clause 1.4.2.3). This ensures that designers consider the forms of deterioration based on the material choices and detailing to achieve durability in bridges.

2.2.2 Loads

Section 3 of CSA S6:19 specifies loads, load factors, and load combinations to be used in calculating load effects for design. Bridge design according to CSA S6:19 shall be on the limit states philosophy, satisfying the Ultimate Limit States (ULS), Fatigue Limit State (FLS), and Serviceability Limit States (SLS). Under ULS, Clause 3.4.2 of CSA S6:19 (2019) specifies that designs shall provide a factored resistance that exceeds the total factored load effect.

The loads considered in bridge deck design according to CSA S6:19 (2019) are divided into three major categories: 1) permanent loads which consist of dead load, loads due to earth pressure and hydrostatic pressure, and secondary prestress effects; 2) transitional loads which consist of traffic loads, wind load on structure, wind load on traffic, and loads due to differential settlement and/or movement of the foundation; 3) exceptional loads which consist of earthquake load, loads due to stream pressure and ice forces or to debris torrents, ice accretion load, and collision load arising from highway vehicles or vessels.

CHAPTER 2: LITERATURE REVIEW

Clause 3.5.1 of CSA S6:19 (2019) states that the calibration of load factors and resistance factors shall be based on a minimum annual reliability index of 3.75 for traffic loading, including special load vehicles with no travel restriction or supervision, and 3.50 special load vehicles travelling alone on a bridge under supervision in accordance with Clause 3.8.3. Further discussion on the implications of the code specified minimum reliability limits is provided in Section 3.4.3.

2.2.3 Methods of Analysis

Section 5 of CSA S6:19 specifies the methods of analysis for the design and evaluation of bridge superstructures. Some of the general requirements from CSA S6:19 (2019) are that: 1) the geometry, boundary conditions, structural characteristics, and loading shall be modelled to accurately reflect the behaviour of the bridge at each relevant limit state; 2) for the purpose of analysis, materials shall be treated as elastic unless otherwise permitted in Section 5 of CSA S6:19 or approved; and 3) beams, girders, trusses, braced frames, grillages, slabs, and connections designed in accordance with the Code shall be considered structures to which small-deflection theory applies.

Clause 5.7 of CSA S6:19 addresses Analysis of Decks and discusses the methods of analysis for different deck types. Clause 5.7.1.1 of CSA S6:19 (2019) states that concrete deck slabs are required to be analysed for positive and negative bending moments resulting from loads applied on the slabs. The analysis shall consider the bending moments induced in the longitudinal direction that agree with the assumptions used in the analysis of the transverse negative bending moments. CSA S6:19 (2019) also requires that cantilever portions of concrete deck slabs are analysed for transverse negative bending moments resulting from loads on the cantilever portions of the slabs or horizontal loads on barriers and railings (CSA S6:19, 2019).

CHAPTER 2: LITERATURE REVIEW

CSA S6:19 (2019) allows deck slabs to be analysed for transverse moments using one of the following methods: 1) in accordance with Clause 5.7.1.2 for portions between supporting elements and Clause 5.7.1.3 for the cantilever portion; 2) using the yield line theory at ULS; or 3) using the refined method in accordance with Clause 5.9.

2.2.4 Concrete Structures

Section 8 of CSA S6:19 specifies requirements for the design of concrete structural components that are made of precast or cast-in-place normal-density, low-density, or semi-low-density concrete and reinforced with prestressed or non-prestressed steel. Clause 8.4.6 of CSA S6:19 (2019) specifies the material resistance factor for concrete, ϕ_c , as 0.75. Clause 8.8.2 states the assumptions for the SLS and FLS while Clause 8.8.3 states the assumptions for the ULS.

2.2.5 Fibre-Reinforced Structures

Section 16 of CSA S6:19 applies to components containing fibre reinforcement such as non-prestressed concrete beams, slabs, columns, and deck slabs. This Section of CSA S6:19 also covers fibre reinforcement with fibres comprising of glass, carbon, aramid, steel, and low modulus polymers as well as matrices such as epoxy resin, saturated and unsaturated polymer resin, vinylester resin, polyethene or concrete.

Clause 16.4.5 of CSA S6:19 (2019) states that the minimum clear cover and its construction tolerance shall be 35 ± 10 mm for FRP bars and grids and 50 ± 10 mm for FRP tendons. The resistance factor, ϕ_{frp} , for GFRP reinforcement is 0.65 according to Clause 16.5.6 (CSA S6:19, 2019). For crack control-reinforcement, CSA S6:19 (2019) provides requirements such that when the maximum tensile strain in FRP reinforcement under full-service loads exceeds 0.0015, cross

CHAPTER 2: LITERATURE REVIEW

sections of the component in maximum positive and negative moment regions shall be proportioned to have the crack width not exceed 0.5 mm for members subjected to aggressive environments and 0.7 mm for other members.

For internally restrained cast-in-place deck slabs, CSA S6:19 recognizes two methods for designing FRP reinforced bridge decks which are: 1) Design by empirical method as specified in Clause 16.8.8.1; and 2) Design for flexure as specified in Clause 16.8.8.2.

When designing using the empirical method, Clause 16.8.8.1 of CSA S6:19 (2019) states that the requirements of Clause 8.18 pertaining to cast-in-place deck slabs shall apply to cast-in-place deck slabs with FRP bars or grids, except when the deck slab is designed using the empirical method of Clause 8.18.3. The following requirements stated in Clause 16.8.8.1 need to be met in lieu of those specified in items a) and c) of Clause 8.18.3.3:

- a) the deck slab shall contain two orthogonal assemblies of FRP bars, with the clear distance between the top and bottom transverse bars being at least 55 mm. The diameter of reinforcement bars shall not be less than 15 mm;
- b) for the transverse FRP bars in the bottom assembly, the minimum area of cross-section in mm^2/mm shall be $500d_s/E_{frp}$, where d_s is the distance from the top of the slab to the centroid of the bottom transverse FRP bars and E_{frp} is the modulus of elasticity of the FRP bar; and
- c) the longitudinal bars in the bottom assembly and the transverse and longitudinal bars in the top assembly shall be of GFRP with a minimum ρ_{frp} of 0.0035, where ρ_{frp} is the ratio of the cross-sectional area of the longitudinal FRP reinforcement to the effective cross-sectional area of the beam.

CHAPTER 2: LITERATURE REVIEW

To maintain consistency with the requirements of Clause 8.18.1, CSA S6:19 states that the requirements of Clause 16.8.2.3 which specify crack-control reinforcement details shall be waived for decks designed using the empirical method.

When designing for flexure, Clause 16.8.8.2 of CSA S6:19 (2019) states that for cast-in-place deck slabs with FRP bars or tendons designed for flexure, the requirements of Clauses 16.8.2 to 16.8.6 shall apply, which are the Clauses that provide requirements for deformability and minimum reinforcement, minimum flexural resistance, crack-control reinforcement, deflection and rotations, non-prestressed reinforcement, development length for FRP bars, and tendons. CSA S6:19 (2019) specifies that the spacing of the reinforcement in each direction shall not exceed 300 mm and the diameter of reinforcement bars shall not be less than 15 mm when designing for flexure in FRP reinforced decks.

2.3 FACTORS INFLUENCING BRIDGE DECK SERVICE LIFE

The service life of bridge decks is reduced due to two main factors that cause early deterioration in the bridge decks. One of them being obsolescence which can be described as a functional planning issue. The second reason being degradation in materials that affect service-life performances, which could be load-induced, man-made or natural, or due to defects in construction materials, processes, designs (Azizinamini et al., 2013). Departments of transportation are generally responsible for maintaining bridges by executing good functional and maintenance plans, whereas deterioration in materials due load induced, man-made, or natural considerations can be less controlled and managed. The load-induced and natural or man-made hazards considerations are reviewed in the following subsections.

2.3.1 Load-Induced Considerations

Bridge decks are subject to deterioration due to loads caused by traffic or by the bridge system itself. Figure 2 shows a breakdown of the load-induced deficiencies of cast-in-place concrete bridge decks and corresponding deterioration mechanism. Load-induced considerations consists of two types of loads: traffic-induced loads, and system-dependent loads. The load types are briefly reviewed in the following subsections in reference to Figure 2.

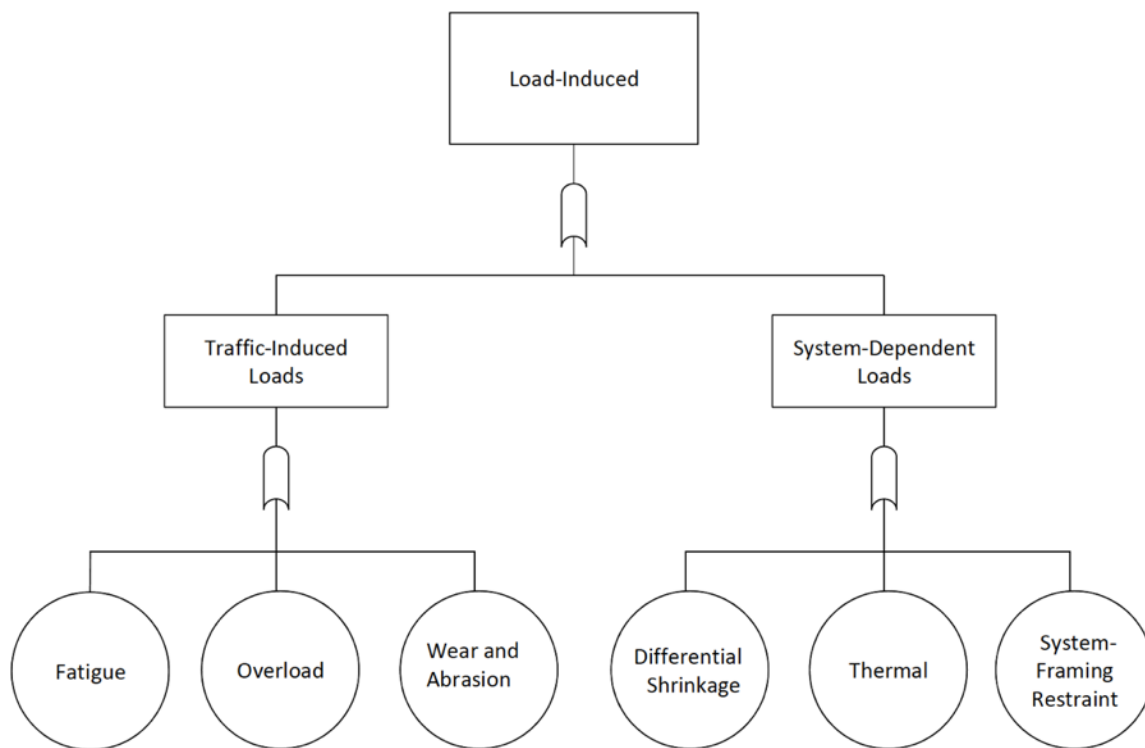


Figure 2. Load-induced deficiency fault tree for bridge decks (Azizinamini et al., 2013).

2.3.1.1 Traffic-Induced Loads

Loads induced by traffic such as trucks and other vehicles can take various forms and affect the bridge deck in different ways such as **fatigue, overload, wear, and abrasion** (Azizinamini et al., 2013). Bridges are primarily made of concrete, with steel or GFRP reinforcement or a combination

CHAPTER 2: LITERATURE REVIEW

of both, and these materials can fail by fatigue, therefore bridges are designed to resist failure by fatigue by satisfying FLS requirements. Although vehicles and trucks have weight restrictions, some vehicles still use the bridges while being overweight and in-turn overload the bridge. This results in additional flexural stresses, deflections, and cracking which can propagate other issues on bridges service life.

The surface of the deck is always subject to wearing and abrasion, hence why bridge deck slabs are topped by a wearing surface, usually concrete or asphalt. High traffic volumes, tire loads, and the types of tires such as studded tires which exhibit much higher road surface erosion rates than non-studded tires cause wearing on the surface of bridge decks (Wagner et al., 2018). This loss of wearing surface leads to reduction in the deck thickness and concrete cover thereby creating a pathway for corrosion to occur, lower capacity, higher stresses, and severe cracking and spalling.

2.3.1.2 System-Dependant Loads

When the bridge deck concrete is cast on-top of previously cast concrete or steel girders, there is a high chance of **differential shrinkage** occurring as the fresh concrete is restrained by the cured concrete or steel girders. Temperature changes can lead to the development of axial forces in the deck such as **thermal** stresses which may be due to a uniform internal temperature and gradient changes on the overlays (Beushausen and Alexander, 2006).

System-framing restraint implies that bridge decks are subject to an additional axial force which are a result of the design choice made by designers regarding the boundary conditions of the deck (type of abutment). This implies that allowing rotation at the ends of the deck close to the abutment by designing expansion joints at the abutment versus casting the bridge deck integral with the abutments could lead to additional load on the structure (Azizinamini et al., 2013).

2.3.2 Natural or Man-Made Hazard Considerations

Bridges and their decks are subjected to various environmental conditions throughout their design life. The bridge deck is the part of the bridge that is most exposed to the environment considering its surface area and direct exposure to the traffic loads and environment. The environmental considerations affecting the bridge deck service life such as extreme thermal climates, chemical climates, fires, and others are shown in Figure 3 (Azizinamini et al., 2013). Two of the major natural hazard categories are discussed in the following subsections.

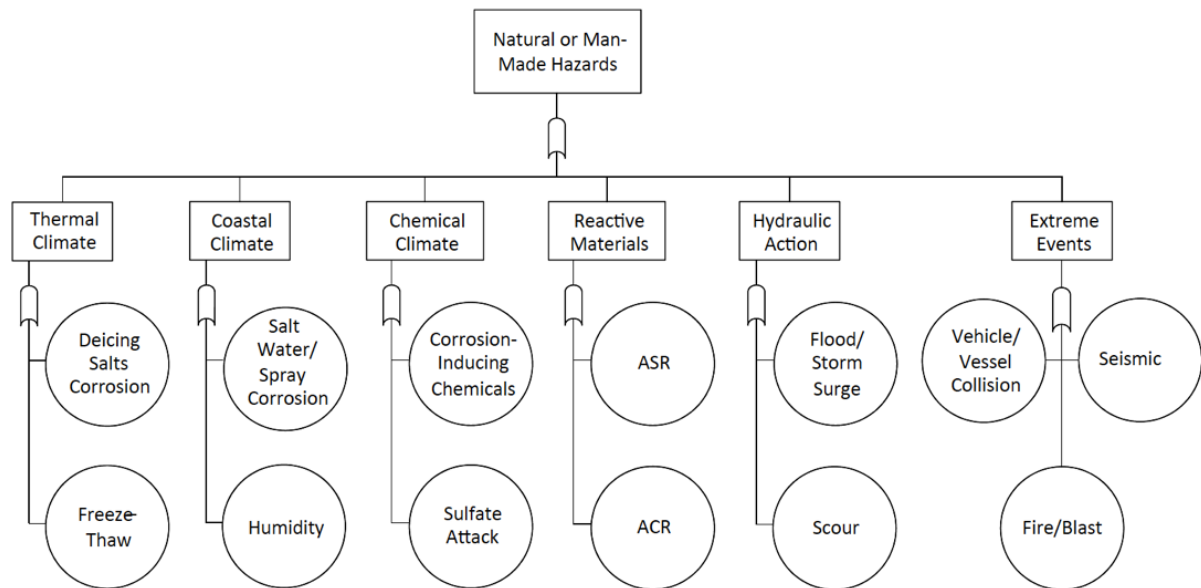


Figure 3. Bridge deck hazards fault tree (Azizinamini et al., 2013).

2.3.2.1 Thermal Climate

The deterioration considerations stemming from thermal climate are mostly due to cold weather and deteriorating hazards coming primarily from the following two sources:

De-icing Salts – Canada is a generally cold country and transportation agencies use de-icing salts in the winter season to help keep the roads safe. When the de-icing salt melts, it

CHAPTER 2: LITERATURE REVIEW

finds its way through cracks or pores in the concrete deck and eventually initiates corrosion that then causes deterioration of the reinforcement through chemical reactions. This phenomenon is very dependent of the type of reinforcement used in the concrete. It should be noted that structures very close to the coastline can see similar chemical reactions from salt-laden moisture coming off the ocean.

Freeze-Thaw Cycles – Water from rain and snow can also find its way into the pores or cracks in the concrete deck and freeze during the winter season and causes frost damage. The frozen water then expands inside the concrete causing stresses in the concrete and when the temperature rises, the water thaws releasing the developed stresses and the process is repeated with every freeze-thaw cycle (Ebrahimi et al., 2018). This phenomenon is very much dependant on the quality and properties of the concrete.

2.3.2.2 Reactive Materials

Reinforced concrete is a material made from combining several constituents and products and sometimes not all its constituents are compatible with each other. Meaning that chemical reactions may occur and lead to degradation of parts of the concrete or its reinforcement. Alkali-silica reactivity (ASR) is a chemical reaction between aggregates containing reactive silica and the alkalis in the concrete which causes the breakdown of the siloxy bonds in the GFRP due to the presence of the alkaline environment in the concrete (Azizinamini et al., 2013). This phenomenon is discussed further in Section 2.4.2.

2.4 DEGRADATION MECHANISM OF GFRP BARS

Even though FRP is non-corrosive, literature indicates that FRP can degrade over time which could lead to loss of material or loss of strength in the bars thereby causing long-term performance and durability issues (Robert et al., 2009). The extent of deterioration in FRP bars is dependent on the fundamental factors that make up the composite such as the fibre type, fibre/matrix volume fraction, resin type, the adhesion of the fibre-matrix interface and the environmental conditions. Most GFRP bars are made of E-glass fibres which is very susceptible to degradation in harsh environments such as moisture and alkalinity (Benmokrane and Ali, 2018).

2.4.1 Effect of Moisture on GFRP Bars

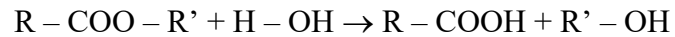
Glass fibres used in GFRP bars are known to degrade over time when in the presence of water (Dejke, 1999). The moisture can reduce the glass transition temperature (T_g) of the resin and make it act as a plasticizer, potentially causing adverse effects on the flexural strength. The sorption rate is controlled by the matrix's chemical structure, interface, and manufacturing process (Daly et al., 2007).

Research studies have been performed to control the moisture-diffusion process by using resin matrices that have a lower permeability, improving the interface by using sizing chemistry, and selecting appropriate molding processes to reduce void content (Benmokrane et al., 2018). The time of exposure to these environmental conditions and the exposure temperatures become important considerations for designing structures using GFRP.

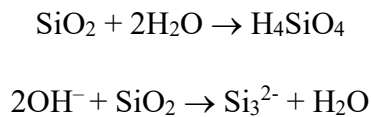
2.4.2 Effects of Alkalinity on GFRP Bars

The concrete environment has been classified as a high pH environment due to its range of 12 and 13. This high alkalinity damages the glass fibres and leads to loss of toughness and strength and increase in embrittlement (Benmokrane et al., 2018). The alkalinity of concrete structures usually depends on the concrete properties such as the cement and the admixtures used in construction. Chen et al. (2007) performed testing which included immersing FRP bars in different solutions at different temperatures and at different times of exposure. Testing indicated that GFRP bars showed significant loss of strength when exposed to the adverse conditions, especially in alkaline solutions where the temperature was at 60 °C.

The interfacial bond between the fibres and the resin are destroyed when water molecules penetrate the resin. The void of the resin becomes occupied, and the free volume of the composite changes causing large cracks and hydrolyzes the resin (Jin et al., 2020). The chemical reaction as described by Jin et al. (2020) is as follows:



The water molecules as well as the OH⁻ penetrates through the resin to the fibre surface, which causes damage to the SiO₂ in the glass described by the two chemical reactions below (Jin et al., 2020):



2.5 DURABILITY AND LIFE PREDICTION METHODS FOR GFRP BARS

Several methods have been proposed in literature to assess the durability and life performance predictions of GFRP bars. The following subsections describe key methods existing in literature.

2.5.1 Arrhenius Relation

The long-term performance of GFRP bars has been estimated by the popular Arrhenius relations, in terms of degradation rate, given by Equations (1) to (3) below (Robert et al., 2009):

$$k = A \exp\left(\frac{-E_a}{R_g T}\right) \quad (1)$$

$$\frac{1}{k} = \frac{1}{A} \exp\left(\frac{E_a}{R_g T}\right) \quad (2)$$

$$\ln\left(\frac{1}{k}\right) = \frac{E_a}{R_g} \frac{1}{T} - \ln(A) \quad (3)$$

where k is the degradation rate (1/time); A is constant relative to the material and degradation process; E_a is the activation energy of the reaction causing the degradation of tensile strength of the GFRP bars; R_g is the universal gas constant; T is the temperature (Kelvin).

The model by Robert et al. (2009) assumes that there is only one degradation mechanism that is dominant for the material during the reaction and the degradation mechanism does not change with temperature or time. From Equation (2), k can be determined as the inverse of time required for a material property to degrade to a given value (100% reduction for a service life prediction) (Chen et al., 2006). In Equation (3), the logarithm of the degradation rate is expressed by a linear function of $1/T$ with a slope of E_a/R_g (Chen et al., 2006).

2.5.2 FRP Strength Degradation Models

According to Davalos et al. (2012), there are mainly four types of FRP strength models, and their prediction procedures are all based on the Arrhenius Relations (Equations (1) to (3)). There are two main approaches to the time-dependant performance prediction of FRP bars: either measuring their “strength retention” or their “moisture absorption” (Benmokrane et al., 2018).

The first model proposed by Tannous (1998) which uses a “moisture absorption” model is shown in Equation (4). This model assumes that the affected area of the bar is completely degraded and unable to carry any load, and the determination of C and D_c from moisture absorption tests makes its use complicated (Benmokrane et al., 2018).

$$Y = 100 \left(1 - \frac{\sqrt{2D_c C t}}{r_o} \right) \quad (4)$$

where Y is the predicted tensile strength retention (%) in this equation and all others in this document; t is the exposure time; D_c is the diffusion coefficient; C is the normalized or relative term describing the alkaline or chloride concentration; r_o is the radius of the FRP bar.

The second model uses an exponential relationship between strength retention and aging time with debonding at the fibre-matrix interface as the major degradation mechanism as expressed in Equation (5). In this model, the tensile strength retention (%) at an infinite exposure time (t) is assumed to be zero (Benmokrane et al., 2018).

$$Y = 100 \cdot \exp\left(\frac{-t}{\tau}\right) \quad (5)$$

where τ is a fitted coefficient using least squares method.

CHAPTER 2: LITERATURE REVIEW

The third model adopts a linear relationship between the strength retention and the logarithm of the aging of time, expressed in Equation (6), which is a widely used equation but does not hypothesize the degradation mechanism (Benmokrane et al., 2018).

$$Y = a_y \cdot \log(t) + b_y \quad (6)$$

where a_y and b_y are regression constants.

The fourth model uses a double logarithmic scale from experiments as expressed in Equation (7), but with different values for the regression constants (Benmokrane et al., 2018).

$$\log(Y) = a_y \cdot \log(t) + b_y \quad (7)$$

Researchers have used these various models of the degradation laws from Equation (4) to Equation (7) to suit their needs depending on what works best for their intended purpose.

2.5.3 Tensile Strength Prediction Based on Environmental Reduction Factor (C_E)

The ACI 440.1R-15 (ACI 2015) uses the environmental reduction factor, C_E , to reflect the effects of harsh environmental conditions that structures reinforced with GFRP bars may experience. The factor is incorporated into ACI 440.1R-15 using Equation (8) (Benmokrane et al., 2020).

$$f_{fu} = C_E \cdot f_{fu}^* \quad (8)$$

where f_{fu} is the design tensile strength of the GFRP bar; f_{fu}^* is the guaranteed tensile strength of the GFRP bar, defined as the average tensile strength minus three times the standard deviation.

CHAPTER 2: LITERATURE REVIEW

In this approach, the model proposed by Huang and Aboutaha (2010) is used to establish the environmental reduction factor, C_E . This model encompasses the effects of seasonal temperature fluctuations, relative humidity (RH) of exposure, and service year into the factor C_E , according to the Equation (9) (Benmokrane et al., 2020).

$$C_E = 1 - [\Delta_1 - \alpha \cdot \log(DL \cdot TSF)] \cdot n_H \quad (9)$$

where C_E is the environmental reduction factor of tensile strength reflecting the effects of service lifetime, temperature, and relative humidity (RH); n_H is a correction factor equal to the ratio of the mobile water in the concrete under different RHs as shown Figure 4; Δ_1 and α can be obtained by accelerated aging test data through linear regression of the experimental data for a minimum of two different temperatures, T_1 and T_2 .

The values of Δ_1 and α are determined by plotting a graph with time on the x -axis on a logarithmic scale (log-time) and the tensile strength retention value on the y -axis on a linear scale (see Figure 5). Lines are then fitted through the experimental data set (one for each conditioning temperature) using linear regression. The slopes of the regression line represent the value of α , where Δ_1 is equal to the tensile strength-reduction after a period corresponding to the time t_1 of experimental exposure at T_1 (see Figure 5) (Benmokrane et al., 2020).

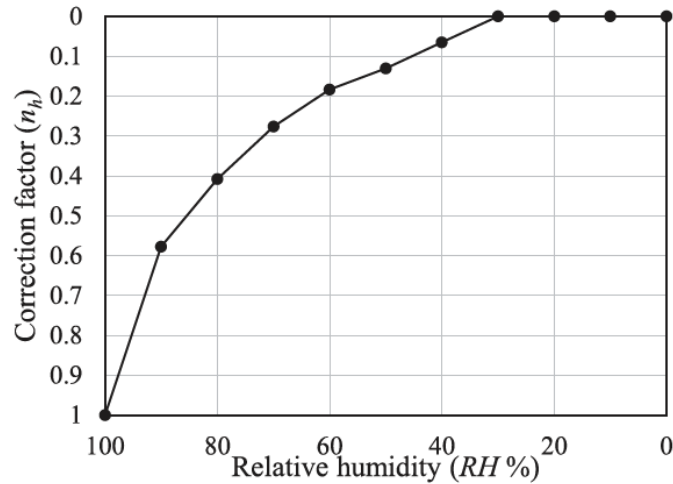


Figure 4. Relationship between the correction factor, n_H , and relative humidity for GFRP bars (Benmokrane et al., 2020).

In Equation (9), DL is the service life in years; and TSF is the time-shift factor for temperature T and temperature T_1 which can be calculated based on the approach proposed by Dejke and Tepfers (2001) as expressed in Equation (10).

$$TSF = e^{\frac{B}{T_1+273.15} - \frac{B}{T+273.15}} \quad (10)$$

where B is a constant determined using the time shift of two known curves; Δ_1 is tensile-strength reduction after t_1 experimental exposure at T_1 ($^{\circ}C$); Δ_2 is the tensile-strength reduction between t_1 experimental exposure and design life (t_D) at T_1 ; Δ_3 is the additional tensile-strength reduction due to effects of elevated temperature at T ($^{\circ}C$) under design lifetime exposure (Benmokrane et al., 2020).

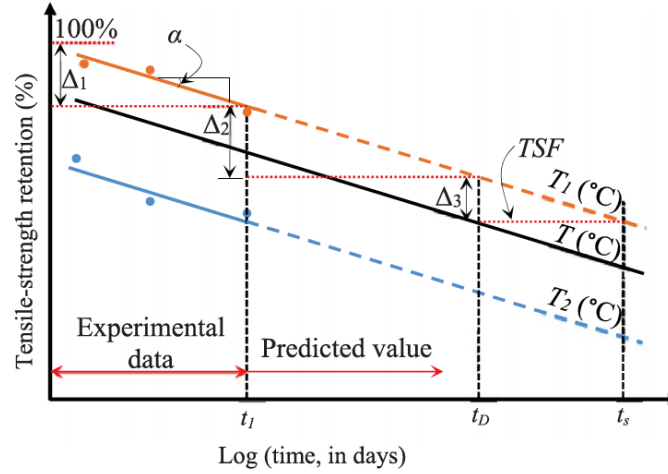


Figure 5. Illustration of the prediction method for calculating tensile-strength retention factor for GFRP bars, C_E , (Benmokrane et al., 2020).

2.5.4 Life Prediction Approach Using Time-Variant Capacity of GFRP Bars Embedded in Concrete

Trejo et al. (2009) proposed a probabilistic time-variant parameter to predict the tensile strength of GFRP bars embedded in concrete at a given time, σ_t , expressed in Equation (11). The basis of this method uses Arrhenius relation with a set of experimental data and error terms to account for uncertainty in the prediction, while accounting for physical terms such as temperature, relative humidity, and radius of GFRP bars (Kim et al., 2012).

$$\sigma_t(x_b, \Theta_\sigma) = \left\{ (1 + s_0 \cdot e_0) - \lambda_1 \left[\frac{D_{T,23} \cdot \exp \left[\frac{E_a}{R_g} \left(\frac{1}{T_{23}} - \frac{1}{T} \right) \right] \cdot t}{r^2} \right]^\alpha (1 + s_1 \cdot e_1) \right\} \cdot \mu_{\sigma_0} \quad (11)$$

where $x_b(D_{T,23}, E_a, R_g, r, T)$ is a vector of basic variables (i.e., material properties geometry, and temperature); $D_{T,23}$ is the diffusion coefficient at a defined reference temperature; $T_{23} = 296$ K[23°C (73°F)], E_a is the activation energy (KJ); R_g is the universal gas constant (KJ/mol-K); r

CHAPTER 2: LITERATURE REVIEW

is the radius of GFRP reinforcement; T is exposure temperature (in K); $s_0 \cdot e_0$ is the error term that captures the variability of s_0 around its mean μ_{s0} ; and $s_1 \cdot e_1$ is the error term that captures the variability in the reduction term $\lambda_1 \{D_{T,23} \cdot \exp[E_a/R_g \cdot (1/T_{23} - 1/T)] \cdot t/r^2\}^\alpha$

The terms e_0 and e_1 are statistically independent identically distributed random variables with zero mean and unit variance, s_0 and s_1 are the standard deviation of the two error terms, and $\Theta_\sigma = (\lambda_1, \alpha, s_0, s_1)$ is a vector of unknown parameters introduced to fit the data whose posterior statistics can be found in Table 1 of Kim et al. (2012) to solve Equation (11).

In this approach, the stress-strain model of concrete used is with the parabolic stress-strain relationship developed by Todeschini et al. (1964) as expressed in Equation (12).

$$f_{cm}(\varepsilon) = \frac{1.8 \cdot f_{cm} \cdot (\varepsilon_{cm}/\varepsilon_{cc})}{1 + (\varepsilon_{cm}/\varepsilon_{cc})^2} \quad (12)$$

where $f_{cm}(\varepsilon)$ is the compressive stress at the compressive strain ε_{cm} [MPa] (ε_{cm} ranges from zero to the ultimate compressive strain, ε_{cu} , (herein 0.0035)); f_{cm} is the measured compressive strength [MPa]; ε_{cc} is the peak strain computed as $1.7f_{cm}/E_c$; and E_c is the modulus of elasticity of the concrete [MPa] computed using Equation (13) (Kim et al., 2012).

$$\ln(E_c) = \theta_1 + \theta_2 \cdot \ln(f_{cm}) + \theta_3 \cdot \ln(w) + s_E \cdot e_E \quad (13)$$

where w is the unit weight of concrete; $s_E \cdot e_E$ is the model error; s_E is the standard deviation of the model error; e_E is a normally distributed random variable with zero mean and unit variance; and $\Theta_E(\theta_1, \theta_2, \theta_3, s_E)$ is a vector of unknown parameters introduced to fit the data, whose posterior statistics can be found in Table 2 of Kim et al. (2012). Note that this method does not consider the deterioration of concrete over time, which could influence the concrete crushing capacity (Kim et al., 2012).

CHAPTER 2: LITERATURE REVIEW

The moment capacity of the bridge deck can be calculated using the time-variant bar capacity model, the dominant failure mode (concrete crushing failure vs GFRP bar failure), the mechanical properties of the concrete deck, the strain compatibility and moment and force equilibrium (Kim et al., 2012). Figure 6 shows the two possible failure modes: (a) crushing of concrete (i.e., compression-controlled failure); and (b) tensile rupture of the GFRP bar (tension-controlled failure). Figure 6 also shows the strain compatibility in the cross-sectional analysis. The moment capacity of the bridge deck at any time, t , is then calculated using Equation (14).

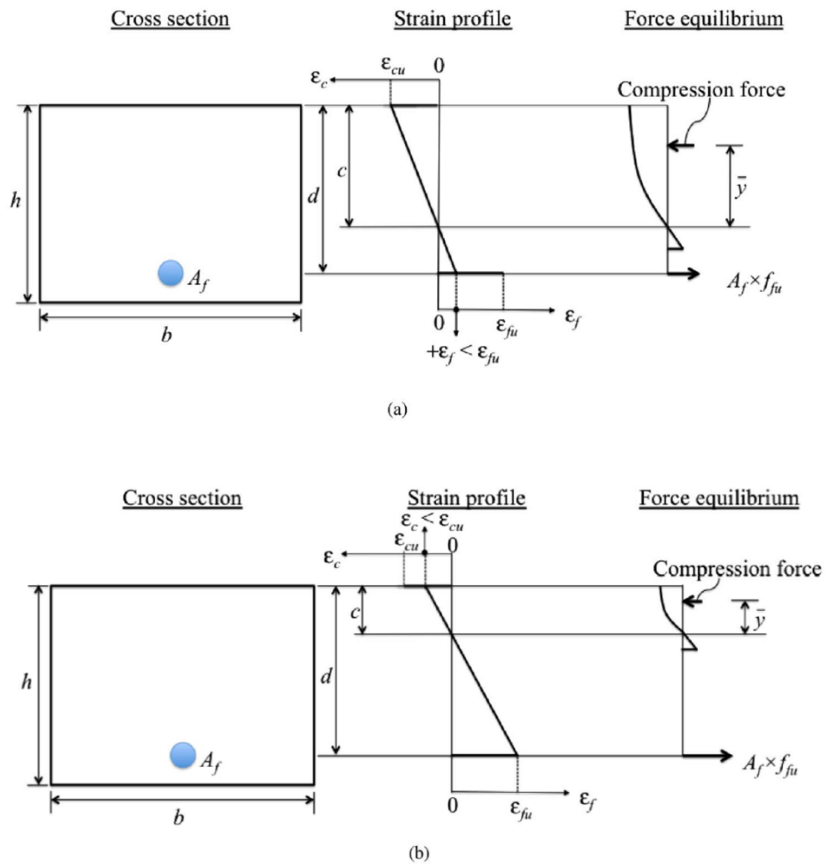


Figure 6. Failure modes of GFRP-reinforced bridge deck: (a) concrete crushing failure; and (b) GFRP bar failure (Kim et al., 2012).

$$C_t(x, \Theta) = \min[C_{CF,t}(x, \Theta), C_{BF,t}(x, \Theta)] \quad (14)$$

where $C_{CF,t}$ is the nominal moment capacity of the deck when the concrete crushing failure occurs at time, t ; $C_{BF,t}$ is the nominal moment capacity of the deck when the GFRP bar rupture occurs at time, t , $\Theta = (\Theta_\sigma, \Theta_E)$, and $x = (x_b, x_d)$, where $x_d(f_{cm}, E_c, \varepsilon_{cu}, b, h, d, A_{frp}, r, \sigma_{t(i)}, E_{frp}, \varepsilon_f, n_b)$ is a vector that includes design and mechanical properties of the deck; b is the width of the cross-section [mm]; h is depth of the section [mm]; d is the distance from the extreme compression fibre to the centroid of tension reinforcement [mm]; A_{frp} is the area of the GFRP reinforcement in the given section [mm²]; $\sigma_{t(i)}$ is the capacity of the i th GFRP bar at time t (years) determined using Equation (11); ε_f is the strain of the GFRP reinforcement at the concrete crushing strain in the top fibre, ε_{cu} ; and n_b is the number of GFRP bars in the given section (Kim et al., 2012).

The nominal moment capacity is then calculated using Equation (15).

$$C_t = A_{frp} E_{frp} \varepsilon_f (d - c + \bar{y}) \quad (15)$$

where c is distance measured from the top extreme fibre to the neutral axis; \bar{y} is the distance from the neutral axis to the location of the resultant compression force; and ε_f is the strain in the GFRP reinforcement when the concrete strain reaches crushing failure.

2.5.5 Performance of GFRP-Reinforced Concrete Beams Under Sustained Load and Natural Aging

Esmaili et al. (2020) performed lab testing on load sustained GFRP-reinforced beams that were exposed to natural aging in Nova Scotia as opposed to accelerated aging. The objective was to compare the flexural behaviour of the conditioned beams under the combined effect of natural

CHAPTER 2: LITERATURE REVIEW

weathering and sustained loads with the flexural behaviour of unconditioned beams. Eight beams were cast where four beams were conditioned for 10 years (exposed to the environment) and the remaining four were unconditioned (cured in a lab environment). Figure 7 shows the schematics of the test specimens.

The conditioned beams were subjected to high sustained bending stress (40% of the ultimate tensile strength of the GFRP bars) applied by a tensioned steel frame as shown in Figure 8 and left in aggressive natural weathering conditions in Halifax for 10 years as shown in Figure 9. The conditioning included freeze-thaw and wet-dry cycles and temperatures varying from -25°C to 35°C . The unconditioned beams were stored in a standard laboratory condition (i.e., at $23^{\circ}\text{C} - 24^{\circ}\text{C}$ and 50% relative humidity) with three of the beams tested till failure using a four-point bending setup after a year of curing (Esmaeili et al., 2020).

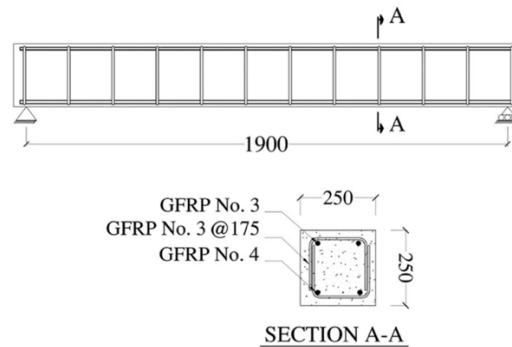


Figure 7. Geometric and reinforcement details of beams tested by Esmaeili et al. (2020) (dimensions are in millimeters).

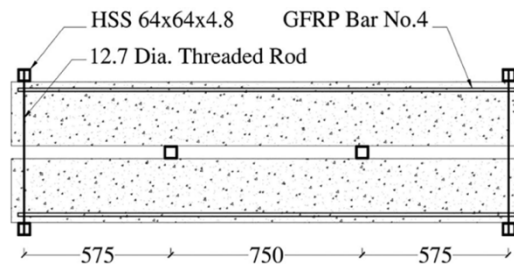


Figure 8. Apparatus used to apply sustained load of beams tested by Esmaeili et al. (2020) (dimensions are in millimeters).

CHAPTER 2: LITERATURE REVIEW



Figure 9. Photos of beams tested by Esmaeili et al. (2020): (a) beams under the sustained load and natural weather conditioning (December 2008); (b) beams under the sustained load and natural weather conditioning (October 2009); (c) number of cracks formed along the length of a conditioned beam; and (d) a close-up photo of a crack. (Images by John Newhook).

CHAPTER 2: LITERATURE REVIEW

After 10 years of exposure, three of the conditioned beams were tested till failure using a four-point bending setup. The stiffness, ultimate flexural strength, and deflection at the ultimate for all tested beams were recorded and summarized in Table 1. On average, the ultimate strength for the conditioned beams was 19% lower than the conditioned beams (Esmaeili et al., 2020).

Table 1. Flexural response of GFRP-reinforced beams before and after conditioning in Nova Scotia (Esmaeili et al., 2020).

Beam No.	Ultimate deflection (mm)		Ultimate strength (kN-m)		Stiffness (kN-m/m)	
	Uncond.	Cond.	Uncond.	Cond.	Uncond.	Cond.
1	37.8	32.0	33.8	27.2	771.0	661.0
2	43.2	35.6	35.1	29.4	648.6	655.7
3	39.4	31.2	34.3	26.5	885.2	666.0
Average	40.2	33.3	34.4	27.7	780.2	660.9
Stand. Dev.	2.1	2.1	0.7	1.5	100.6	5.2
COV	5.2%	6.3%	1.9%	5.4%	12.9%	0.8%

Note: COV is the coefficient of variation

2.5.6 Creep Rupture and Long-Term Performance of GFRP bars Under Sustained Load

Esmaeili et al. (2021) presented results from a series of lab tests to assess the creep-rupture strength of GFRP bars subjected to severe environmental exposure throughout a comprehensive experimental investigation. A total of 160 GFRP bars of various sizes and types were tested in the study by Esmaeili et al. (2021) under different conditioning types and a wide range of imposed sustained stress levels. There were three bar sizes used in the tests: #3, #4, and #5 bars (10, 13, 16 mm, respectively), with two types of #5 GFRP bars used. Type A was sand coated with helically wrapped surface, and Type B was helically grooved as shown in Figure 10.



Figure 10. GFRP bars used for creep-rupture tests by Esmaeili et al. (2021).

There were three exposure conditions: (a) Group A, which consisted of 70 bars bearing sustained load without environmental conditioning, (b) Group B, which consisted of 60 bars subjected to sustained load and exposed to alkaline solution at ambient temperature (23°C), and (c) Group C, which consisted of 30 bars subjected to sustained load and exposed to alkaline solution and a temperature of 60 °C. The sustained loads applied on the bars varied between 40% and 90% of the average UTS of the bars until failure as shown in Table 2 (Esmaeili et al., 2021).

Esmaeili et al. (2021) adopted a Weibull distribution for the time-to-failure to account for the high variability in the test results while a normal distribution was adopted for the variability of GFRP ultimate tensile strength at time zero as shown in Figure 11. Note that in Figure 11, $F_{u,m}$ is the average ultimate tensile strength at time zero, $F_{u,k}$ is the characteristic tensile strength, and F_u^* is the guaranteed tensile strength.

CHAPTER 2: LITERATURE REVIEW

Table 2. Loading and environmental conditioning of GFRP bars tested for creep rupture by Esmaeili et al. (2021).

Group	Bar size	Loading level (% of UTS)	Exposure Medium	Temperature
A	#3	40, 60, 70, 80, and 90	-	Ambient temperature (23 °C)
	#4	60, 70, and 90		
	#5A	60, 80, and 90		
	#5B	60, 80, and 90		
B	#3	50, 60, and 70	Alkaline solution (pH ≥ 12.5)	Ambient temperature (23 °C)
	#4	40, 50, and 70		
	#5A	40, 50, and 70		
	#5B	40, 50, and 70		
C	#4	50, 60, and 70	Alkaline solution (pH ≥ 12.5)	High temperature (60 °C)
	#5A	40, 50, and 60		

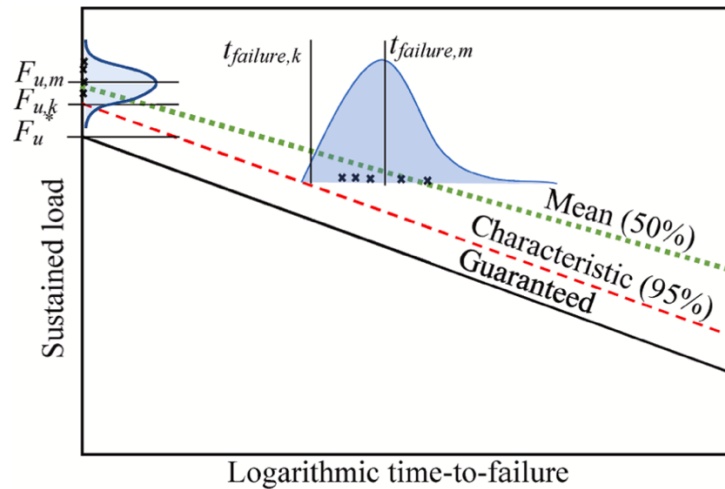


Figure 11. Creep-rupture curves of GFRP bars by Esmaeili et al. (2021).

2.6 RELIABILITY ANALYSIS OF GFRP-REINFORCED BRIDGE DECKS

Extensive research examined the reliability of steel reinforced bridge decks (Stewart and Rosowsky, 1998; Ghodoosi et al., 2015; Lounis and Daigle, 2008), but very limited work assessed the time-dependent reliability and capacity of bridge decks reinforced with GFRP bars. Assessing the time-dependent reliability of GFRP reinforced bridge decks is critically needed since literature indicate an evident reduction in tensile capacity of GFRP bars embedded in concrete due to moisture and ASR.

Kim et al. (2012) assessed the time-variant structural reliability of a typical bridge deck reinforced with GFRP bars using the time-variant probabilistic model developed by Trejo et al. (2009). The model uses a time-variant capacity of GFRP bars embedded in concrete and the reliability of GFRP-reinforced bridge decks is expressed using fragility curves. According to Gardoni et al. (2002), fragility is defined as the conditional probability of attaining or exceeding prescribed limit states for a given set of boundary variables. The limit state function $g(\cdot)$ is introduced such that the event of $[g(\cdot) \leq 0]$ denotes not meeting a specified performance level for a given moment demand, D (Kim et al., 2012). Therefore, the probabilistic model for the time-variant capacity of a GFRP-reinforced deck shown in Equation (14) is used to describe the performance function, g_t , and the fragility, F_t , at any time t in Equations (16) and (17) respectively.

$$g_t(x, \Theta) = C_t(x, \Theta) - D \quad (16)$$

$$F_t(D, \Theta) = P[g_t(x, \Theta) \leq 0 | D] \quad (17)$$

CHAPTER 2: LITERATURE REVIEW

Although the fragility approach for estimating the reliability of GFRP-reinforced bridge decks used by Kim et al. (2012) is applicable, it only considered applications to interior deck section subjected to positive flexural moment. This method also does not directly account for the damage to the concrete due to freeze-thaw effect, the effect of variation in the concrete cover over the deck surface, the variation in the traffic loads, and is also based on data that are not directly calibrated for NS. This presents an opportunity for finding an alternative approach to solving the time-dependent reliability problem for GFRP-reinforced bridge decks and to also tailor the solution to tackle issues faced in the NS environment.

CHAPTER 3 FRAMEWORK OF THE TIME-DEPENDENT RELIABILITY ANALYSIS

3.1 INTRODUCTION

This chapter presents the development of a robust time-dependent reliability analysis of concrete bridge decks reinforced using GFRP by considering the time-dependent environmental degradation in resistance and the time-dependent changes in load effects (Phase I of the project scope as discussed in Section 1.2). The input statistical parameters used in the reliability model were carefully selected to fit the conditions experienced in NS. The framework for the time-dependent reliability analysis involved defining the limit state criterion for the analysis, collecting model and statistical parameters for both time-dependent and time-independent random variables, and developing a MATLAB[®] code to solve the reliability analysis using Monte Carlo (MC) simulation.

3.2 ULTIMATE LIMIT STATE (ULS) FOR BRIDGE DECKS

The limit state function (LSF) used in the time-dependent reliability analysis relates to the ULS of a bridge deck subjected to bending as expressed in Equation (18). The difference between the factored bending moment demand, $M_f(t)$, expressed in Equation (19) and the factored bending moment of resistance, $M_r(t)$, expressed in Equation (20) shall be greater than or equal to zero to consider the bridge deck safe, where (t) signifies that the parameters are time dependent. The symbol (t) may be dropped in some equations for clarity purposes.

$M_r(t)$ is expressed as a function of two time-dependent damage parameters with mean values ranging from zero to unity, where zero describes damage-free capacity to account for the

degradation in the section capacity with time: time-dependent GFRP damage parameter, $\psi_{frp,d}(t)$, and time-dependent concrete-related damage parameter, $\psi_{fc,d}(t)$. The LSF reduces to the ULS specified in CSA S6:19 at time t equal zero because $\psi_{frp,d}(t)$ and $\psi_{fc,d}(t)$ would equal zero upon the complete construction of the bridge deck.

$$M_r(t) - M_f(t) \geq 0 \quad (18)$$

$$M_f(t) = \alpha_{D_{sw}} M_{D_{sw}} + \alpha_{D_{ws}} M_{D_{ws}} + \alpha_L M_L(t)(1 + DLA) \quad (19)$$

$$M_r(t) = \phi_{frp} (1 - \psi_{frp,d}(t)) f_{frp} A_{frp} \left[d - \frac{\phi_{frp} (1 - \psi_{frp,d}(t)) f_{frp} A_{frp}}{2b\alpha_1\phi_c (1 - \psi_{c,d}(t)) f'_c} \right] \quad (20)$$

where $\alpha_{D_{sw}}$ is the dead load factor for self-weight; $\alpha_{D_{ws}}$ is the dead load factor for wearing surface; α_L is the live load factor; DLA is the dynamic load allowance; $M_{D_{sw}}$ is the dead load moment due to self-weight; $M_{D_{ws}}$ is the dead load moment due to wearing surface; $M_L(t)$ is the live load moment; ϕ_{frp} is the FRP material resistance factor (0.65); ϕ_c is the concrete resistance factor (0.75); f_{frp} is the FRP tensile strength; f'_c is the concrete compressive strength; A_{frp} is the tension FRP reinforcement cross-sectional area; d is the distance measured from the extreme compression fiber to the centroid of the tension reinforcement; b is the width of the concrete section; and $\alpha_1 = 0.85 - 0.0015f'_c \geq 0.67$ according to Clause 8.8.3 of CSA S6:19 (2019).

There are two failure modes for GFRP-reinforced sections designed for flexure as discussed in Section 2.5.4: tension-controlled (FRP rupture) failure mode; and compression-controlled (concrete crushing) failure mode. CSA S6:19 permits the design of sections using either failure mode but Clause 16.8.2.2 of CSA S6:19 states that if the ULS design of the section is governed by FRP rupture, M_r shall be greater than $1.5M_f$. This 1.5 factor was not considered in the reliability analysis in this project as the reliability index for tension-controlled sections with the 1.5 factor

would be far greater than the minimum acceptable target reliability index, which is proven and discussed in the time-dependent reliability analyses performed in Chapter 4.

3.3 MODELS AND STATISTICAL PARAMETERS OF RANDOM VARIABLES

Fifteen random variables were considered in the reliability analysis. The random variables were divided into three categories: loads, resistance, and methods of structural analysis. The variables and their corresponding distribution type, bias ratio (predicted-to-specified), λ , and coefficient of variation, V , are summarised in Table 3. The load and resistance mathematical models and their corresponding statistical parameters were primarily based on measurements taken in NS. The random variables are discussed in detail in the following subsections.

Table 3. Input statistical properties of the random variables for the reliability analysis.

Category	Variable	Definition	Distribution	λ	V	Reference
Loads	$M_L(t)$	Live load moment	Gumbel	Eq. (26)/ Eq. (28)	Eq. (27)/ Eq. (26)	This study
	$M_{D_{sw}}$	Dead load moment due to concrete deck self-weight	Normal	1.068	0.014	Kennedy et al. (1992)
	$M_{D_{ws}}$	Dead load moment due to wear surface self-weight	Normal	1.437	0.532	Kennedy et al. (1992)
	DLA	Dynamic load allowance	Normal	1.186	0.301	This Study
	x_{LL}	Model error in live load analysis	Normal	1.000	0.150	Slobbe et al. (2020)
Resistance	f'_c	Concrete compressive strength	Lognormal	Eq. (30)	0.100	Nowak and Szerszen (2003)
	$f_{frp}(t)$	Time-dependent GFRP tensile capacity	Normal	Eq. (32)	Eq. (33)	This study
	E_{frp}	FRP modulus of elasticity	Normal	1.000	0.068	Shield et al. (2011)
	d_c	Concrete cover thickness	Truncated Lognormal	0.962	0.045	This Study
	$x_{FT,N}$	Model uncertainty in predicting number of freeze-thaw cycles	Normal	1.000	0.1500	Oudah (2022)
	$x_{FT,NA}$	Model variance in field measured freeze-thaw cycles	Normal	1.000	0.1733	Oudah (2022)

Category	Variable	Definition	Distribution	λ	V	Reference
	$x_{FT,f}(t)$	Model uncertainty in predicting concrete strength damage parameter	Normal	1.000	0.0911	Oudah (2022)
	$x_{FT,Ec}(t)$	Model uncertainty in predicting static concrete modulus of elasticity	Normal	1.000	0.0593	Oudah (2022)
Methods of Structural Analysis	x_{FE}	Model error in FE analysis of live loads	Normal	1.100	0.120	Castaldo et al. (2019)
	PF	Model error in simplified analysis of structural resistance (i.e., Professional factor)	Normal	1.020	0.060	Nowak and Szerszen (2003)

3.3.1 Load Model

The load model consists of five random variables comprising of the time-dependent live load moment, $M_L(t)$, dead load moment due to concrete deck self-weight, $M_{D_{sw}}$, dead load moment due to wear surface self-weight, $M_{D_{ws}}$, dynamic load allowance, DLA , and model error in live load analysis, x_{LL} . The approach to obtain the statistical parameters for each of the five random variables is explained in the following subsections.

3.3.1.1 Live load moment, $M_L(t)$

The analysis to determine $M_L(t)$ is detailed in this section. The discussion is broken into three sequential parts presented in the following paragraphs: Statistical analysis of weigh-in-motion live load data, finite element analysis of live load moment on bridge decks, and statistical analysis of live load moments on bridge decks.

Statistical Analysis of Weigh-In-Motion Live Load Data

To obtain the statistical parameters for the time-dependent live load moment intensity on bridge decks, a comprehensive statistical analysis was performed on a year's worth of live load data (from

CHAPTER 3: FRAMEWORK OF RELIABILITY ANALYSIS

September 2019 to September 2020), obtained from a weigh-in-motion (WIM) truck scale in Enfield, NS. A representative finite element (FE) analysis was developed to correlate between the wheel loads of the WIM trucks loads and its load effect on bridge decks. The established load effects were extrapolated for longer return periods since only a year of WIM data was used. The purpose of the statistical analysis was to establish a distribution type and the values of λ and V for $M_L(t)$, on bridge decks in NS. The value of λ is found by dividing the maximum moment demand from the WIM traffic loads to the maximum live load moment demand calculated in accordance with CSA S6:19. The details pertaining to the analysis of the WIM, FE analysis, and determining the statistical parameters are described in the following paragraphs.

The obtained WIM data consisted of vehicles from Class 1 to Class 13 following the category classification defined in the “Traffic Monitoring Guide” by the Federal Highway Administration (FHWA, 2014) as shown in Figure 12. The data was categorized into sections such as, gross vehicle weight (GVW), number of axles, axle weights, and distance between axles. Class 13 vehicles recorded the highest gross vehicle weights and axle weights, with approximately 33,300 vehicles. Figure 13 shows a histogram of the gross vehicle weights of Class 13 vehicles in kilonewtons (kN), which show three peaks. It was recognized that the three peaks show the weight distribution of unloaded trucks, partially-loaded trucks, and fully-loaded trucks (Schmidt et al., 2016). Histograms of the axle loads were also plotted and analyzed.

A Gaussian Mixture Model (GMM) distribution was used to fit normal distributions to each of the peaks and obtain the mean and standard deviation for each peak. The third axle (Axle 3) of Class 13 vehicles had the highest mean axle load for fully-loaded trucks with a mean of 89 kN and standard deviation of 5.69 kN as seen in Figure 14. Since the live load moment intensity on bridge

CHAPTER 3: FRAMEWORK OF RELIABILITY ANALYSIS

decks according to CSA S6:19 uses wheel loads of the CL-625 design truck, the wheel loads were used in the statistical analyses as half the axle loads.



























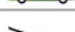







Class 1 Motorcycles		Class 7 Four or more axle, single unit	
Class 2 Passenger cars		Class 8 Four or less axle, single trailer	
			
			
			
Class 3 Four tire, single unit		Class 9 5-Axle tractor semitrailer	
			
			
Class 4 Buses		Class 10 Six or more axle, single trailer	
			
		Class 11 Five or less axle, multi trailer	
Class 5 Two axle, six tire, single unit		Class 12 Six axle, multi-trailer	
			
		Class 13 Seven or more axle, multi-trailer	
			
			
			

Figure 12. FHWA vehicle category classification (FHWA, 2014).

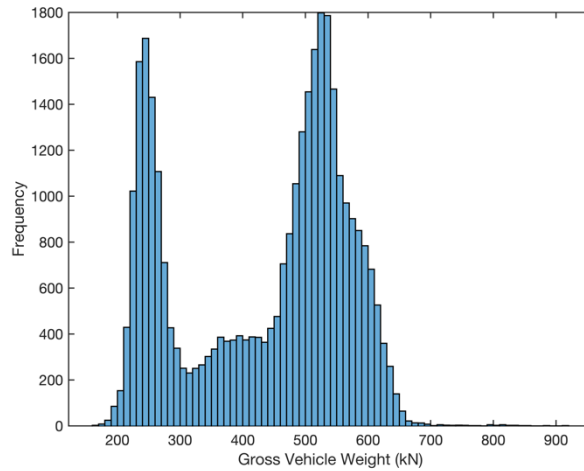


Figure 13. Histogram of gross vehicle weights (GVW) of Class 13 vehicles in NS.

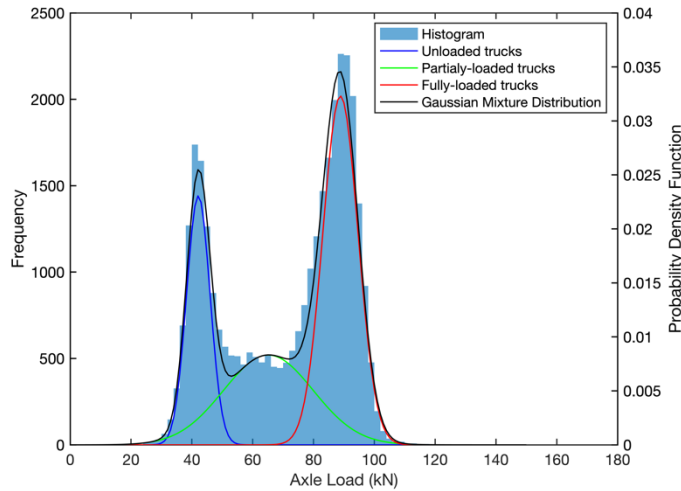


Figure 14. Probability density functions (PDFs) and histograms for Axle 3 of Class 13 vehicles in NS.

Finite Element Analysis of Live Load Moment on Bridge Decks

A finite element (FE) analysis model was developed using SAP2000® to determine the moment demand induced in the bridge deck due to the obtained peak wheel loads. The bridge configuration chosen for the model was based on a real-life bridge deck in NS that represents the typical design practice in the province. The bridge was single-span with a span length of 36 meters from the north

CHAPTER 3: FRAMEWORK OF RELIABILITY ANALYSIS

abutment bearing point to the south abutment bearing point, with a 12.71-meter deck width, a deck concrete compressive strength of 45 MPa, and a 225 mm thick GFRP-reinforced concrete deck resting on four New England Bulb Tee (NEBT) girders. A cross-section of the bridge deck is shown in Figure 15.

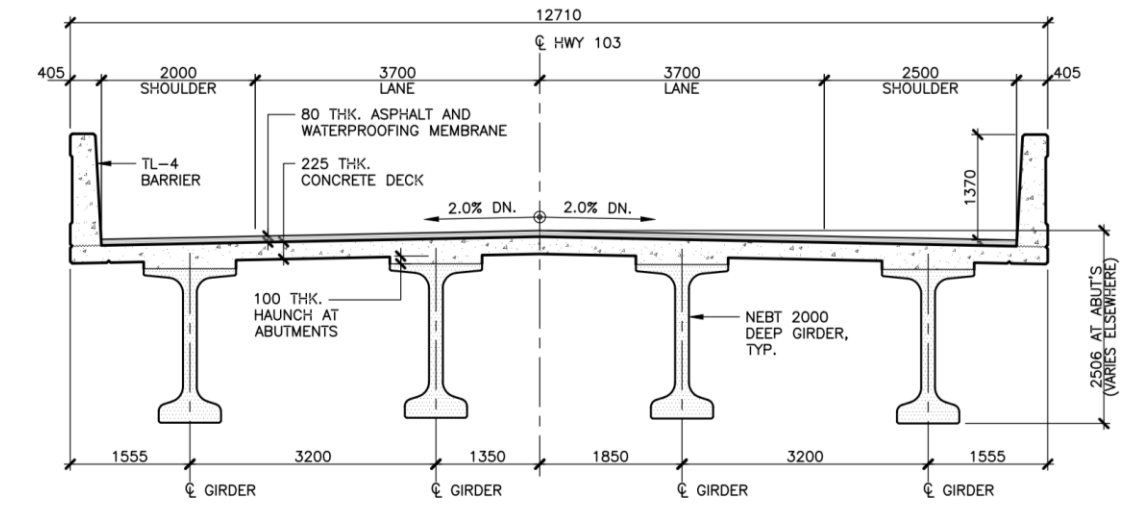


Figure 15. Cross-section of bridge analysed using finite element (FE) extracted from bridge drawings provided by NS-PW (all dimensions in millimeters).

The bridge deck was modelled using 2D thin-shell elements and concrete NEBT girders which were modelled as beam elements. Composite-bending behaviour was considered between the deck and the girders using fixed link elements (links restrained from translating and rotating in all directions). The shell elements representing the deck were approximately 0.25 m by 0.25 m in size with an aspect ratio of 1. Although the abutments were not modelled, the boundary conditions were assumed to be pinned (restrained from translation in all directions) on one end of the girders, and as rollers (restrained from translation in the z -direction only) on the other end. The isometric view and extruded cross-section of the bridge model are shown in Figure 16 and Figure 17 respectively.

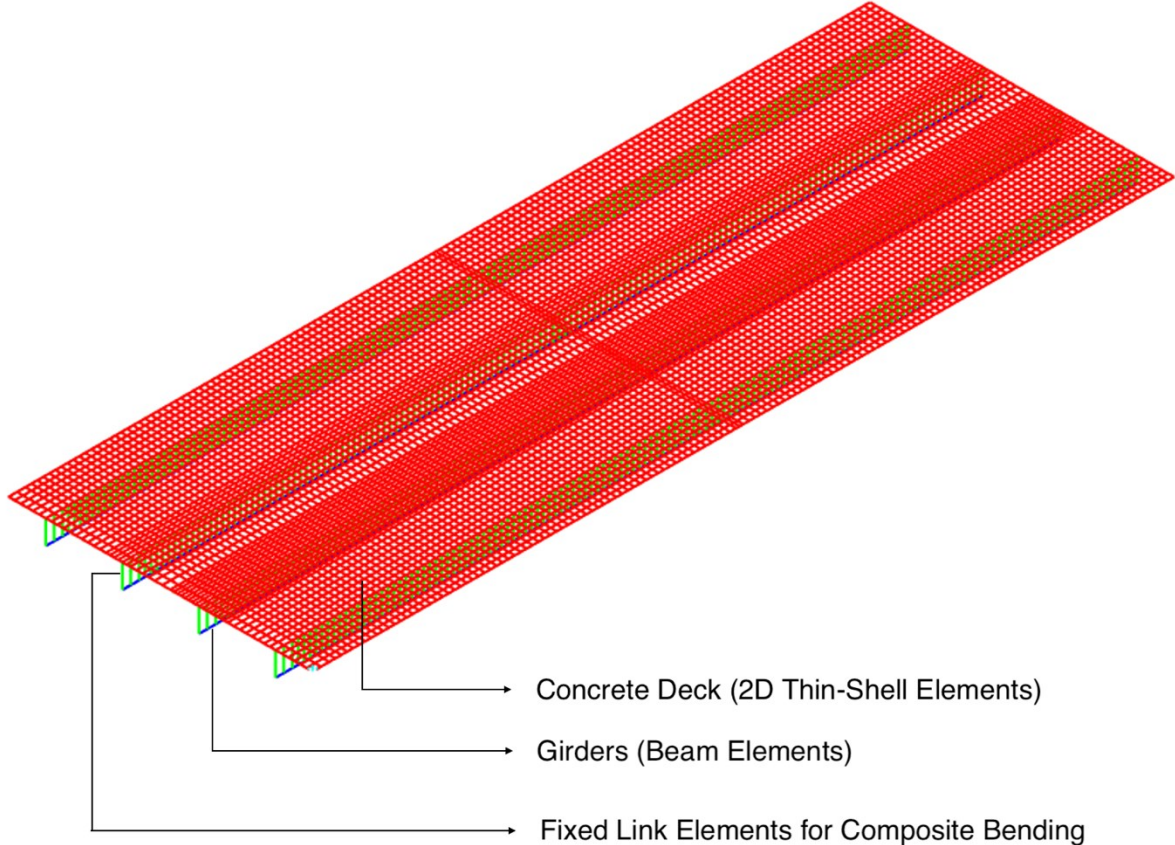


Figure 16. Isometric view of the bridge FE model.

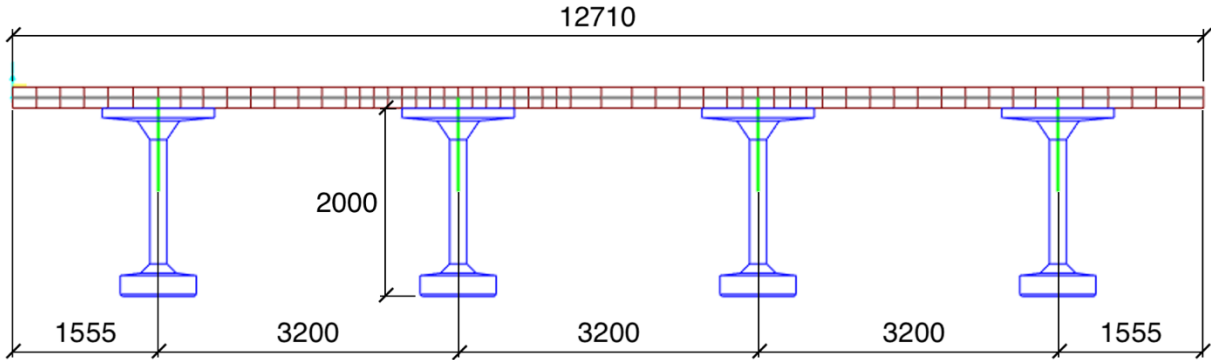


Figure 17. Extruded cross-section view of the bridge FE model (all dimensions in millimeters).

CHAPTER 3: FRAMEWORK OF RELIABILITY ANALYSIS

The following assumptions were used in developing the FE model:

- Linear-elastic response of the bridge deck (i.e., material, and geometric nonlinearities were not considered). This is an acceptable assumption since the bridge deck response under working loads is elastic
- The contribution of the barriers to the stiffness of the bridge deck was not considered as well as the live load effects from the barriers.
- The effect of abutment on M_L induced in the bridge deck was not considered. This is an acceptable assumption since the maximum value of M_L was found to occur at mid-span where the effect of the boundary condition diminishes.

The loading consisted of two-wheel loads each applied on a 0.25 m by 0.60 m area on the surface of the deck spaced 1.8 m apart (center-to-center) in the transverse direction, with a load magnitude of 1 kN each. This loading geometry represents the wheel dimensions and the spacing configuration of axle 4 of the CL-625 vehicle in CSA S6:19. The load was applied at the bridge mid-span to obtain results around the region furthest from both supports (abutments). Several loading positions along the transverse direction of the deck were selected and checked. The loading positions checked include one wheel load placed directly between two of the interior girders, both wheel loads straddling an interior girder, and one of the wheels at a defined distance from the edge of the interior girders.

A parametric analysis was conducted to examine the impact of the bridge deck design parameters and the mesh density of the FE model on the magnitude and distribution of M_L . The parametric analysis considered varying three parameters: loading condition, deck mesh size, and girder spacing as shown in Table 4. Although the thickness of the concrete deck affects the

CHAPTER 3: FRAMEWORK OF RELIABILITY ANALYSIS

distribution of the transverse moment across the length of the deck, the parametric analysis did not account for the variation in the deck thickness since the typical deck thickness in the NS is 225 mm. The parametric analysis was focused on varying the influential parameters regarding the response of the model and was bounded by practical range of values. The positive and negative transverse moments on the deck were obtained and compared.

Table 4. Model descriptions for finite element model sensitivity analysis.

Model #	Loading Condition	Deck Mesh Size (m x m)	Girder Spacing (m)
1	Wheel loads straddling interior girder	0.25 x 0.25	3.2
2	Wheel loads straddling interior girder	0.125 x 0.125	3.2
3	Wheel loads straddling interior girder	0.5 x 0.5	3.2
4	One wheel mid-distance between interior girders and other wheel 1.8 m away	0.25 x 0.25	3.2
5	One wheel 0.6 m from an interior girder and another wheel 1.8 m away	0.25 x 0.25	3.2
6	Wheel loads straddling interior girder	0.25 x 0.25	2.5
7	Wheel loads straddling interior girder	0.25 x 0.25	3.0
8	Wheel loads straddling interior girder	0.25 x 0.25	3.5

The maximum positive and negative transverse moments on the deck were obtained at the nodes after the sensitivity analysis was completed and the results were compiled into a spreadsheet where they were plotted against the longitudinal distance along the bridge as shown in Figure 18, for 3.5 m (most sensitive region) of the decks measure from the point of axle load application. The plots are symmetrical about point “0 m” due to symmetry in deck geometry and loading about the middle of the deck. The results for Model 4 shown in Figure 18b for the negative transverse moment indicates reduced moment when one of the wheels is acting on the girder.

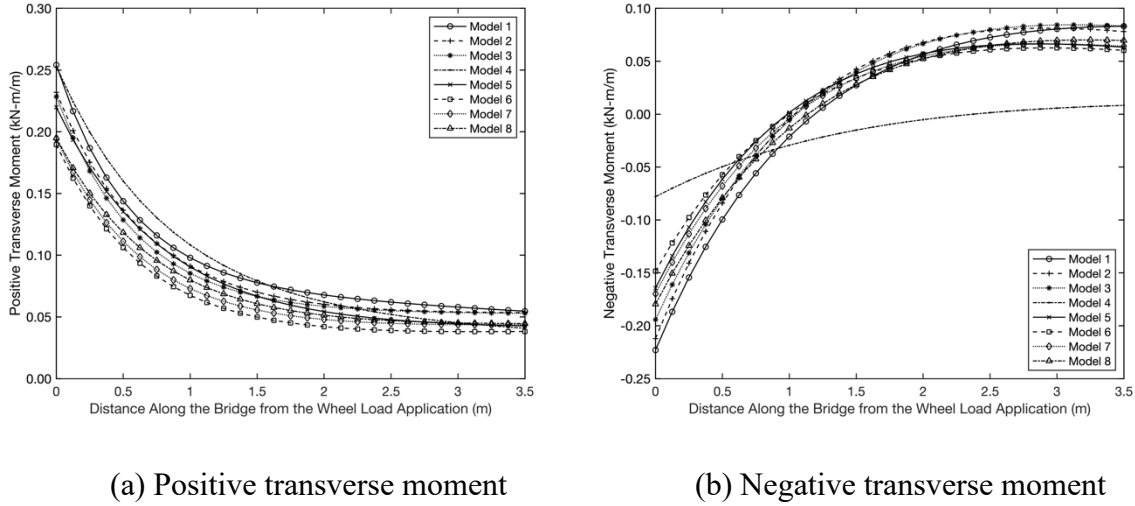


Figure 18. Sensitivity analysis results for positive and negative transverse moments on bridge deck FE model.

Figure 19a shows the maximum positive transverse moment on the bridge deck which occurs in Model 4, when the load is applied by one wheel positioned mid-distance between interior girders and another wheel 1.8 m away, as defined in Table 4. The positive transverse moment has its peak at the location of the loading and tapers off to zero towards the abutments. Figure 19b shows maximum negative transverse moment on the bridge deck which occurs in Model 1, when the wheel loads are straddling an interior girder, as defined in Table 4. A regression analysis was performed and Equations (21) and (22) were proposed to estimate the maximum positive, M_T^+ , and negative, M_T^- , transverse moments on the bridge deck respectively.

$$M_T^+ = P_W(0.1952 \exp(-1.232x) + 0.05791 \exp(-0.1191x)) \quad (21)$$

$$M_T^- = P_W(-0.419 \exp(-0.8098x) + 0.196 \exp(-0.1708x)) \quad (22)$$

where P_W is the wheel load in kN; and x is the distance along the bridge.

CHAPTER 3: FRAMEWORK OF RELIABILITY ANALYSIS

The negative transverse moment has its peak negative value at the loading point and transitions into a positive value and back towards zero at 18 m (i.e., the abutment). This behaviour is supported by the results of the experimental work by Shafei et al. (2020). The strain profiles shown for the top and bottom of the deck tested in Shafei et. al. (2020), are similar to the negative and positive moment profile found in this study.

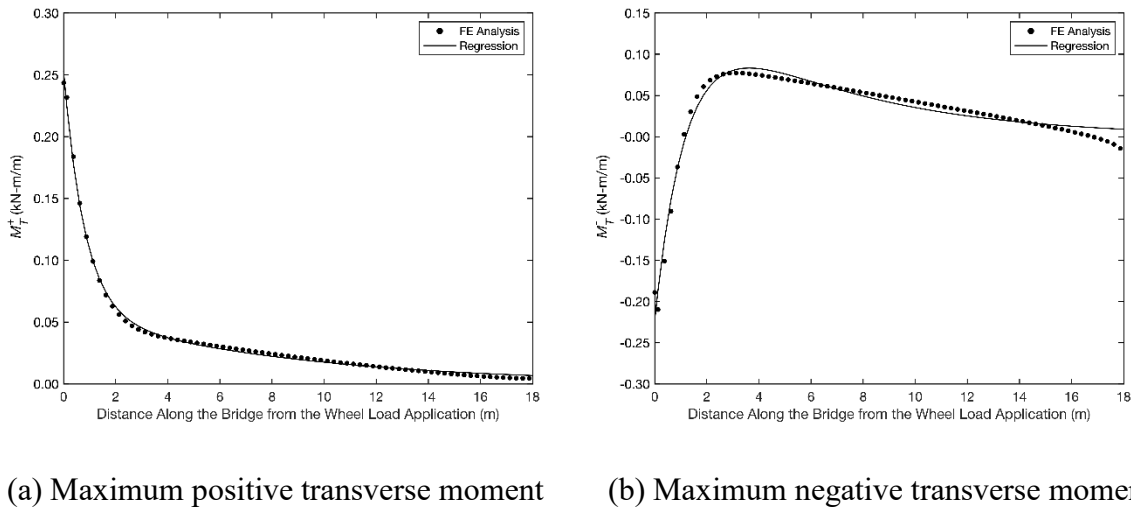


Figure 19. Maximum positive transverse moments along the span of the bridge deck FE model.

After performing the FE analyses, Equations (21) and (22) were applied to the wheel loads of the WIM Class 13 vehicles to obtain the positive and negative transverse moments on the deck. Unlike the CSA S6:19 which uses only the maximum wheel load of the CL-625 Truck to calculate the transverse moments, the influence from adjacent axle loads were accounted for where applicable by using Equations (21) and (22). For most Class 13 vehicles, axles 2 and 3 (axle group 1) are closely spaced, similarly axles 4, 5, and 6 (axle group 2), and axles 7, 8, and 9 (axle group 3). Therefore, the combined load effects of these three groups of axles were calculated using the principle of superposition and the recorded axle spacing for each vehicle. The load effect from

axle 1 was always smaller compared to the three axle groups and was therefore discarded from the analysis.

The influence from adjacent axle loads maximizes the positive transverse moment on the decks, whereas it reduces the negative moments for negative transverse moments. Therefore, the influence from adjacent axles was only accounted for in the positive transverse moment, and the negative transverse moments were only due to the individual wheel loads in order to maximize the moment effects on the bridge deck. The statistical distribution for the positive and negative transverse moments were obtained for the peak axle loads of Class 13 vehicles using a GMM distribution, and they showed a similar multi-peak distribution to the distribution of the gross-vehicle loads shown in Figure 14. The peaks with the highest mean value were selected for the three axle groups and the means, standard deviations, and mixing proportions of the GMM distribution were collected.

Statistical Analysis of Live Load Moments on Bridge Decks

The mean maximum live load effects on the bridge deck (positive and negative transverse moments) were then extrapolated for longer return periods because the collected WIM data only contained traffic information for one year. The extrapolation was based on the procedures outlined in the report by Sivakumar et al. (2011) which assumes that the tail end of the histogram and PDF of the maximum load effect over a given return period approaches an Extreme Value Type I (Gumbel) distribution.

The mean, μ_e , standard deviation, σ_e , and mixing proportion of the GMM, m_p , of the peak distribution with the highest mean moment due to the individual axles and axle groups 1 to 3 defined previously were obtained using a GMM distribution. The total number of trucks within

CHAPTER 3: FRAMEWORK OF RELIABILITY ANALYSIS

the return period, N_{RP} , is calculated using Equation (23). The most probable value, u_N , and the dispersion coefficient, α_N , for the Gumbel distribution are calculated using Equations (24) and (25) respectively. The mean maximum load effect (live load moment), μ_{max} , and its corresponding standard deviation, σ_{max} , for a predefined return period, RP , are then calculated using Equations (26) and (27) respectively.

$$N_{RP} = n_{yr} \cdot RP \cdot m_p \cdot 365 \quad (23)$$

$$u_N = \mu_e + \sigma_e \left[\sqrt{2 \ln(N_{RP})} - \frac{\ln(\ln(N_{RP})) + \ln(4\pi)}{2\sqrt{2 \ln(N_{RP})}} \right] \quad (24)$$

$$\alpha_N = \frac{\sqrt{2 \ln(N_{RP})}}{\sigma_e} \quad (25)$$

$$\mu_{max} = u_N + \frac{0.577216}{\alpha_N} \quad (26)$$

$$\sigma_{max} = \frac{\pi}{\sqrt{6} \alpha_N} \quad (27)$$

where $n_{yr} = 33301$, is the number of trucks in the 1-year WIM data obtained for NS.

The maximum transverse moment (positive or negative) on an interior portion of a concrete bridge deck that is continuous over three or more supports, M_{S6} , according to Clause 3.8.4.5.3 of CSA S6:19 (2019) is calculated using Equation (28) following the simplified elastic method.

$$M_{S6} = 0.8 \frac{(S_e + 0.6)P}{10}, (\text{kN} \cdot \text{m}/\text{m}) \quad (28)$$

where S_e is the equivalent transverse span (m); and $P = 87.5 \text{ kN}$, is the maximum wheel load of the CL-625 Truck.

The value of λ of the time-dependent live load moment is calculated by dividing the mean calculated in Equation (26) by the moment calculated according to CSA S6:19 in Equation (28),

CHAPTER 3: FRAMEWORK OF RELIABILITY ANALYSIS

while the V is calculated by dividing the standard deviation calculated in Equation (27), by the mean calculated in Equation (26).

3.3.1.2 Model error in live load analysis, x_{LL}

The time-dependent live load moment demand calculated in the reliability analysis makes use of real traffic loads from the WIM data which was processed to establish the statistical distribution for fully-loaded vehicles. A random variable called the model error in live load analysis, x_{LL} , was introduced to account for the uncertainty in the approach used to obtain the live load statistical distribution.

Limited research has been published in literature about quantifying the error in the approach for analysing traffic load. In Table 2 of Slobbe et al. (2020), the traffic load model uncertainty is quantified as a normal distribution, with a mean of 1.00 (λ of 1.00) and a V of 0.15. These statistical parameters were adopted for x_{LL} since a more relevant study has not yet been published at the time this research was conducted.

3.3.1.3 Dynamic load allowance, DLA

Billing (1984) performed dynamic tests on a representative selection of bridges to quantify the dynamic amplification factor for bridges in Ontario using the Ontario Highway Bridge Design Code (OHBDC). The dynamic amplification factor refers to the dynamic load allowance (DLA) specified in CSA S6:19. The statistics of the dynamic amplification were presented in Table 3 of Billing (1984) which was represented as a normal distribution and showed that V of dynamic amplification are quite large ranging from 0.56 and 1.11, with a mean of approximately 0.82. Billing (1984) concluded that the mean dynamic amplification factor is inversely proportional to

CHAPTER 3: FRAMEWORK OF RELIABILITY ANALYSIS

the GVW up to GVW of 580 kN. Kennedy et al. (1992) proposed Equation (29) to express the inversely varying relationship between the dynamic amplification factor and the weight based on the work by Billing (1984).

$$I = 41.5/W \leq 0.415 \quad (29)$$

where I is the dynamic amplification factor; and W is the gross vehicle weight.

Clause 5.7.1.2 of CSA S6:19 (2019) specifies that the bending moment demand in the analysis of concrete deck slabs shall be increased by the dynamic load allowance, DLA , for a single axle, using the maximum wheel load of the CL-625 Truck, P , which is 87.5 kN. Therefore, the value of W used when evaluating Equation (29) was set to 87.5 kN, which gave an I of 0.474. Although Equation (29) proposed by Kennedy et al. (1992) sets an upper limit for I as 0.415, the mean impact factors reported in Billing (1984) were above 0.415, so the upper limit set in Equation (29) was not considered in this study.

The value of λ of DLA was then calculated by dividing the dynamic impact factor (which is named DLA in CSA S6:19) of 0.474 obtained using Equation (29) by the DLA value set by CSA S6:19 (2019) in Clause 3.8.4.5.3 of 0.4, where only one axle of the CL-W Truck is used. The resulting value of λ was 1.186, while the value of V was taken as 0.301 as used by Kennedy et al. (1992).

3.3.1.4 Dead load moments, $M_{D_{sw}}$ and $M_{D_{ws}}$

The distribution type and values of λ and V for $M_{D_{sw}}$ and $M_{D_{ws}}$ were based on the study by Kennedy et al. (1992) which included an extensive survey of bridge statistics in Alberta. The distribution

CHAPTER 3: FRAMEWORK OF RELIABILITY ANALYSIS

type was a normal distribution and the values of λ and V for $M_{D_{sw}}$ were 1.068 and 0.1399 respectively, and 1.437 and 0.5316 respectively for $M_{D_{ws}}$.

3.3.2 Resistance Model

The resistance model consists of eight random variables including the specified concrete compressive strength, f'_c , the time-dependent GFRP tensile capacity, $f_{frp}(t)$, FRP modulus of elasticity, E_{frp} , concrete cover thickness, d_c , and time-dependent concrete damage parameter, $\psi_{FT,f}(t)$, and its respective model prediction uncertainties. The approach to obtain the statistical parameters of the eight random variables is explained in the following subsections.

3.3.2.1 Concrete compressive strength, f'_c

Nowak and Szerszen (2003) provide statistics for the distribution type, λ and V used in calibrating ACI 318-19 for concrete compressive strength, f'_c . The distribution type for f'_c was a lognormal distribution. The bias of the concrete compressive strength, λ_{f_c} , is calculated as a function of the specified f'_c as expressed in Equation (30). The quality control in the North American construction industry is largely consistent meaning that the values obtained using Equation (30) are acceptable for typical Canadian and American construction (Oudah and Hassan, 2022).

$$\lambda_{f_c} = -2.4713 \times 10^{-5} f'_c{}^3 + 0.003174 f'_c{}^2 - 0.135436 f'_c + 3.064 \text{ (MPa)} \quad (30)$$

3.3.2.2 Time-dependent GFRP tensile capacity, $f_{frp}(t)$

The time-dependent bias of GFRP tensile capacity, $\lambda_{\psi_{frp,d}}$, and coefficient of variation, $V_{\psi_{frp,d}}$, were introduced in this project to determine the time-dependent GFRP tensile capacity damage

CHAPTER 3: FRAMEWORK OF RELIABILITY ANALYSIS

parameter, $\psi_{frp,d}(t)$, expressed in Equation (31). $\lambda_{\psi_{frp,d}}$ and $V_{\psi_{frp,d}}$ are variables created to quantify damage to the time-dependent tensile capacity of GFRP bars, $f_{frp}(t)$, as they degrade over time due to sustained loads and/or ASR.

$$\psi_{frp,d} = 1 - (\lambda_{\psi_{frp,d}}/1.15) \quad (31)$$

From the test results of Esmaeili et al. (2021), the time-to-failure values for the creep-rupture tests on the GFRP bars were obtained and a Weibull distribution was found to best fit the values. Using the Weibull distribution, random time-to-failure values were generated to show the variation in the failure times for bars tested under the same sustained load. Esmaeili et al. (2021) performed tests on bars at three exposure condition, and the results from exposure condition B (submerged in alkaline solution and at 23°C) were used in this project as it best represents the conditions of the concrete decks in Nova Scotia.

The experiments conducted on the sand-coated and helically-wrapped surface #5 bars (#5A) showed the shortest average failure times under conditioning B and were used to evaluate the mean and standard deviation for $f_{frp}(t)$. The time-to-failure values were plotted on a logarithmic scale against the corresponding sustained load level and extrapolated for a 30% sustained load level. The 30% sustained load was selected to represent the upper bounds of sustained load expected for a bridge deck, which would include the total loads due to self-weight of the concrete deck and barrier, and a portion of the live load on the bridge decks as discussed by Huang (2011).

The variability in the ultimate tensile strength (UTS) at time zero was considered by randomly generating numbers using a normal distribution with a λ of 1.15 and a V of 0.068 based on detailed statistical analysis by Shield et al. (2011) aimed at quantifying the variability in the FRP bar tensile capacity. The number of points generated for both the Weibull distribution time-to-failure values and the normal distribution UTS values (normalized by the specified UTS value at time zero) were

CHAPTER 3: FRAMEWORK OF RELIABILITY ANALYSIS

the same and were connected via linear lines as shown in Figure 20. The value of V for the normalized UTS was calculated along the range of time-to-failure values at intervals of 1000 hours.

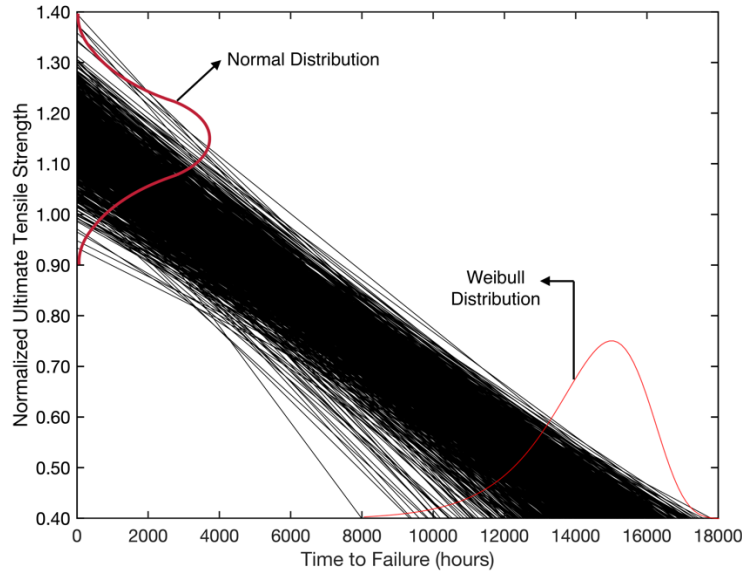


Figure 20. Distribution of normalized GFRP ultimate tensile strength (UTS) against distribution of time-to-failure values.

Esmaili et al. (2020) showed an average of 80% tensile strength retention in the GFRP reinforcement bars in the concrete beams exposed to NS environment under a 40% sustained load for 10 years which is rather conservative when compared to the actual stresses sustained in bridge deck reinforcement (El-Salakawy et al., 2005). Based on those results, the estimated failure time of the beam can be extrapolated for a sustained load of 30% assuming it follows a linear trend. The estimated sustained load percentage was based on preliminary design checks of bridge decks in NS. The assumption of the linear trend was made since the GFRP capacity was evaluated at only two points in time (zero and failure time). Should future testing indicate that the trend is non-linear, the prediction model for GFRP degradation can be readily updated.

CHAPTER 3: FRAMEWORK OF RELIABILITY ANALYSIS

The estimated failure time of the concrete beam was then compared to the failure rate of the GFRP bars in the creep-rupture tests at the same sustained load ratio (30%) extrapolated from the tests performed by Esmaeili et al. (2021). The work from Esmaeili et al. (2021) makes it possible to correlate between the time-to-failure values provided in hours for the creep-rupture tests and the years of exposure for the beams in Esmaeili et al. (2020). This correlation provides an approximate degradation rate for the GFRP bars which yields a first order polynomial for $\lambda_{\psi_{frp,d}}$ expressed in Equation (32). $V_{\psi_{frp,d}}$ is expressed as a second-order polynomial obtained from a regression analysis and calculated as shown in Equation (33). Figure 21 shows how the values of $\lambda_{\psi_{frp,d}}$ and $V_{\psi_{frp,d}}$ vary with time.

$$\lambda_{\psi_{frp,d}} = 1.15 - 0.0009543 t \quad (32)$$

$$V_{\psi_{frp,d}} = 3.545 \times 10^{-6} t^2 - 8.845 \times 10^{-5} t + 0.06827 \quad (33)$$

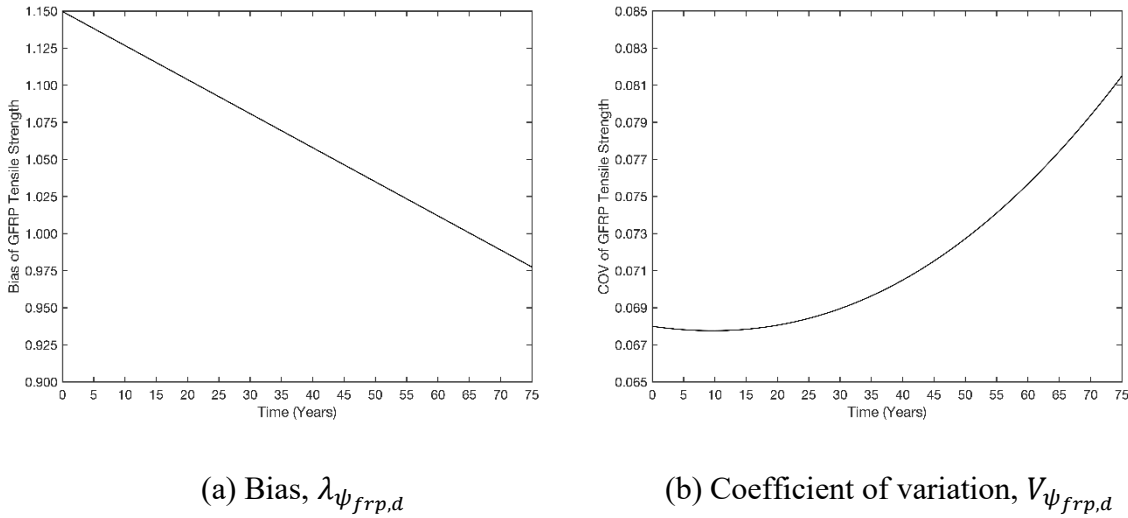


Figure 21. Bias, $\lambda_{\psi_{frp,d}}$, and coefficient of variation, $V_{\psi_{frp,d}}$, of GFRP tensile strength with respect to time.

3.3.2.3 FRP modulus of elasticity, E_{frp}

The FRP modulus of elasticity, E_{frp} , was considered as a time-dependent random variable. The statistical parameters for E_{frp} were obtained from Shield et al. (2011) with a normal distribution and values of λ and V of 1.00 and 0.068 respectively.

3.3.2.4 Concrete cover thickness, d_c

Binmerdah (2018) presents results from Ground Penetrating Radar (GPR) tests performed on two NS bridges, with concrete cover depths ranging from 40 mm to above 100 mm for Upper Durham Bridge and between 55 mm and 95 mm for Lower Durham Bridge, including histograms showing GPR-recorded cover thickness values.

The histograms showing the cover thickness variation in Binmerdah (2018) were recreated and combined into one histogram as shown in Figure 20 to establish the statistical properties of d_c , including the distribution type, λ and V . The resulting distribution type followed a lognormal distribution as shown in Figure 22, with a mean of 67.37 mm and V of 0.045. The specified concrete cover thickness for Upper and Lower Durham Bridges according to Table 8.5 of CSA S6:19 is 70 ± 20 mm, which yields a value of λ of 0.962 when compared to the mean of 67.37 mm. The lognormal distribution was truncated between 15 mm and 125 mm in the present reliability analysis, as those were the minimum and maximum cover thicknesses respectively recorded in the study by Binmerdah (2018). The truncation was necessary to prevent generating unrealistic values of d_c in the reliability analysis.

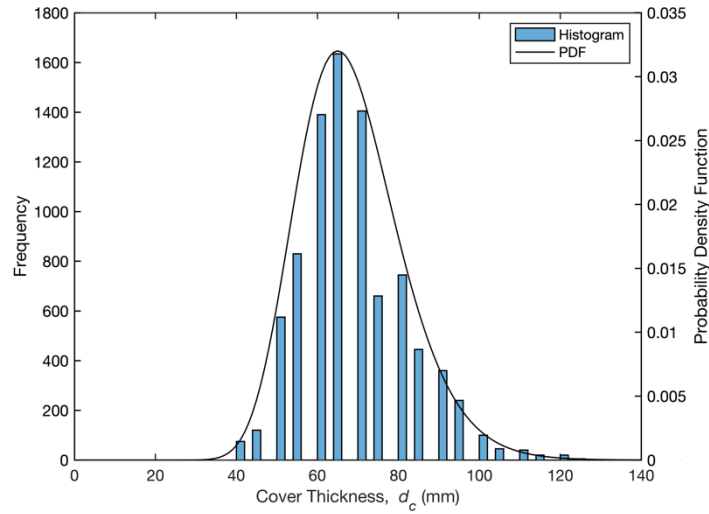


Figure 22. Histogram and probability density function (PDF) of concrete cover thickness based on GPR data from Upper and Lower Durham Bridges.

3.3.2.5 Time-dependent concrete damage due to freeze-thaw effect,

$$\psi_{FT,f}(t)$$

There is limited reliable literature available to predict the concrete compressive strength damage factor, $\psi_{FT,f}(t)$. Oudah (2022) proposed a polynomial equation based on the work by Anbang et al. (2017) to predict the relationship between the damage to the static elastic modulus of concrete, $\psi_{FT,EC}$, and $\psi_{FT,f}$ using Equation (34).

$$\psi_{FT,f}(t) = x_{FT,f}(-0.9833 \psi_{FT,EC}(t)^2 + 1.871 \psi_{FT,EC}(t)) \quad (34)$$

where $x_{FT,f}$ is a random variable to account for model uncertainty in predicting $\psi_{FT,f}(t)$

Lee et al. (2017) performed research to relate the number of freeze-thaw cycles to the damage in the dynamic elastic modulus of concrete, $\psi_{FT,Ed}$. Oudah (2022) accordingly expressed $\psi_{FT,EC}(t)$

CHAPTER 3: FRAMEWORK OF RELIABILITY ANALYSIS

as a function of $\psi_{FT,Ed}(t)$ using the equations proposed by Lee et al. (2017), while introducing random variables to account for the variance in the prediction. Lee et al. (2017) proposed Equation (35) which relates f'_c , E_c , and E_d , where a_c and b_c are functions of the test type for determining E_d ($a_c = 0.33$ and $b_c = 1.24$ for E_d determined using transverse resonant frequency, $k_1 = k_2 = 0.95$).

$$f'_c = \eta(E_c)^3 = \eta(a_c E_d^{b_c})^3 \quad (35)$$

where,

$$E_c = k_1 k_2 33500 (f'_c/60)^{1/3} \quad (36)$$

$$E_d = (E_c/a_c)^{1/b_c} \quad (37)$$

Multiplying E_c and E_d in Equation (35) by $(1 - \psi_{FT,EC})$ and $(1 - \psi_{FT,Ed})$, respectively, rearranging the equation to express $\psi_{FT,EC}$ as a function of $\psi_{FT,Ed}$, and introducing a random variable to account for model uncertainty in predicting E_c , $x_{FT,EC}$, yields Equation (38) as presented by Oudah (2022).

$$\psi_{FT,EC} = 1 - x_{FT,EC} a_c ((1 - \psi_{FT,Ed}) E_d)^{b_c} / E_c \quad (38)$$

Chen and Qiao (2015) conducted reliability-based analysis to construct curves that correlate the total number of freeze-thaw cycles, N_T , to $\psi_{FT,Ed}$, where $\psi_{FT,Ed}$ (whose variation was found to be best represented by a Weibull distribution) is determined as per ASTM C215-19. Equation (39) presents the relationship between N_T and $\psi_{FT,Ed}$ for 50% reliability.

$$N_T = 1315 e^{1.4\psi_{FT,Ed}} - 1356 \quad (39)$$

CHAPTER 3: FRAMEWORK OF RELIABILITY ANALYSIS

Re-arranging Equation (39) to express $\psi_{FT,Ed}$ as a function of N_T , and introducing a random variable to account for model uncertainty in predicting N_T using Equation (39), $x_{FT,N}$, yields Equation (40) as presented by Oudah (2022).

$$\psi_{FT,Ed} = 5 \ln \left[\frac{N_T/x_{FT,N} + 1356}{1315} \right] / 7 \quad (40)$$

A conversion factor, γ_N , is required to correlate the annual number of freeze-thaw cycles in a specific geographical region, N_A , to the number of cycles used in experimental studies (i.e., laboratory conditions) as expressed in Equation (41) in order to determine N_T (Oudah, 2022).

$$N_T = x_{FT,NA} (N_A t) / \gamma_N \quad (41)$$

where $x_{FT,NA}$ is a random variable to account for the variance in field measured N_T (Oudah, 2022); and γ_N is a conversion factor.

The value of γ_N was determined in this research based on the work of Esmaeili et al. (2020). Figure 10 of Esmaeili et al. (2020) presents the load-deflection curves for unconditioned (cured under lab conditions) and conditioned (load-sustained and exposed to NS climate for 10 years) beams reinforced with GFRP bars. Using the load-deflection curves, the change in the stiffness of the concrete can be inferred by comparing the estimated average slope of the load-deflection curve of conditioned beams to the average slope for the unconditioned beams before cracking.

The pre-cracking loss of stiffness in the conditioned vs. the unconditioned beams was approximated to be 1% using Figure 10 of Esmaeili et al. (2020), which shows that there was little change in the uncracked stiffness after 10 years of exposure in Nova Scotia climate. The post cracking stiffness was not compared because the post-cracking behaviour of the beam includes the influence from the GFRP reinforcement. Therefore, the damage parameter to the static elastic

CHAPTER 3: FRAMEWORK OF RELIABILITY ANALYSIS

modulus of concrete, $\psi_{FT,EC}$, was extrapolated for 75 years as 7.5% using the trend from the load-deflection curves, which lead to a concrete compressive strength damage factor, $\psi_{FT,f}(t)$, of approximately 13.5% after 75 years of exposure in NS calculated using Equation (34).

The annual number of freeze-thaw cycles, N_A , was set to 84.9 cycles/year following the projected values for the Halifax Regional Municipality (HRM) region for the 2020's presented by Richards and Daigle (2015). The annual number of freeze-thaw cycles in NS is projected to drop to approximately 73.8 cycles/year in the 2050's and 66.3 cycles/year in the 2080's, which may reduce the amount of degradation that occurs in the concrete strength. The conversion factor, γ_N , was updated to 85 for NS to reflect the same level of degradation in the concrete as seen in the load-deflection curves from Esmaeili et al. (2020). The distribution type for all the freeze-thaw related damage parameters was a normal distribution and the values of λ and V are given in Table 3. The concrete damage model presented herein is based on the response of normal weight concrete.

3.3.3 Methods of Structural Analysis

The methods of structural analysis consist of two random variables which are the model error in the FE analysis of live loads, x_{FE} , and model error in the simplified analysis of structural resistance, PF . The approach to obtain the statistical parameters for the two random variables is explained in the following subsections.

3.3.3.1 Model error in FE analysis of live loads, x_{FE}

The calculation of the λ for M_L in Section 3.3.1.1 was based on an FE analysis of a typical bridge in NS. The analysis was linear elastic and used shell elements to simulate the bending effect at the

bridge deck. Shell elements are formulated based on the bending flexural theory while accounting for the shear deformation. Experimental testing of bridge decks indicates that the flexural theory may misrepresent the moment demand on the bridge deck which is best predicted using a strut-and-tie model. The random variable x_{FE} was introduced to account for the uncertainty in the prediction process of M_L using FE analysis. The statistical parameters of x_{FE} were obtained from Castaldo et al. (2019) as a normal distribution with values of λ and V of 1.10 and 0.12 respectively.

3.3.3.2 Model error in simplified analysis of structural resistance, PF

The prediction of M_r in the reliability analysis is based on the nominal value obtained using Equation (20) (i.e., M_r is evaluated using Equation (20) at every trail). The random variable PF was introduced to account for the uncertainty of using Equation (20) to predict the flexural capacity of the bridge deck section. This method is aligned with the approach taken by ACI 318 in calibrating the safety of concrete members using reliability analysis (Oudah and Hassan, 2022). The statistical parameters for PF were adapted from Nowak and Szerszen (2003) with values of λ and V of 1.02 and 0.060 respectively.

3.4 TIME-DEPENDENT RELIABILITY ANALYSIS USING MC SIMULATION

Time-dependent reliability analysis is used to assess the reliability of structures under various random processes and degradation in the resistance (Lopez and Beck, 2012; Melchers and Beck, 2018). Monte Carlo (MC) Simulation is known to be computationally expensive and several alternative analytical solutions to time-dependent engineering problems have been proposed in literature to improve the computational efficiency as compared with MC simulation.

CHAPTER 3: FRAMEWORK OF RELIABILITY ANALYSIS

Gong and Frangopol (2019) summarized the existing analytical methods in literature into three groups: the Poisson process load method, the extreme value-based method, and the FORM-based outcrossing rate method. The Poisson process load method uses a nested numerical integral of conditional probability of failure on resistance assuming the occurrence of external loading follows a random process, while the extreme value-based method focuses on the extreme maximum of the structural response within the forecast time using a Gaussian process model (Gong and Frangopol, 2019).

The FORM-based outcrossing rate method uses First-Order Reliability Method (FORM) to estimate the reliability by taking advantage of the concept of outcrossing events, defined as the system response passing through a prescribed threshold to the failure domain. These outcrossing events are characterized by the Poisson process and the failure probability is presented as the sum of outcrossing rates within the forecast time such as the PH12 model by Sudret (2008) and the NEWREL model by Gong and Frangopol (2019).

Although these existing alternative analytical methods are proven to be more computationally efficient in predicting the failure probability of different engineering problems as compared with MC simulation, these methods provide approximate results or results that are specific to problems involving limited number of random variables (Kroetz et al., 2020).

Since the benefits of accurately calculating the probability of failure outweighs the benefits of reducing the computational cost, and no accurate analytical solution to the time-dependent problem presented in this research is available, a MC simulation was used in this research to solve the time-dependent reliability problem. MC simulation has been utilized in literature for solving large scale engineering problems that include a large number of random variables similar to this research (Roubos et al., 2020).

3.4.1 Procedure of Time-Dependent Reliability Analysis

The procedure for conducting the time-dependent reliability analysis consists of two steps: deterministic evaluation of the ULS (Step 1), and probabilistic evaluation of the ULS (Step 2). In Step 1, M_r , is calculated based on Equation (20) at time t equal zero using a fibre analysis and by applying the corresponding material resistance factors. M_f is then obtained by setting the utilization ratio (U.R.) equal to unity as expressed in Equation (42), while the nominal M_L , $M_{D_{sw}}$, and $M_{D_{ws}}$ are sequentially obtained by applying the corresponding load combination and introducing the dead-to-live load ratios for self-weight, $(D/L)_{sw}$, and wearing surface $(D/L)_{ws}$ as expressed in Equations (43), (44), and (45) respectively. The nominal corresponds to the mean load effects divided by the corresponding bias values.

$$U.R. = \frac{M_f}{M_r} \quad (42)$$

$$M_L = \frac{M_r \cdot U.R.}{\alpha_L(1 + DLA) + \alpha_{D_{sw}}(D/L)_{sw} + \alpha_{D_{ws}}(D/L)_{ws}} \quad (43)$$

$$M_{D_{sw}} = M_L[(D/L)_{sw}] \quad (44)$$

$$M_{D_{ws}} = M_L[(D/L)_{ws}] \quad (45)$$

In Step 2, the values of M_L , $M_{D_{sw}}$, and $M_{D_{ws}}$ are multiplied by the corresponding bias ratios to obtain the mean of the moments using the reliability analysis. MC simulation is then employed to calculate the annual reliability index, β_A , and the design lifetime reliability index, $\beta_R(t)$.

The detailed procedure followed to calculate $\beta_A(t)$ is described as follows (Roubos et al. (2020)): The time-dependent performance function, $G(X(t))$, is set equal to the difference in the resistance, $R(t)$, and the load effects, $S(t)$, as shown in Equation (46), where X is a vector of random variables. The time-dependent probability of failure, $P_f(t)$, corresponds to the probability of $G(X(t))$ equal to or less than zero. $P_f(t)$ equal to the integration of the joint probability density

CHAPTER 3: FRAMEWORK OF RELIABILITY ANALYSIS

function (PDF) of the vector X of random variables as a function of time, $f_{X(t)}(x(t))$ as shown in Equation (47).

$$G(X(t)) = R(t) - S(t) \quad (46)$$

$$P_f(t) = P(G(X(t)) \leq 0) = \int_{G(X(t)) \leq 0} f_{X(t)}(x(t)) \quad (47)$$

For each year, the conditional probability of failure at year $t = i$ was determined as the probability that failure occurs during year i given that the structure has survived until time t . This approach utilizes a probability of failure per year i , given that the bridge has survived all previous years, $P_{f,i|S}$, as expressed in Equation (48). $\beta_A(t)$ is subsequently calculated using Equation (49). In addition to $\beta_A(t)$, the design lifetime reliability index, $\beta_R(t)$, was evaluated at select reference years, t_{ref} , as expressed in Equation (51) using the cumulative probability of failure from year i to t_{ref} , $P_{f,i_{ref}}(t)$, expressed in Equation (50).

$$P_{f,i|S} = P(F_i | S_1 \cap \dots \cap S_{i-1}) \quad (48)$$

$$\beta_A(t) = -\Phi^{-1}(P_{f,i}(t)) \quad (49)$$

$$P_{f,i_{ref}} = \frac{F_{i_{ref}}}{n} \quad (50)$$

$$\beta_R(t) = -\Phi^{-1}(P_{f,i_{ref}}(t)) \quad (51)$$

where F_i is the number failure points in year i of the MC simulation; S_i is the number of survival points in year i of the MC simulation; $F_{i_{ref}}$ is the number of failure points from year i to year t_{ref} ; n is the number of trials; and $\Phi(\cdot)$ is the cumulative distribution function of the standardised normal distribution.

The performance function in Equation (46) is evaluated and the number of failed points at $t = i$ is recorded. The failed points at $t = i$ are removed from the obtained M_L , $M_{D_{sw}}$, and $M_{D_{ws}}$ in

CHAPTER 3: FRAMEWORK OF RELIABILITY ANALYSIS

Equations (43), (44), and (45) respectively, as well as the corresponding M_r . The removal of the failed points was necessary to ensure that only the survival points at time $t = i$ feed into the reliability analysis at time $t = i + 1$ years. Equation (49) is then used to calculate the corresponding β_A for year i . The probability of failure and reliability index is established by utilizing statistical and reliability analysis methods to perform the reliability analysis using both time-dependant and time-independent random variables.

3.4.2 Accuracy of MC simulation

The accuracy of the MC is a function of the number of trails, n , used in the reliability analysis. A sensitivity analysis was conducted to examine the influence of increased number of trails on the accuracy of predicting β_A and β_R at 75 years of service. The sensitivity analysis considered evaluating β_A and β_R for three bridge deck configurations for n values ranging from 10 million to 150 million. The common design parameters of the three bridge deck configurations were as follows: $h = 225$ mm, $b = 1000$ mm, $\phi_b = 15.9$ mm, $A_b = 285$ mm², $(D/L)_{sw} = 0.1577$, $(D/L)_{ws} = 0.0541$, $f_{frpu} = 1100$ MPa, $E_{frp} = 60$ GPa, $f'_c = 35$ MPa, $U.R. = 1$, where ϕ_b , A_b , and f_{frpu} , are the GFRP reinforcement bar diameter, bar area, and ultimate tensile strength respectively. Three combinations of the parameters d_c and ρ_{frp} were selected to achieve a minimum M_r of 140 kN-m/m to produce three typical bridge deck configurations. The values of d_c checked were 35, 45, and 55 mm and their corresponding ρ_{frp} were 0.99, 1.30, and 1.80, respectively.

The mean β_A and β_R at 75 years of service and the corresponding standard deviation of three identical runs per bridge configuration described above were obtained using the framework of analysis described in this chapter. The analysis results are shown in Figure 23. Based on the results,

CHAPTER 3: FRAMEWORK OF RELIABILITY ANALYSIS

an n value of 50 million trials was selected because the standard deviation of the β_A and β_R values appeared to stabilize and not exhibit high volatility when n reaches 50 million trials. Although the computational cost of using 50 million trials is relatively high, it is the most suitable number of trials to run the MC simulation without compromising the accuracy of the results. The error for β_A of 4.36 and β_R of 3.50 for a confidence level of 99% evaluated at 75 years based on the mean values of the three simulations at n of 50 million is 14.5% and 2.5%, respectively. The calculated error is considered acceptable. The confidence level, maximum tolerable error, and the number of trials are correlated as per Equation (52) (Fenton and Griffiths, 2008):

$$n = \frac{z_{\alpha}^2 \hat{p} \hat{q}}{e^2} \quad (52)$$

where z_{α} is the z-value for a selected confidence level; e is the maximum tolerable error on the expected probability of failure; \hat{p} is the expected probability of failure; and $\hat{q} = 1 - \hat{p}$ is the expected probability of survival.

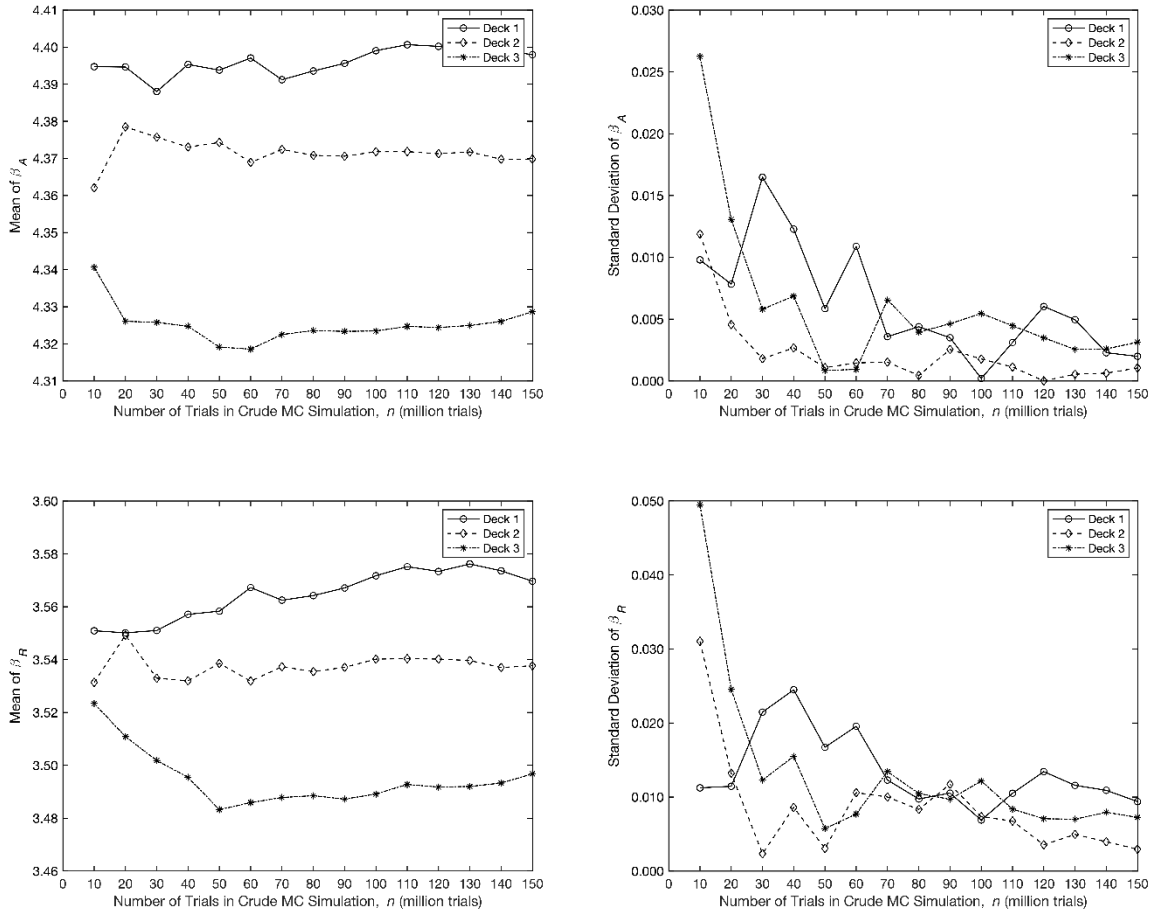


Figure 23. Sensitivity analysis of the number of trails, n , considered in the MC analysis.

3.4.3 Target Reliability Index

The calculated bridge deck reliability needs to be compared with a target value to evaluate the adequacy of the bridge deck design against a target service life. The target value can be set based on the annual reliability approach (i.e., target reliability based on β_A) or the design lifetime approach (i.e., target reliability based on β_R).

Clause 3.5.1 of CSA S6:19 (2019) states that the calibration of load factors shall be based on a minimum β_A of 3.75, while review of the Commentary to CSA S6:19 indicates the use of a

minimum of β_R of 3.50 for a service life of 75 years for the calibration of the load and material resistance factors. β_A and β_R have been historically correlated in design code calibration by assuming independent failure event per year for the considered reference year, t_{ref} , as expressed in Equation (53) since code calibration does not account for the time-dependent degradation in the structural resistance.

$$\beta_R = \Phi^{-1}\{[\Phi(\beta_A)]^{t_{ref}}\} \quad (53)$$

The value of β_R obtained from Equation (53) by using the CSA S6:19 specified β_A of 3.75 as in Clause 3.5.1 is 2.48, which is significantly less than β_R of 3.50 which was used in calibrating CSA S6:19 and other internationally recognized bridge codes like AASHTO LRFD (2017). Therefore, the target reliability index, β_T , was set to β_R of 3.50 for a design life of 75 years in this research. This approach aligns with the values used in calibrating CSA S6:19 and AASHTO LRFD (2017) and avoids using Equation (53) to correlate β_R to β_A since the equation is not valid when considering the time-dependent degradation in the structural resistance as concluded in Section 4.2.2.

3.5 MATLAB CODE STRUCTURE

The time-dependent reliability analysis was conducted using an algorithm programmed in MATLAB®. Figure 24 shows a flowchart of the main script for the time-dependent reliability analysis which graphically shows how the steps described in Section 3.4 are executed in sequence to obtain β_A and β_R . The section, material, load, and resistance properties are firstly inputted into the algorithm, followed by the time-independent and time-dependent properties. The deterministic evaluation of the ULS (Step 1) is then performed to obtain the mean load and resistance values.

CHAPTER 3: FRAMEWORK OF RELIABILITY ANALYSIS

The probabilistic evaluation of the ULS (Step 2) is performed sequentially and the realizations of the random variables are generated, and the reliability analysis is performed. The algorithm makes use of a main script which is graphically represented in Figure 24 and eight functions which:

- calculate the time-independent (deterministic) moment resistance – M_r Function,
- generate n time-independent random variables – *MC Direct Sampling*,
- calculate the time-dependent statistical parameters of M_L – $M_L(t)$ Function,
- generate n time-dependent random variables – *MC Direct Sampling*,
- calculate the time-dependent statistical parameters of GFRP – $f_{frp}(t)$ Function,
- calculate the time-dependent concrete freeze-thaw damage $\psi_{frp,d} - f'_c(t)$ Function,
- calculate the time-dependent (probabilistic) moment resistance – M_r Function, and
- calculate the annual and design lifetime reliability indexes – *Beta Function*.

CHAPTER 3: FRAMEWORK OF RELIABILITY ANALYSIS

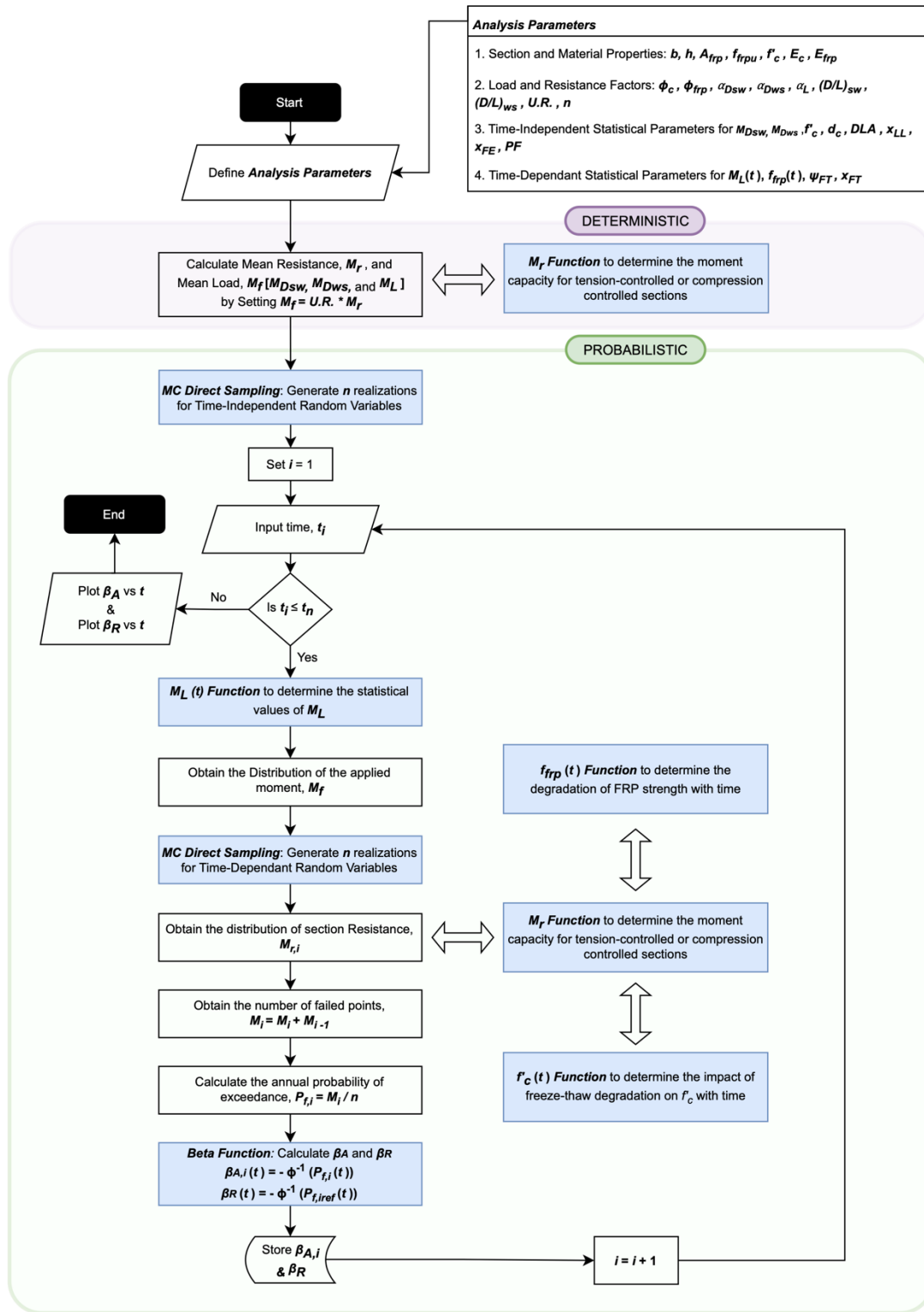


Figure 24. Flowchart describing the main algorithm for the time-dependent reliability analysis.

CHAPTER 3: FRAMEWORK OF RELIABILITY ANALYSIS

The time-dependent $M_r(t)$ is calculated using the M_r Function shown in Figure 24 which is an optimized MATLAB[®] function that was developed within the Structural Assessment and Retrofit (SAR) research group at Dalhousie University to calculate the moment resistance of both tension-controlled (FRP rupture) and compression-controlled (concrete crushing) FRP-reinforced cross-sections. The function was updated and modified to address the needs of this project.

The M_r Function uses an iterative approach to solve for the depth of the neutral axis, c , by first assuming a compression-controlled failure mode, and checking if the force in the FRP is equal to the force in the concrete. The function then checks if the strain in the FRP, ε_{frp} , is less than the ultimate FRP strain, ε_{frpu} . If that check is positive, the function outputs the M_r for a compression-controlled failure mode, otherwise it assumes a tension-controlled failure mode and repeats the process to output the M_r for a tension-controlled failure mode. Figure 25 shows a flowchart describing the steps taken within the M_r Function to solve for M_r . The accuracy of the M_r Function was validated against hand calculations and showed less than 1% error between results.

The $f_{frp}(t)$ Function and the $f'_c(t)$ Function shown in Figure 24 are functions created using MATLAB[®] that calculate the λ and V of the time-dependent GFRP tensile strength, and the damage to the concrete compressive strength due to freeze-thaw effect respectively according to methods discussed in Sections 3.3.2.2 and 3.3.2.5 respectively. The $M_L(t)$ Function calculates λ and V of $M_L(t)$ according to the methods described in Section 3.3.1.1. The MC Direct Sampling functions generate n realizations of either time-independent or time-dependent random variables when required. The Beta Function calculates β_A and β_R according to the procedure described in Section 3.4.

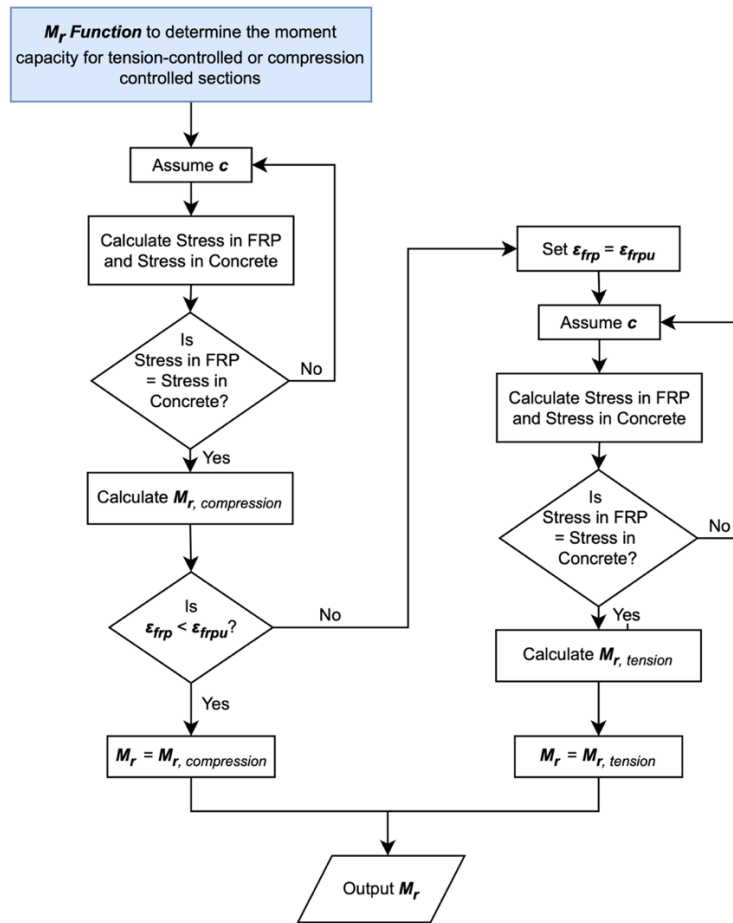


Figure 25. Flowchart describing the moment resistance function for GFRP-reinforced bridge deck sections (M_r Function).

CHAPTER 4 TIME-DEPENDENT RELIABILITY-BASED ASSESSMENT OF BRIDGE DECK DESIGN OPTIONS IN NS

4.1 INTRODUCTION

This chapter proposed reliability-based durable alternative bridge deck design options for NS (Phase II of the project scope as discussed in Section 1.2). The methodology for proposing the alternative bridge deck design options consists of two steps: time-dependent reliability-based assessment of select NS bridge decks (Step 1); and time-dependent reliability-based parametric analysis of representative bridge deck configurations (Step 2). The objectives of Step 1 are to assess the reliability of select NS bridge decks and help in bounding the values of the design parameters used in the parametric analysis conducted in Step 2. The objective of Step 2 is to propose alternative durable bridge deck designs for NS that meet the structural safety requirements of CSA S6:19 using the developed time-dependent reliability framework of analysis. The performance objectives for proposing the alternative bridge deck designs are to minimize the specified concrete compressive strength, concrete cover thickness, and overall deck section depth while satisfying the ULS and reliability requirements.

4.2 TIME-DEPENDENT RELIABILITY-BASED ASSESSMENT OF SELECT NS BRIDGE DECKS (STEP 1)

4.2.1 Description of the Select Bridge Decks

A database comprising of the design details of select bridges in NS was developed, summarizing the bridges into categories such as date of construction, abutment type, girder type, concrete compressive strength, deck thickness, span length, and other relevant categories. Information for

CHAPTER 4: RELIABILITY ASSESSMENT OF DECK OPTIONS IN NS

these bridges was obtained, such as stamped engineering design drawings, inspection reports, and strength testing reports. The database currently consists of 20 bridges and the key design parameters are summarized in Table 5.

Five bridges with GFRP-reinforced bridge decks were selected and analysed at ULS. The five bridges were selected to capture different regions in NS from the Northern, Central, Cape Breton, and South Shore regions of the province as shown in Figure 26. The names and IDs of the select bridges are included in Table 6.

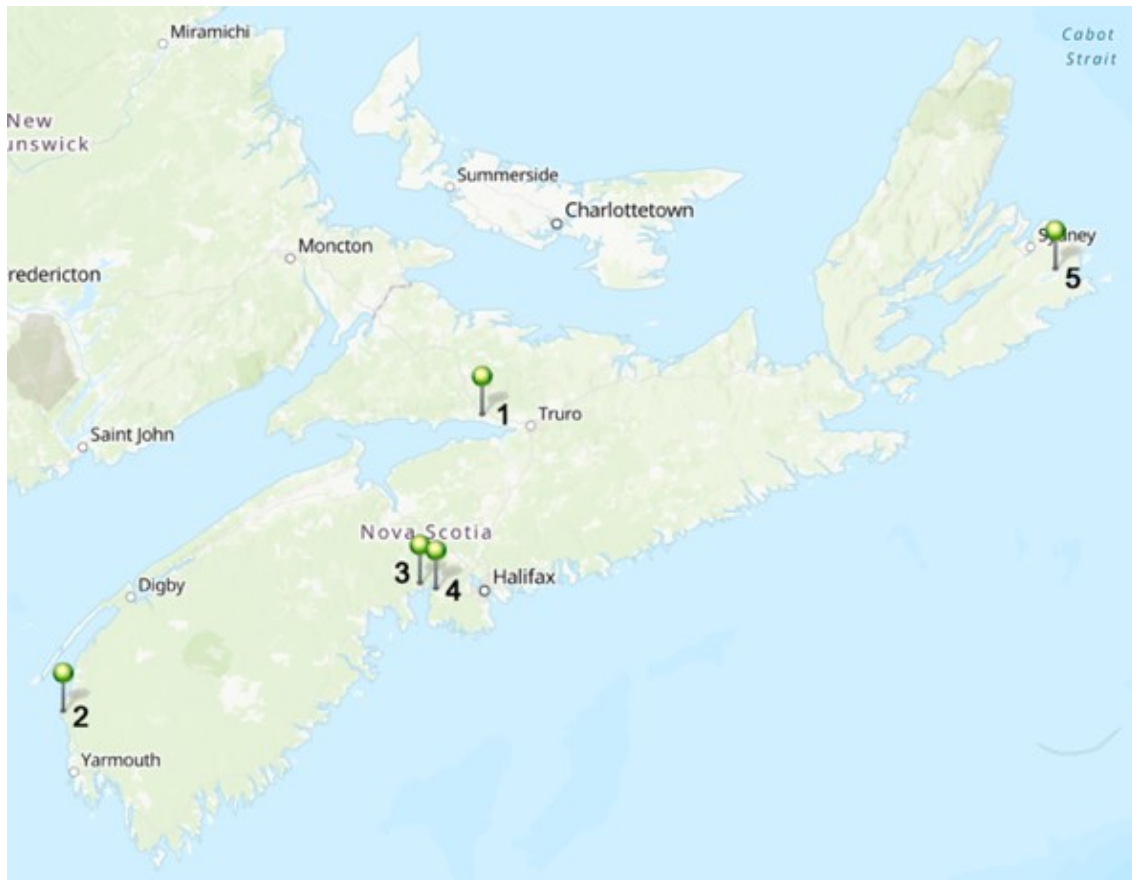


Figure 26. Locations of NS bridges analysed using time-dependent reliability analysis.

Table 5. Summary of Nova Scotia bridges in created database.

Parameter	Value/ Range	Number of Bridges	
		Database (20)	Analysed (5)
Date of construction	2011 – 2015	12	2
	2016 – 2020	8	3
Abutment type	Integral Abutment	18	5
	Semi-Integral Abutment	2	0
Girder type	New England Bulb Tee (NEBT)	15	5
	Box Girder	3	0
	Next Beam Type B	1	0
	28F Next Beam	1	0
Concrete compressive strength	45 MPa	19	5
	50 MPa	1	0
Deck thickness	175 mm	1	0
	200 mm	1	0
	225 mm	14	4
	250 mm	4	1
Span length	15 m – 24 m	3	0
	25 m – 34 m	5	2
	35 m – 44 m	9	3
	45 m – 54 m	0	0
	55 m – 65 m	3	0

Table 6. Nova Scotia bridges analysed using time-dependent reliability analysis.

Bridge #	Bridge Name	Bridge ID
1	Great Village River Bridge	COL 010
2	Cape St. Mary's #2 Bridge	DIG 176
3	Ingramport Connector Underpass	HFX 469
4	Ingram River Bridge	HFX 559
5	Lower Black Brook Bridge	CB 048

A detailed structural design check was performed on the five selected existing NS bridge decks to obtain the design loads, resistances, and U.R. The deck section details are summarised in Table 7 and the details of the structural design checks are shown in Appendix A. The results of the

detailed design check indicate that the five selected NS bridge decks meet the ULS requirement of CSA S6:19 of having a U.R. less than or equal to unity.

The objective of the reliability-based assessment of the NS bridge decks in Step 1 is to examine the sensitivity of bridge decks designed per CSA S6:19 on the long-term reliability. Therefore, the utilization ratio in Equation (42) was set to unity. The reliability indexes of the bridge decks were checked in the positive transverse, negative transverse, and longitudinal bending directions. The number of trails in the MC simulation was set to 50 million as described in Section 3.4.2.

Table 7. Summary of section details for analysed NS bridge decks.

Direction	Parameter	Bridge 1	Bridge 2	Bridge 3	Bridge 4	Bridge 5
General	h (mm)	225	225	250	225	225
	$d_{c_{top}}$ (mm)	50	50	50	50	50
	$d_{c_{bot}}$ (mm)	30	35	35	38	38
	f'_c (MPa)	45	45	45	45	45
Positive Transverse Direction	d_{bar} (mm)	19.1	19.1	19.1	19.1	19.1
	s (mm)	200	150	300	200	200
	ρ_{frp} (%)	0.768	1.053	0.462	0.803	0.803
	f_{frpu} (MPa)	1105	1000	1100	1100	1100
	M_r (kN-m/m)	140	148	132	129	129
	Failure Mode	Comp.	Comp.	Tens.	Comp.	Comp.
Negative Transverse Direction	d_{bar} (mm)	15.9	19.1	19.1	15.9	19.1
	s (mm)	250	300	300	225	225
	ρ_{frp} (%)	0.474	0.574	0.499	0.527	0.766
	f_{frpu} (MPa)	1184	1000	1100	1100	1100
	M_r (kN-m/m)	93	95	121	96	110
	Failure Mode	Comp.	Tens.	Comp.	Comp.	Comp.
Positive Longitudinal Direction	d_{bar} (mm)	15.9	19.1	19.1	15.9	15.9
	s (mm)	248	300	300	247	248
	ρ_{frp} (%)	0.475	0.589	0.51	0.501	0.499
	f_{frpu} (MPa)	1184	1000	1100	1100	1100
	M_r (kN-m/m)	94	95	118	85	84
	Failure Mode	Comp.	Tens.	Comp.	Comp.	Comp.

Note: $d_{c_{top}}$ and $d_{c_{bot}}$ are the specified top and bottom cover thicknesses respectively; s is the bar spacing; d_{bar} is the bar diameter; and f_{frpu} is the specified GFRP tensile strength.

4.2.2 Time-Dependent Reliability Analysis Results

The annual reliability index, β_A , values for the five selected NS bridge decks were plotted as shown in Figure 27 as a function of the number of years in service for the positive transverse, negative transverse, and positive longitudinal moments. The values of β_A exhibited a higher variance within the first 20 years and the trend got smoother as the number of years in service increased. The number of failures in the initial years of service is relatively low because the bridge decks have not lost much of their capacity due to GFRP and concrete degradation, and the live load moment has not increased substantially. In the later years, the trend starts to stabilize as the number of failures increases. From Figure 27, it is observed that the common method used in structural reliability to derive the target annual reliability index based on the target reliability index for a selected design life by assuming independent failure events in subsequent years is inaccurate. This common assumption is reported in AASHTO LRFD (2017) and used in the calibration of the load and resistance factors in Canadian standards including the CSA S6:19.

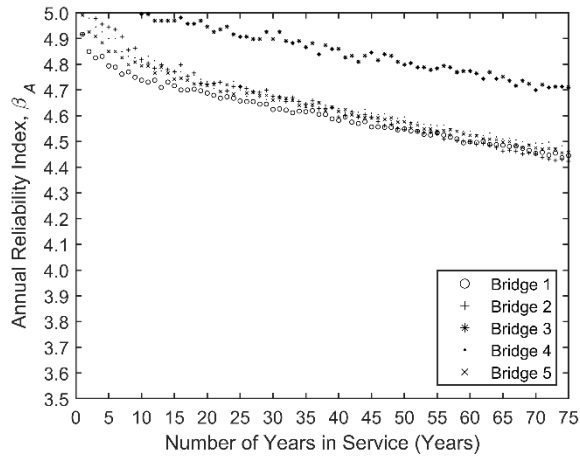
The design lifetime reliability index, β_R , values for the five NS bridge decks are plotted as shown in Figure 28 for the positive transverse, negative transverse, and positive longitudinal moments up to a design life of 75 years. The range of β_R was approximately 4.85 to 5.0 at a design life of 1 year, which signifies a low probability of failure as defined in Equation (47). As the design life increases, β_R reduces. This reduction in β_R is a result of the increase in the probability of an extreme live load occurrence and reductions in M_r due to damage in the concrete compressive strength and reduction of the GFRP tensile capacity with time. The reduction in GFRP tensile strength and the concrete compressive strength was approximately 6.15% and 7.11% respectively from year 1 to year 75, and depending on the design failure mode, either one of the two would govern the reduction of M_r .

CHAPTER 4: RELIABILITY ASSESSMENT OF DECK OPTIONS IN NS

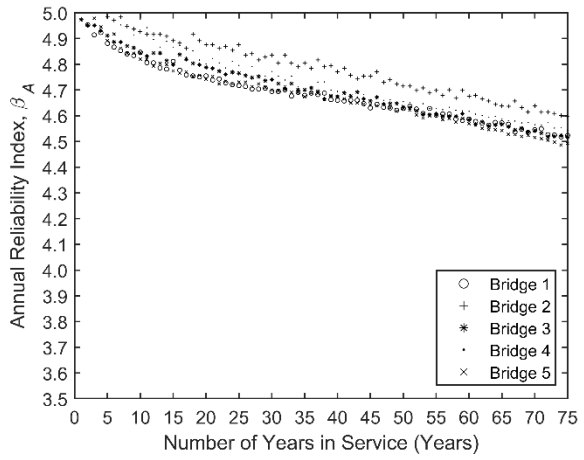
Each bridge has a unique curve of $\beta_R(t)$, and this variation is due to the choice of design parameters for the bridge decks. For example, Bridge 3 has a 250 mm thick deck and a concrete cover of 35 mm, to achieve an M_r of 132 kN-m/m, whereas Bridge 1 has a 225 mm thick deck and a concrete cover of 30 mm, to achieve an M_r of 140 kN-m/m in the positive transverse bending direction. Both bridges have a specified GFRP tensile strength of 1100 MPa, and concrete compressive strength of 45 MPa, but Bridge 3 was designed to fail in a tension-controlled failure mode (FRP rupture), while Bridge 4 was designed to fail in a compression-controlled failure mode (concrete crushing). Bridge 3 has a β_R of 3.90 at 75 years while Bridge 1 has a β_R of 3.58 at 75 years as seen in Figure 28a. This difference in $\beta_R(t)$ is due to the different design parameter choices made by their respective designers.

Based on the results for the NS bridges, the decks designed for a tension-controlled failure mode exhibited higher β_R and β_A values at year 75 than compression-controlled failure decks which is also seen in the positive longitudinal bending direction. This trend occurs because the reduction of the tensile capacity of GFRP with time is less than the reduction in the concrete compressive strength with time, therefore decks designed for tension-controlled failure mode appear to be more reliable.

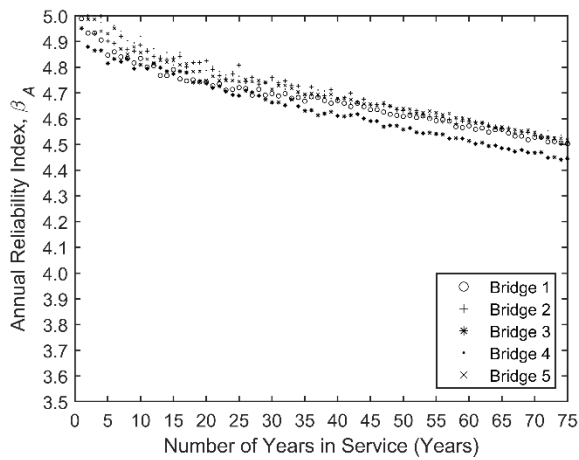
Comparing the bridge response in Figure 28 with the target β_T of 3.50 described in Section 3.4.3 indicates that all considered bridge deck details meet or exceed the structural safety requirements. It also indicates that a room exists for refining bridge deck design in NS to minimize certain design specifications while satisfying the target reliability index at the design life of 75 years. This observation is utilized in Step 2 of the time-dependent reliability analysis to propose alternative durable bridge decks that yield reduced construction cost while meeting the reliability requirement of CSA S6:19.



(a) Positive transverse moment

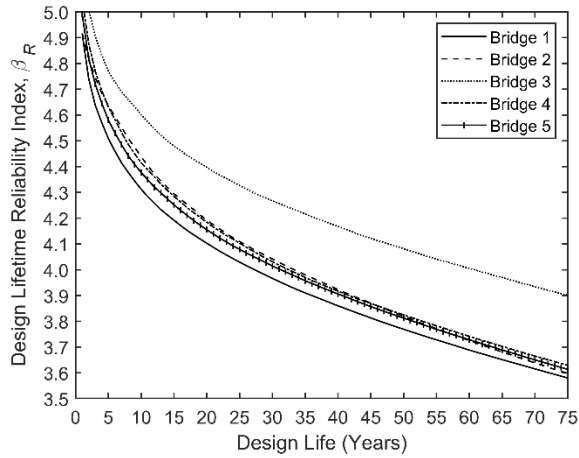


(b) Negative transverse moment

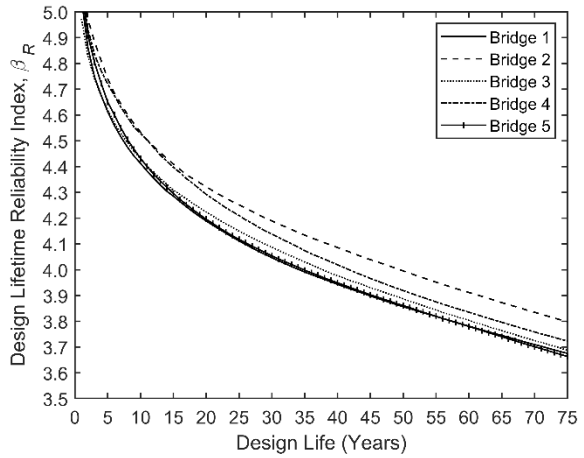


(c) Positive longitudinal moment

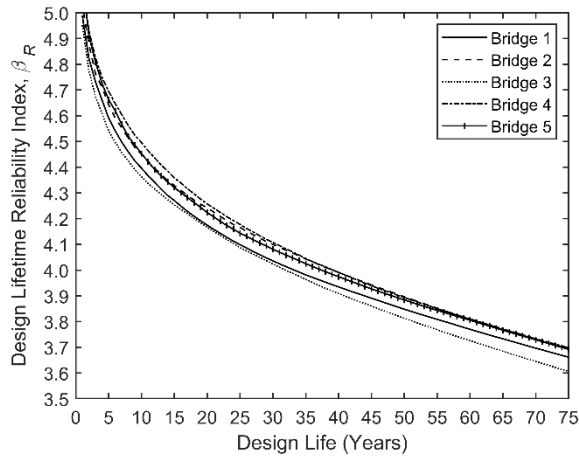
Figure 27. Annual reliability index, β_A , for the positive transverse, negative transverse, and positive longitudinal moments for NS bridge decks.



(a) Positive transverse moment



(b) Negative transverse moment



(c) Positive longitudinal moment

Figure 28. Design lifetime reliability index, β_R , for the positive transverse, negative transverse, and positive longitudinal moments for NS bridge decks.

4.3 TIME-DEPENDENT RELIABILITY-BASED PARAMETRIC ANALYSIS OF REPRESENTATIVE BRIDGE DECK CONFIGURATIONS (STEP 2)

4.3.1 Description of the Considered Bridge Deck Configurations

Based on the results of Step 1, it is evident that the current bridge deck practice in NS is reliable but there is room for creating designs with reduced specified material and geometric properties to further reduce the construction cost. The performance objectives for proposing the alternative bridge deck designs in Step 2 are to minimize the specified concrete compressive strength, concrete cover thickness, and overall deck section depth while satisfying the ULS and service-life reliability index of 3.50 at 75 years.

The design variables varied in the parametric study are h , d_c (top and bottom), and f'_c . Parameters such as the reinforcement size and reinforcement spacing can be selected by designers to meet the required moment capacities after the section details have been selected. Based on the design drawings in the created NS bridge database, design trends were observed for NS bridges such as specifying an h of 225 mm, using a d_c of 50 mm on the top of decks, using a d_c higher than 35 mm on the underside of decks, and specifying an f'_c of 45 MPa for decks. The rebar material properties were kept consistent following typical NS practice with an f_{frrpu} of 1100 MPa and E_{frrpu} of 60 GPa.

A sequential parametric analysis was conducted in which the effect of reducing the specified f'_c is first investigated followed by investigating the feasibility of reducing d_c and h . The reliability index is evaluated for each analysis and compared with the target value. To perform the sequential parametric analysis, six groups of analyses were considered to assess the reliability of 36 unique concrete bridge deck configurations as summarized in Table 8. The target bending moment capacities for the Analyses 1 to 4 were based on the range of moment capacities observed

CHAPTER 4: RELIABILITY ASSESSMENT OF DECK OPTIONS IN NS

in the selected five NS bridge decks and the typical moment capacities generally encountered in the design of bridge decks, whereas the target moment capacities for Analysis Group 5 and 6 were based on the configurations in the first four analyses that produce the lowest design lifetime reliability index at 75 years. The actual design M_r for each configuration was greater than or equal to the target M_r within a range of 7% or less. The rationale for the considered bridge deck configurations per analysis group is outlined in the following paragraphs.

Table 8. Bridge deck configuration details for reliability-based parametric study for proposing alternative deck design options.

Analysis Group No.	Config. No.	M_r (kN-m/m)	h (mm)	d_c (mm)	f'_c (MPa)	d_{bar} (mm)	s (mm)	ρ_{frp} (%)	Failure Mode	$\beta_A(75)$	$\beta_R(75)$
1	1	90	225	50	35	22.2	300	0.789	Comp.	4.43	3.59
	2	100	225	50	35	22.2	270	0.877	Comp.	4.45	3.65
	3	110	225	50	35	22.2	210	1.127	Comp.	4.41	3.60
	4	120	225	50	35	22.2	165	1.434	Comp.	4.37	3.54
	5	130	225	50	35	22.2	130	1.821	Comp.	4.33	3.50
	6	140	225	50	35	22.2	105	2.254	Comp.	4.29	3.45
	7	150	225	50	35	22.2	85	2.784	Comp.	4.25	3.42
2	8	80	225	50	35	22.2	260	1.053	Comp.	4.41	3.58
	9	90	225	50	35	22.2	190	1.441	Comp.	4.38	3.56
	10	100	225	50	35	22.2	140	1.955	Comp.	4.32	3.48
	11	110	225	50	35	22.2	105	2.607	Comp.	4.29	3.46
	12	120	225	50	35	22.2	80	3.422	Comp.	4.23	3.38
3	13	90	225	35	35	15.9	265	0.410	Tens.	4.41	3.56
	14	100	225	35	35	19.1	290	0.545	Comp.	4.46	3.64
	15	110	225	35	35	19.1	230	0.687	Comp.	4.42	3.59
	16	120	225	35	35	19.1	185	0.854	Comp.	4.42	3.60
	17	130	225	35	35	19.1	150	1.053	Comp.	4.39	3.57
	18	140	225	35	35	19.1	120	1.316	Comp.	4.35	3.51
	19	150	225	35	35	19.1	100	1.579	Comp.	4.35	3.51
4	20	80	225	35	35	19.1	300	0.589	Comp.	4.45	3.59
	21	90	225	35	35	19.1	240	0.736	Comp.	4.45	3.64
	22	100	225	35	35	19.1	185	0.955	Comp.	4.41	3.61
	23	110	225	35	35	19.1	145	1.218	Comp.	4.39	3.55

CHAPTER 4: RELIABILITY ASSESSMENT OF DECK OPTIONS IN NS

Analysis Group No.	Config. No.	M_r (kN-m/m)	h (mm)	d_c (mm)	f'_c (MPa)	d_{bar} (mm)	s (mm)	ρ_{frp} (%)	Failure Mode	$\beta_A(75)$	$\beta_R(75)$
5	24	120	225	35	35	19.1	110	1.606	Comp.	4.33	3.51
	25	140	200	35	35	28.6	110	3.869	Comp.	4.17	3.31
	26	140	200	35	45	22.2	115	2.192	Comp.	4.35	3.53
	27	140	200	35	55	22.2	155	1.626	Comp.	4.36	3.53
	28	150	200	35	35	28.6	85	5.006	Comp.	4.13	3.26
	29	150	200	35	45	22.2	95	2.653	Comp.	4.33	3.48
	30	150	200	35	55	22.2	125	2.016	Comp.	4.32	3.50
6	31	110	200	35	35	28.6	65	8.080	Comp.	4.03	3.15
	32	110	200	35	45	28.6	120	4.377	Comp.	4.22	3.36
	33	110	200	35	55	22.2	145	2.031	Comp.	4.34	3.50
	34	120	200	35	35	28.6	45	11.67	Comp.	3.95	3.04
	35	120	200	35	45	28.6	90	5.836	Comp.	4.19	3.33
	36	120	200	35	55	22.2	115	2.561	Comp.	4.30	3.44

Analysis 1 consisted of seven deck configurations for satisfying the positive and negative transverse moments on bridge decks while Analysis 2 consisted of five deck configurations for satisfying the positive longitudinal moments based on the configurations from the first analysis. The first two analyses had decks with an h of 225 mm, top and bottom d_c of 50 mm, and f'_c of 35 MPa. The h and d_c of 225 mm and 50 mm, respectively, were selected to follow the typical NS design as a starting point while reducing the f'_c .

Similar to the first two analyses, Analyses 3 and 4 consisted of seven configurations for satisfying the positive and negative transverse moments and five configurations for satisfying the positive longitudinal moments respectively. The Configurations in Analyses 3 and 4 investigated the effect on the reliability index when the top and bottom d_c values are reduced from 50 mm to 35 mm, which corresponds to the minimum concrete cover thickness for GFRP-reinforced deck sections according to Clause 16.4.4 of CSA S6:19 (2019).

Analyses 5 and 6 each consisted of six deck configurations for satisfying the positive and negative transverse moments and the positive longitudinal moments respectively. Analyses 5 and

6 were performed to investigate the effects on the reliability index for configurations with a reduced h of 200 mm, f'_c values of 35, 45, and 55 MPa, and the same top and bottom d_c values as Analyses 3 and 4 (35 mm). Given that the reliability index for some of the configurations in the first four analysis groups met the target reliability index, as will be discussed in the Section 4.3.2, the feasibility of using a reduced h was checked.

4.3.2 Time-Dependent Reliability Analysis Results

The design lifetime reliability index, $\beta_R(t)$, for all 36 configurations in the six analyses were obtained and plotted as shown in Figure 29, while the values of β_A and β_R at year 75 are reported in Table 8. The plots of $\beta_A(t)$ versus the number of years in service are included in Appendix B. The results from Analysis Group 1 and 2 show that for a bridge deck section with an h of 225 mm, d_c of 50 mm, and f'_c of 35 MPa, the $\beta_R(t)$ values satisfy the recommended β_T for decks with M_r values up to 130 kN-m/m for transverse moments and 90 kN-m/m for positive longitudinal moment. Configurations with a reduced d_c of 35 mm as seen in Analyses 3 and 4, with M_r values up to 150 kN-m/m for transverse moment and 120 kN-m/m for positive longitudinal moment have $\beta_R(t)$ values that are up to or exceed the recommended β_T .

The values of $\beta_R(t)$ for Analyses 5 and 6, with sections that reduce both h and d_c to 200 mm and 35 mm respectively, only satisfy the recommended β_T for the configurations that have f'_c values of 45 or 55 MPa. To achieve the relatively high target M_r values for Analyses 5 and 6 using an h of 200 mm, ρ_{frp} would have to increase significantly, as high as 8%, because the internal moment arm between the effective concrete block and the tensile reinforcement is reduced. For example, both Configurations 18 and 25 have a target M_r of 140 kN-m/m and d_c of 35 mm, but Configuration 18 has an h of 225 mm and a ρ_{frp} of 1.316% and Configuration 25 has an h of 200

CHAPTER 4: RELIABILITY ASSESSMENT OF DECK OPTIONS IN NS

mm and a ρ_{frp} of 3.969%, meaning that the ρ_{frp} needs a 201% increase to meet the target M_r . To reduce the high values of ρ_{frp} required to satisfy the target M_r values, higher f'_c values were required as seen in some of the configurations in Analyses 5 and 6.

As determined in Step 1, sections with a compression-controlled failure mode are less reliable. With majority of the configurations in Step 2 being designed for compression-controlled failure mode, it is no surprise that there are configurations of lower reliability especially in Analyses 5 and 6 where ρ_{frp} values are high. It can be concluded from these results that as the amount of GFRP reinforcement increases, the reliability index decreases.

Based on the results of the six analyses, it is evident that some configurations do not meet the target reliability index and are therefore not viable options. But there are also configurations with reduced material and geometric properties that are validated for the range of moment resistances checked in this project. The section details for the durable alternative GFRP-reinforced bridge deck configurations that are feasible are summarised in Table 9 along with a general schematic shown in Figure 30. The current design practice in NS has been validated to be durable, and the sections details presented in Table 9 are for sections with either the same or reduced material and geometric properties as the typical NS design.

Table 9 may be used by design engineers as a basis to select preliminary section details for their design once the design factored loads have been calculated for the respective bending directions. For example, if the factored design load in the positive transverse bending direction for a GFRP-reinforced concrete bridge deck was 140 kN-m/m, then the designer may opt for either Options 1, 3 or 4 from Table 9, depending on the value of f'_c specified by NS-PW for the concrete bridge deck and the designers choice of preferred concrete cover.

CHAPTER 4: RELIABILITY ASSESSMENT OF DECK OPTIONS IN NS

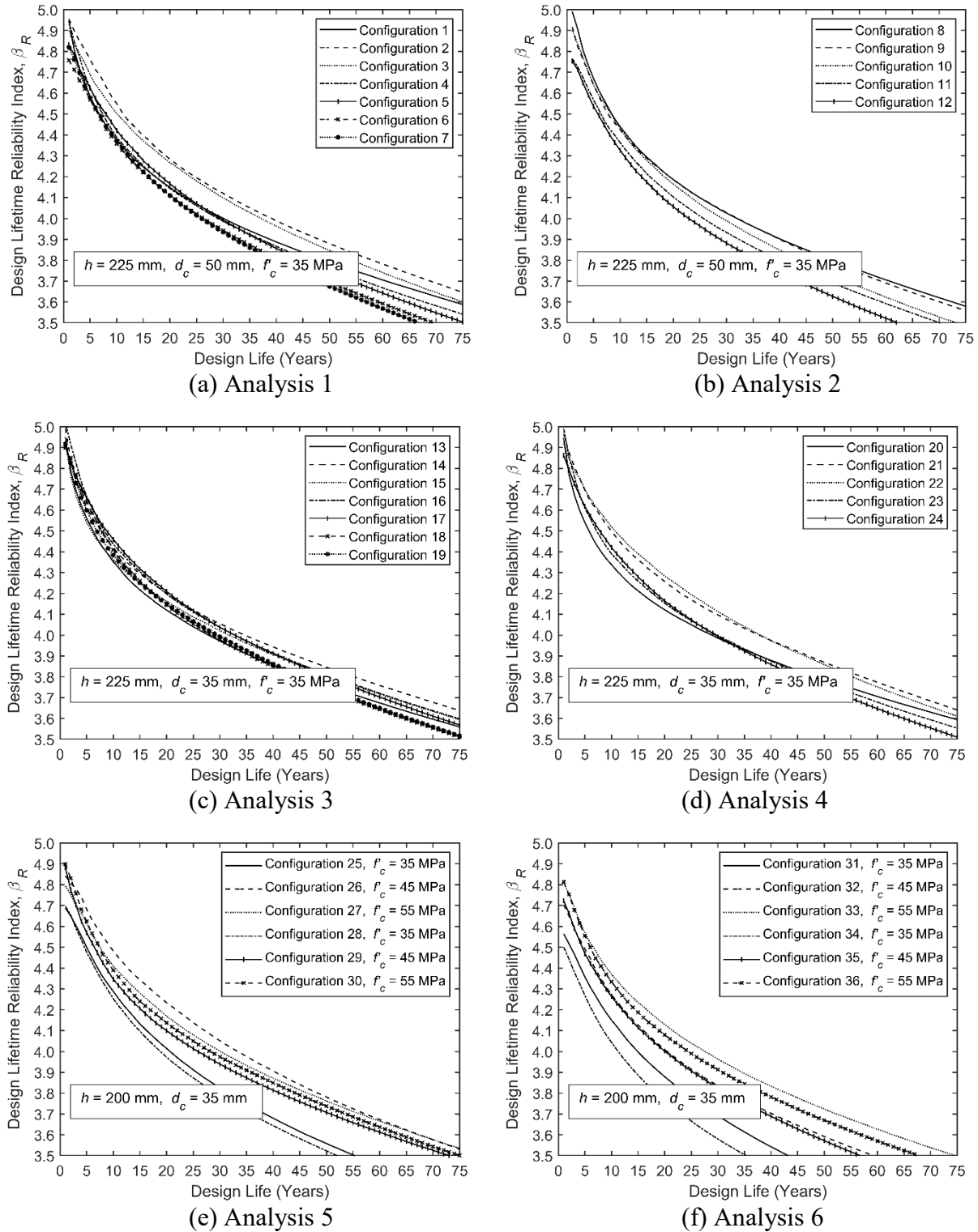


Figure 29. Design lifetime reliability index, β_R , for the six analyses of the parametric study.

Table 9. Section details for feasible durable alternative GFRP-reinforced bridge deck configurations for NS validated for a range of moment resistances.

Option Number	f'_c (MPa)	Minimum h (mm)	Maximum d_c (mm)	Range of Moment Resistances (kN-m/m)	
				Transverse Direction	Longitudinal Direction
1	35	225	35	≤ 150	≤ 120
2	35	225	50	≤ 130	≤ 90
3	45	225	35	≤ 150	≤ 120
4	45	225	50	≤ 150	≤ 120

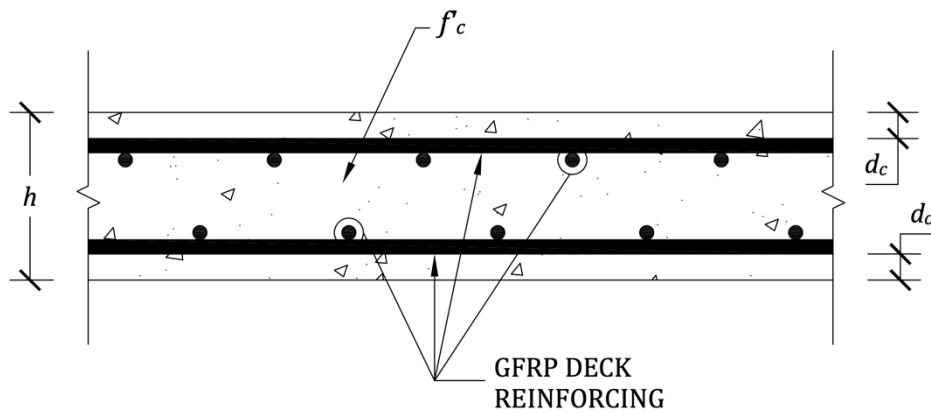


Figure 30. General schematic of GFRP-reinforced bridge deck variables for durable alternative deck designs.

CHAPTER 5 CONCLUSIONS AND RECOMMENDATIONS

5.1 SUMMARY

The durability of bridges is largely influenced by the durability of their decks which are directly subjected to high traffic loads and adverse environmental conditions. The use of GFRP-reinforced bridge deck sections is proving to be a durable solution to the durability issues faced by the steel-reinforced counterparts. The objective of this research programme is to provide Nova Scotia Public Works (NS-PW) with recommended durable reliability-based design alternatives for GFRP-reinforced bridge decks in NS.

The project was undertaken in two phases: development of a time-dependent reliability analysis framework for bridge decks (Phase I); and the application of the developed analysis framework to propose alternative bridge deck design for NS (Phase II). The framework of the reliability analysis in Phase I consisted of performing Monte Carlo simulations to solve the time-dependent reliability problem on MATLAB[®], consisting of fifteen random variables related to the load model, resistance model, and the methods of structural analysis. The statistical parameters for the following time-dependent random variables were calibrated for NS: live load moment, the GFRP tensile capacity, and the freeze-thaw compressive strength damage factor. The developed MATLAB[®] code is versatile and can be readily updated should more refined statistical parameters of the input variables become available. Phase II consisted of applying the framework to select existing bridge decks in NS and performing a comprehensive parametric study to propose durable design alternatives for bridge decks in NS.

The annual reliability index was calculated using a discrete probability of failure approach using Monte Carlo (MC) simulation and the design lifetime reliability index was also calculated as a function of time. A target reliability index of 3.50 for a 75-year design life was utilized to

CHAPTER 5: CONCLUSIONS AND RECOMMENDATIONS

assess the structural safety of the select bridge decks based on the range of reliability indexes used in calibrating CSA S6:19 and AASHTO LRFD 2017. A reliability analysis was performed on five NS bridges as basis for a comprehensive parametric study to examine the sensitivity of varying the following design parameters on the bridge deck reliability: the overall deck section depth, concrete cover thickness, and specified concrete compressive strength. The research conclusions and recommendations are summarized as follows:

5.2 CONCLUSIONS AND DESIGN RECOMMENDATIONS

The conclusions and design recommendations of applying the developed framework of time-dependent reliability analysis are presented for the two major contribution of the research:

1. Reliability Analysis of Select NS bridge Decks

- The five considered bridge deck details meet or exceed the structural safety requirements. The reliability indexes of the considered bridge decks ranged from 3.58 – 3.90 for a 75-year design life, which are greater than the target reliability index of 3.50 for the design lifetime.
- The bridge's reliability decreased with time as the moment resistance decreased and the live load moment demand increased with time.
- The reduction in GFRP tensile strength and the concrete compressive strength was approximately 6.15% and 7.11% respectively from year 1 to year 75.
- The results of the reliability analysis on NS bridge decks showed that the design choices made by designers for decks such as tension vs. compression-controlled failure mode or the choices in section and material properties can affect the reliability index of the bridge decks with time.

CHAPTER 5: CONCLUSIONS AND RECOMMENDATIONS

- The reliability of the tension-controlled bridge decks was consistently greater than the compression-controlled counterparts which indicates that the 1.5 factor specified in Clause 16.8.2.2 of CSA S6:19 is conservative. Further studies can be conducted to optimize the 1.5 factor.

2. Alternative Durable Bridge Deck Design Options for NS

- The results of the parametric study (36 unique bridge configurations) showed that the minimum deck section depth required to meet the target reliability index at a design lifetime of 75 years for moment resistances up to 150 kN-m/m and 120 kN-m/m for transverse and longitudinal moments respectively is 225 mm, validated for specified concrete compressive strengths between 35 and 55 MPa.
- The reliability index of GFRP-reinforced bridge decks decreases with the increase in the amount of GFRP reinforcement used.
- The specification of the recommended alternative durable GFRP-reinforced bridge decks in NS that meet a reliability index of 3.50 for a 75-year design life are presented in Table 9. The durable alternative GFRP-reinforced bridge deck sections proposed in this project use reduced material and geometric properties which can lead to more economical designs.

5.3 RECOMMENDED FUTURE RESEARCH

- The framework of the time-dependent reliability analysis can be updated to consider the serviceability limits state to investigate the durability of decks based on other criteria such as crack width.
- The framework of the time-dependent reliability analysis approach can be updated in future to include a detailed cost analysis which will allow a cost optimization approach to help

CHAPTER 5: CONCLUSIONS AND RECOMMENDATIONS

designers make their design choices based both on satisfying durability criteria and cost optimization.

- The analysis to predict the time-dependent GFRP tensile capacity in the present research can be further improved, pending more testing and research on the service life performance of GFRP-reinforced sections.
- The framework of the time-dependent reliability analysis can be updated to assess the reliability and optimize the design of bridge decks reinforced using other type of composites and alloys.
- The framework of the time-dependent reliability analysis can be utilized to conduct a time-dependent reliability-based calibration of the GFRP material resistance factor in CSA S6:19 as opposed to the current approach of utilizing a regression-based factor to account for GFRP degradation in the calibration process.
- The framework of the time-dependent reliability analysis can be reconfigured to predict the service life of bridge decks to meet a predefined target reliability index.

BIBLIOGRAPHY

- Ali, A. H., Benmokrane, B., Mohamed, H. M., Manalo, A., & El-Safty, A. (2018). Statistical analysis and theoretical predictions of the tensile-strength retention of glass fiber-reinforced polymer bars based on resin type. *Journal of Composite Materials*, 52(21), 2929-2948.
- Ali, O., Bigaud, D., & Ferrier, E. (2012). Comparative durability analysis of CFRP-strengthened RC highway bridges. *Construction and building materials*, 30, 629-642.
- American Association of State Highway and Transportation Officials. (2017). *AASHTO LRFD bridge design specifications* (8th ed.). Washington, D.C.: Author.
- Anbang, L., Shanhua, X., Youde, W. (2017). Effects of frost-damage on mechanical performance of concrete. *Journal of Wuhan University of Technology – Material Science Edition*, 32, 129-135.
- Andrea, G. (2019). Capital Plan 2019-20. Finance and treasury board: Government of Nova Scotia, Canada. <https://novascotia.ca/news/release/?id=20190307001>
- ASTM C215. (2019). Standard Test Method for Fundamental Transverse, Longitudinal, and Torsional Resonant Frequencies of Concrete Specimens. *In Annual book of ASTM standards*, 4(2). Philadelphia, PA: American Society for Testing and Materials.
- Azizinamini, A., Power, E. H., Myers, G. F., Ozyildirim, H. C., Kline, E. S., Whitmore, D. W., & Mertz, D. R. (2014). *Design guide for bridges for service life* (No. SHRP 2 Report S2-R19A-RW-2).
- Benmokrane, B., & Ali, A. H. (2018). Durability and Long-Term Performance of Fiber-Reinforced Polymer as a New Civil Engineering Material. *In International Congress on Polymers in Concrete* (pp. 49-59). Springer, Cham.

BIBLIOGRAPHY

- Benmokrane, B., Brown, V. L., Ali, A. H., Mohamed, K., & Shield, C. (2020). Reconsideration of the Environmental Reduction Factor CE for GFRP Reinforcing Bars in Concrete Structures. *Journal of Composites for Construction*, 24(4), 06020001.
- Benmokrane, B., Newhook, J., Svecova, D., Mufti, A., & ISIS Canada. (2007). Reinforcing Concrete Structures with Fibre Reinforced Polymers. ISIS Canada.
- Beushausen, H., & Alexander, M. G. (2006). Failure mechanisms and tensile relaxation of bonded concrete overlays subjected to differential shrinkage. *Cement and concrete research*, 36(10), 1908-1914.
- Billing, J. R. (1984). Dynamic loading and testing of bridges in Ontario. *Canadian journal of civil engineering*, 11(4), 833-843.
- Binmerdah, A. (2018). *Service Life Prediction of Reinforced Concrete Bridge Deck*. [Master's thesis, Dalhousie University].
- Canadian Standards Association. (2019). *Canadian Highway Bridge Design Code* (CSA Standard No. S6-19). Mississauga, ON: Author.
- Canadian Standards Association. (2019). *Commentary on CSA-S6-19, Canadian Highway Bridge Design Code*, (CSA Standard No. S6.1-19). Mississauga, ON: Author.
- Canadian Standards Association. (2019). *Design of Concrete Structures* (CSA Standard No. A23.3-19). Mississauga, ON: Author.
- Castaldo, P., Gino, D., & Mancini, G. (2019). Safety formats for non-linear finite element analysis of reinforced concrete structures: discussion, comparison and proposals. *Engineering Structures*, 193, 136-153.
- Chen, F., & Qiao, P. (2015). Probabilistic damage modeling and service-life prediction of concrete under freeze-thaw action. *Materials and Structures*, 48, 2697-2711.

BIBLIOGRAPHY

- Chen, Y., Davalos, J. F., & Ray, I. (2006). Durability prediction for GFRP reinforcing bars using short-term data of accelerated aging tests. *Journal of Composites for Construction*, 10(4), 279-286.
- Chen, Y., Davalos, J. F., Ray, I., & Kim, H. Y. (2007). Accelerated aging tests for evaluations of durability performance of FRP reinforcing bars for concrete structures. *Composite Structures*, 78(1), 101-111.
- Daly, B., Benmokrane, B., Hfaied, N., Harchay, M., & Boukhili, R. (2007). Investigation of water absorption in pultruded composites containing fillers and low-profile additives. *Polymer composites*, 28(3), 355-364.
- Davalos, J. F., Chen, Y., & Ray, I. (2012). Long-term durability prediction models for GFRP bars in concrete environment. *Journal of Composite Materials*, 46(16), 1899-1914.
- Dejke, V. (1998). Durability of fibre reinforced polymers (FRP) as reinforcements in concrete structures - an update of knowledge and an overview of current research activities. *Technical Report, Department of Building Materials, Chalmers University of Technology* (pp. 98-108).
- Ebrahimi, K., Daiezadeh, M. J., Zakertabrizi, M., Zahmatkesh, F., & Korayem, A. H. (2018). A review of the impact of micro-and nanoparticles on freeze-thaw durability of hardened concrete: Mechanism perspective. *Construction and Building Materials*, 186, 1105-1113.
- El-Salakawy, E., Benmokrane, B., El-Ragaby, A., & Nadeau, D. (2005). Field investigation on the first bridge deck slab reinforced with glass FRP bars constructed in Canada. *Journal of composites for construction*, 9(6), 470-479.
- Esmacili, Y., Eslami, A., Newhook, J., & Benmokrane, B. (2020). Performance of GFRP-Reinforced Concrete Beams Subjected to High-Sustained Load and Natural Aging for 10 Years. *Journal of Composites for Construction*, 24(5), 04020054.

BIBLIOGRAPHY

- Esmaeili, Y., Mohamed, K., Newhook, J., & Benmokrane, B. (2021). Assessment of creep rupture and long-term performance of GFRP bars subjected to different environmental exposure conditions under high sustained loads. *Construction and Building Materials*, *300*, 124327.
- Federal Highway Administration. (2014). *FHWA Traffic Monitoring Guide*. Washington, D.C.: Author.
- Fenton, G. A., & Griffiths, D. V. (2008). *Risk assessment in geotechnical engineering* (Vol. 461). New York: John Wiley & Sons.
- Gardoni, P., Der Kiureghian, A., & Mosalam, K. M. (2002). Probabilistic capacity models and fragility estimates for reinforced concrete columns based on experimental observations. *Journal of Engineering Mechanics*, *128*(10), 1024-1038.
- Gardoni, P., Nemati, K. M., & Noguchi, T. (2007). Bayesian statistical framework to construct probabilistic models for the elastic modulus of concrete. *Journal of materials in civil engineering*, *19*(10), 898-905.
- Ghodoosi, F., Bagchi, A., & Zayed, T. (2015). System-level deterioration model for reinforced concrete bridge decks. *Journal of Bridge Engineering*, *20*(5), 04014081.
- Gong, C., & Frangopol, D. M. (2019). An efficient time-dependent reliability method. *Structural Safety*, *81*, 101864.
- Huang, J. W. (2011). Sustained Load Effect on GFRP Bar Reinforced Concrete Deck. In *Applied Mechanics and Materials*, *99*, 1251-1254.
- Huang, J., & Aboutaha, R. (2010). Environmental reduction factors for GFRP bars used as concrete reinforcement: new scientific approach. *Journal of Composites for Construction*, *14*(5), 479-486.

BIBLIOGRAPHY

- Idemudia, D., Newhook, J., & Oudah, F. (2021). Design and performance of GFRP reinforced bridge decks in Nova Scotia – Preliminary Analysis. In *Proceedings of the 8th International Conference on Advanced Composite Materials in Bridges and Structures (ACMBS-8), Sherbrooke, QC* (pp. 521-527).
- ISIS, Design Manual No. 3. (2007). Reinforcing Concrete Structures with Fibre Reinforced Polymers. *Intelligent Sensing for Innovative Structures Canada*, 449-458.
- Jin, Q., Chen, P., Gao, Y., Du, A., Liu, D., & Sun, L. (2020). Tensile strength and degradation of GFRP bars under combined effects of mechanical load and alkaline solution. *Materials*, 13(16), 3533.
- Kennedy, D. L., Gagnon, D. P., Allen, D. E., & MacGregor, J. G. (1992). Canadian highway bridge evaluation: load and resistance factors. *Canadian Journal of Civil Engineering*, 19(6), 992-1006.
- Khanna, O. S., Mufti, A. A., & Bakht, B. (2000). Experimental investigation of the role of reinforcement in the strength of concrete deck slabs. *Canadian Journal of Civil Engineering*, 27(3), 475-480.
- Kim, Y. H., Trejo, D., & Gardoni, P. (2012). Time-variant reliability analysis and flexural design of GFRP-reinforced bridge decks. *Journal of Composites for Construction*, 16(4), 359-370.
- Kroetz, H. M., Moustapha, M., Beck, A. T., & Sudret, B. (2020). A two-level Kriging-based approach with active learning for solving time-variant risk optimization problems. *Reliability Engineering & System Safety*, 203, 107033.
- Lee, B. J., Kee, S.H., Oh, T., & Kim, Y. Y. (2017). Evaluating the dynamic elastic modulus of concrete using shear-wave velocity measurements. *Advances in Materials Science and Engineering*, 1651753.

BIBLIOGRAPHY

- Li, J., Xu, W., Cao, J., Lin, L., Guan, Y. (1999). Study on the mechanism of concrete destruction under frost action. *Journal of Hydraulic Engineering*, 1, 412–419.
- Lopez, R. H., & Beck, A. T. (2012). Reliability-based design optimization strategies based on FORM: a review. *Journal of the Brazilian Society of Mechanical Sciences and Engineering*, 34, 506-514.
- Lounis, Z., & Daigle, L. (2008). Reliability-based decision support tool for life cycle design and management of highway bridge decks. *In Annual Conference of the Transportation Association of Canada*, 1-19.
- Melchers, R. E., & Beck, A. T. (2018). *Structural reliability analysis and prediction*. Hoboken, NJ: John Wiley & Sons.
- Mufti, A. A., Newhook, J. P., & Khanna, S. O. (1999). Predicting the Punching Behaviour of Reinforced Concrete Bridge Decks. *Proceedings of the Canadian Society for Civil Engineering Annual Conference, Regina, 1*, 325-334.
- Mufti, A., Onofrei, M., Benmokrane, B., Banthia, N., Boulfiza, M., Newhook, J., ... & Brett, P. (2005). Durability of GFRP reinforced concrete in field structures. *In Proceedings of the 7th International Symposium on Fiber-Reinforced Polymer Reinforcement for Reinforced Concrete Structures (FRPRCS-7), Kansas City, MO* (pp. 6-9).
- Nowak, A. S. (2004). System reliability models for bridge structures. *Bulletin of the Polish Academy of Sciences: Technical Sciences*, 321-328.
- Nowak, A. S., & Szerszen, M. M. (1998). Bridge load and resistance models. *Engineering structures*, 20(11), 985-990.
- Nowak, A. S., & Szerszen, M. M. (2003). Calibration of design code for buildings (ACI 318): Part 1-Statistical models for resistance. *ACI Structural Journal*, 100(3), 377-382.

BIBLIOGRAPHY

- Oudah, F. (2022). Time-dependent reliability-based charts to evaluate the structural safety of RC wharf decks exposed to corrosion and freeze-thaw effect. *Engineering Structures*. (under review).
- Oudah, F., & Hassan, A. (2022). Reliability of compression-controlled FRP RC flexural members designed using North American codes and standards: Comparison and FRP material resistance/strength reduction factor calibration. *ACI SP publication*. (Accepted)
- Richards, W., & Daigle, R. (2015). *Scenarios and guidance for adaptation to climate change and sea level rise-NS and PEI municipalities*. Atlantic Climate Adaptation Solutions Association = Solutions d'adaptation aux changements climatiques pour l'Atlantique.
- Robert, M., Cousin, P., & Benmokrane, B. (2009). Durability of GFRP reinforcing bars embedded in moist concrete. *Journal of Composites for Construction*, 13(2), 66-73.
- Roubos, A. A., Allaix, D. L., Schweckendiek, T., Steenbergen, R. D., & Jonkman, S. N. (2020). Time-dependent reliability analysis of service-proven quay walls subject to corrosion-induced degradation. *Reliability Engineering & System Safety*, 203, 107085.
- Schmidt, F., Jacob, B., & Domprobst, F. (2016). Investigation of truck weights and dimensions using WIM data. *Transportation Research Procedia*, 14, 811-819.
- Shafei, B., Phares, B., & Saini, D. (2020). *Field investigation of bridge deck reinforced with glass fiber reinforced polymer (GFRP) rebar* (No. MN 2020-05).
- Shield, C. K., Galambos, T. V., & Gulbrandsen, P. (2011). On the history and reliability of the flexural strength of FRP reinforced concrete members in ACI 440.1 R. *Special Publication*, 275, 1-18.
- Sivakumar, B., Ghosn, M., & Moses, F. (2011). *Protocols for collecting and using traffic data in bridge design* (Vol. 683). Transportation Research Board.

BIBLIOGRAPHY

- Slobbe, A., Rózsás, Á., Allaix, D. L., & Bigaj-van Vliet, A. (2020). On the value of a reliability-based nonlinear finite element analysis approach in the assessment of concrete structures. *Structural Concrete*, 21(1), 32-47.
- Stewart, M. G., & Rosowsky, D. V. (1998). Time-dependent reliability of deteriorating reinforced concrete bridge decks. *Structural safety*, 20(1), 91-109.
- Sudret, B. (2008). Analytical derivation of the outcrossing rate in time-variant reliability problems. *Structure and Infrastructure Engineering*, 4(5), 353-362.
- Tannous, F. E. (1998). Environmental effects on the mechanical properties of E-glass FRP rebars. *ACI Materials Journal*, 95(2), 87–100.
- Todeschini, C. E., Bianchini, A. C., & Kesler, C. E. (1964). Behavior of concrete columns reinforced with high strength steels. *ACI Journal Proceedings*, 61(6), 701–716.
- Trejo, D., Gardoni, P., Kim, J. J., & Zidek, J. (2009). Long-term performance of GFRP reinforcement: technical report (No. FHWA/TX-09/0-6069-1). *Texas Transportation Institute*.
- Wagner, S., Hüffer, T., Klöckner, P., Wehrhahn, M., Hofmann, T., & Reemtsma, T. (2018). Tire wear particles in the aquatic environment-a review on generation, analysis, occurrence, fate and effects. *Water research*, 139, 83-100.

APPENDIX A: DETAILED DESIGN CHECK OF SELECT NS BRIDGE DECKS

This Appendix describes the approach for calculating the loads, resistances, and methods of analysis for bridge decks and provides a detailed sample calculation for the structural design checks. The data collected from the five select bridges identified in Section 4.2 were analysed to determine the demand, capacity, and utilization ratios (U.R.) for various parts of the bridge deck. The analysis basis used for the bridge deck design check includes:

- All analyses and design checks were performed in accordance with the CSA S6:19.
- Project details and designs were extracted from approved and stamped engineering design drawings. The details were provided by NS-PW.
- Design loads were taken from methods specified in Section 3 (Loads) of CSA S6:19.
- The Flexural Method of evaluating bridge decks as described in Section 5 (Methods of analysis) of CSA S6:19 was used to evaluate the flexural capacity of the bridge decks.
- Methods pertaining to the design of concrete structures and FRP-reinforced bridge decks were in accordance with Sections 8 (Concrete structures) and 16 (Fibre-reinforced structures) respectively of CSA S6:19.
- Some of the variables were calculated based on equations presented in ISIS Design Manual No. 3 (2007), while maintaining accordance with CSA S6:19.

A1. DEAD LOAD

Dead loads according to CSA S6:19 includes the weight of all components of the structure and appendages fixed to the structure, including wearing surface, earth cover, and utilities. Table 3.4 of CSA S6:19 (2019) shows the unit material weights for calculating dead loads in the absence of

APPENDIX A: DETAILED DESIGN CHECK OF SELECT NS BRIDGE DECKS

more precise information. The unit weight of reinforced concrete used for the self-weight and bituminous wearing surface were 24.0 kN/m^3 and 23.5 kN/m^3 respectively.

A.2 LIVE LOAD

Traffic Loads –The traffic loads are idealized by a five-axle truck known as the CL-W truck where the W number indicates the gross load of the truck in kilonewtons. Figure A1 shows the wheel and axle loads (shown in terms of W), wheel spacing, weight distribution, and clearance envelopes for the CL-625 Truck. The CL-W loading consists of the CL-W truck shown in Figure A1 or the CL-W Lane Load shown in Figure A2 per Clauses 3.8.3.1.2 and 3.8.3.1.3, respectively, of CSA S6:19 allows designers to use a loading that is lesser or greater than CL-625 only where justified by traffic conditions and approved.

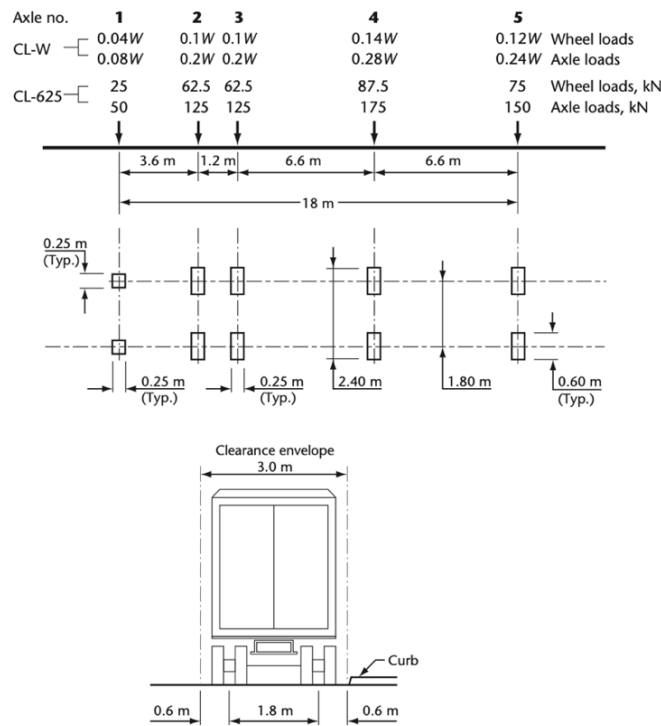


Figure A1. CL-W Truck (CSA S6:19, 2019).

APPENDIX A: DETAILED DESIGN CHECK OF SELECT NS BRIDGE DECKS

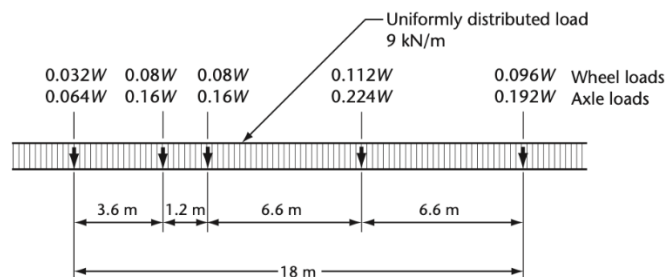


Figure A2. CL-W Lane Load (CSA S6:19, 2019).

Dynamic Load Allowance (DLA) – CSA S6:19 recognizes that the loads from the design trucks are transitional and impose a dynamic effect on bridges, therefore the dynamic effect is applied to the structure using a Dynamic Load Allowance (DLA). The DLA is applied to the CL-W Truck and is included in loads on the superstructure and loads transferred from the superstructure to the substructure but not in loads transferred to footings that are surrounded with earth or parts of piles below ground. CSA S6:19 (2019) states that for components other than buried structures, the DLA is 0.5 for deck joints, 0.4 where only one axle of the CL-W Truck is used, 0.3 where two axles of the CL-W Truck are used, or 0.25 where three or more of the axles of the axles of the CL-W Truck are used per Clause 3.8.4.5.3. Therefore, a DLA of 0.4 was used since the design of bridge decks is based on the maximum wheel load of the CL-W design truck.

Barrier Loads – The traffic barriers on bridge decks are a source of loading classified under live loads. CSA S6:19 (2019) states that the transverse, longitudinal, and vertical loads shall be applied simultaneously as specified in Table A1 and the loads shall be used for the design of traffic barrier anchorages and decks only per Clause 3.8.8.1. The barrier loads on railings are not considered to act simultaneously with the curb load and the dynamic load allowance shall not be applied to the barrier loads.

APPENDIX A: DETAILED DESIGN CHECK OF SELECT NS BRIDGE DECKS

Table A1. Loads on traffic barriers (CSA S6:19, 2019).

Performance level	Transverse load, kN	Longitudinal load, kN	Vertical load, kN
TL-1 (Test Level 1)	25	10	10
TL-2 (Test Level 2)	50	20	10
TL-4 (Test Level 4)	100	30	30
TL-5 (Test Level 5)	210	70	90

A.3 METHODS OF ANALYSIS

According to Clause 5.7.1.2 of CSA S6:19 (2019), concrete deck slabs that are supported on longitudinal girders may be analysed for transverse bending using the simplified elastic method in which the maximum transverse moment intensity in the portion of the deck slab between the outer girders due to the CL-625 Truck shall be determined as described in the following paragraphs.

Other than portions of the deck slab within 1.0 m of a transverse free edge, the deck slab is designed for transverse live load moment intensity, M_{TL} , for simple span deck slabs using Equation A1 and for deck slabs continuous over three or more supports, the maximum bending moment, either positive or negative, is assumed to be 80% of that determined for a simple span calculated in Equation A1. These moments are required to be increased by the dynamic load allowance for a single axle, as specified in Clause 3.8.4.5.3 (CSA S6:19, 2019).

$$M_{TL} = \frac{(S_e + 0.6)P}{10}, (\text{kN} \cdot \text{m}/\text{m}) \quad (\text{A1})$$

where S_e is the equivalent transverse span in metres, which can be determined from Figure A2 for different types of superstructures; P shall be 87.5 kN, the maximum wheel load of the CL-625 Truck.

APPENDIX A: DETAILED DESIGN CHECK OF SELECT NS BRIDGE DECKS

For portions of a deck slab within 1.0 m of a transverse free edge, the reinforcing is required to be twice the level of the transverse reinforcement in the other portions of the deck slab, unless equivalent local stiffening by diaphragms is provided. The longitudinal moment intensity, M_{LL} , for distribution of wheel loads to be used with the transverse moment intensity for portions of the deck slab that are not within 1.0 m of a transverse free edge is taken as $120/(S_e^{0.5})\%$, but not to exceed 67% of the maximum transverse moment intensity and shall be applied as a positive moment that produces tension in the bottom portion of the deck slab (CSA S6:19, 2019). CSA S6:19 (2019) also states that the longitudinal reinforcement necessary to resist the longitudinal moment shall be used in the centre half of the span. The percentage may be reduced by 50% in the end quarters of the span.

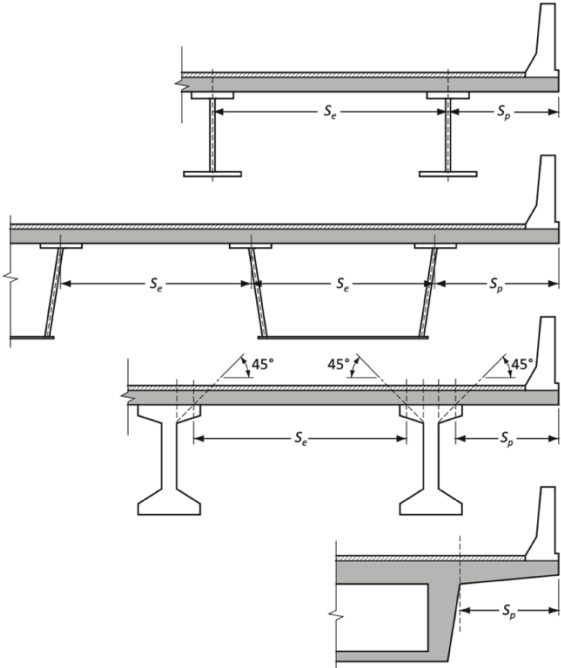


Figure A3. Definition of S_p and S_e (CSA S6:19, 2019).

Clause 5.7.1.3 of CSA S6:19 states the provisions for designing for the transverse moments in the cantilever portion of the deck. The intensity of transverse moment, including dynamic load

APPENDIX A: DETAILED DESIGN CHECK OF SELECT NS BRIDGE DECKS

allowance, shall be obtained from Table 5.15 of CSA S6:19 (2019) for unstiffened and edge stiffened cantilever slabs, where r_t is the ratio of smallest slab thickness to the largest slab thickness of the bridge deck. Linear interpolation can be used to find the intensity for longitudinal length of deck overhang in Table 5.15 of CSA S6:19 are shown in terms of and can be linearly interpolated for lengths between the specified values. CSA S6:19 (2019) specifies that for portions of the cantilever slab that are within a distance S_p of transverse free edge of the slab but not less than 1.0 m, the transverse moment intensity shall be assumed to be $2M_y$ unless a more rigorous analysis is used.

A.4 RESISTANCE

According to Clause 16.8.2.2 of CSA S6:19 (2019), the factored resistance, M_r , shall be at least 50% greater than the cracking moment, M_{cr} and that if the ULS design of the section is governed by FRP rupture for non-prestressed sections, M_r shall be greater than $1.5M_f$. Clause 8.8.4.4 states that a structural component is said to be cracked when the moment at a section is such that the tensile stress of the cracking stress of concrete, f_{cr} , calculated using Equation A2 for normal-density concrete is induced in the concrete.

$$f_{cr} = 0.4\sqrt{f'_c} \quad (\text{A2})$$

The value of the factored resistance, M_r , is calculated in accordance with the assumptions made for the ultimate limit state in Clause 8.8.3 of CSA S6:19 (2019) in addition to the conditions of equilibrium and compatibility of strains.

A.5 CRACK WIDTH

Clause 16.8.2.3 of CSA S6:19 (2019) states that the crack width, w_{cr} , for FRP-reinforced bridge decks is calculated using Equation A3.

$$w_{cr} = 2 \frac{f_{frp}}{E_{frp}} \frac{h_2}{h_1} k_b \sqrt{d_c^2 + (s/2)^2} \quad (A3)$$

where f_{frp} is the stress in the tension FRP reinforcement; E_{frp} is the modulus of elasticity of the FRP bar; d_c is the distance from the centroid of the tension reinforcement to the extreme tension surface of concrete; s is the spacing of the tensile reinforcement; h_1 is the distance from the centroid of tension reinforcement to the neutral axis; h_2 is the distance from the extreme flexural tension surface to the neutral axis; k_b is the coefficient depending on bond between FRP and concrete. The value of k_b is determined by using the test method in CSA S806, but in the absence of test data may be taken as 0.8 for sand-coated and 1.0 for deformed FRP bars.

The design check results for all five bridges are summarised in the form of a Utilization Ratios (U.R.), which is the demand-to-capacity ratio, in Table A2 followed by a detailed sample calculation for Bridge 1.

Table A2. Utilization Ratios (U.R.) for the five analysed bridge decks.

Span	Loading Direction	Utilization Ratio for Bridge Deck					Mean	Standard Deviation
		1	2	3	4	5		
Interior Spans	Negative Transverse Bending	0.68	0.43	0.36	0.48	0.54	0.50	0.121
	Positive Transverse Bending	0.44	0.27	0.32	0.67	0.44	0.43	0.154
	Positive Longitudinal Bending	0.45	0.30	0.25	0.51	0.47	0.40	0.114
Exterior Spans	Negative Transverse Bending	0.67	0.57	0.40	0.53	0.51	0.54	0.098
	Negative Transverse Bending - Barrier Load	0.66	0.60	0.47	0.58	0.54	0.57	0.071
Interior Spans	Crack width: Negative Transverse	1.54	0.99	0.88	1.34	0.88	1.13	0.299

APPENDIX A: DETAILED DESIGN CHECK OF SELECT NS BRIDGE DECKS

Span	Loading Direction	Utilization Ratio for Bridge Deck					Mean	Standard Deviation
		1	2	3	4	5		
	Crack width: Positive Transverse	0.50	0.22	0.68	0.60	0.55	0.51	0.175
	Crack width: Positive Longitudinal	1.01	0.71	0.63	1.20	1.09	0.93	0.247
Exterior Spans	Crack width: Negative Transverse	0.81	0.70	0.51	0.45	0.46	0.59	0.161

A.6 SAMPLE CALCULATIONS FOR BRIDGE 1

General Bridge Information

Bridge number = 1

Bridge name = Great village river bridge

Span type = Single span

Deck type = Continuous deck (Not edge stiffened)

Girder type = Concrete NEBT

Abutment type = Integral

Span length, $L = 36,000 \text{ mm}$

Girder spacing, $l = 3157 \text{ mm}$

Girder flange width, $f_w = 510 \text{ mm}$

Girder flange thickness, $f_t = 135 \text{ mm}$

Girder web thickness, $w_t = 180 \text{ mm}$

Deck width, $w_d = 12,000 \text{ mm}$

Deck section depth, $h = 225 \text{ mm}$

Deck specified concrete compressive strength, $f'_c = 45 \text{ MPa}$

Concrete unit weight, $\gamma_c = 24 \text{ kN/m}^3$ (Table 3.4, CSA S6:19)

Asphalt (wearing surface) thickness, $h_{ws} = 80 \text{ mm}$

Asphalt unit weight, $\gamma_{ws} = 23.5 \text{ kN/m}^2$ (Table 3.4, CSA S6:19)

Maximum length of cantilever, $l_e = 1930 \text{ mm}$

Maximum axle load, $P = 87.5 \text{ kN}$ (Clause 3.8.3.1.2, CSA S6:19)

Maximum strain in concrete, $e_{cu} = 0.0035$ (Clause 8.8.3, CSA S6:19)

Deck unit width, $b = 1000 \text{ mm}$

APPENDIX A: DETAILED DESIGN CHECK OF SELECT NS BRIDGE DECKS

Reinforcement Information (GFRP)

Table A3. Reinforcement information for Bridge 1.

Bar Number	Bar diameter, d_{bar} (mm)	Bar area, A_{bar} (mm ²)	f_{frpu} (MPa)	E_{frpu} (GPa)	ϵ_{frpu}
5	15.9	197.9	1184	62	0.019097
6	19.1	285.0	1105	62	0.017823
7	22.2	387.9	1069	62	0.017242
8	25.6	506.7	1000	62	0.016129

Top cover, $d_{c_{top}} = 50$ mm

Bottom cover, $d_{c_{bot}} = 30$ mm

Load, Resistance and Material Factors

$$\phi_c = 0.75 \text{ (Table 8.1, CSA S6:19)}$$

$$\phi_{frp} = 0.65 \text{ (Table 16.2, CSA S6:19)}$$

$$\alpha_1 = 0.85 - 0.0015(45) = 0.78 \text{ (Clause 8.8.3, CSA S6,19)}$$

$$\beta_1 = 0.97 - 0.0025(45) = 0.86 \text{ (Clause 8.8.3, CSA S6,19)}$$

Loads (Clause 5.7.1.2, CSA S6:19)

Interior Spans

$$l = 3.157 \text{ m}$$

$$S_e = l - 2\left(\frac{w_t}{2}\right) - 2(f_t) = 3.157 - 2\left(\frac{0.180}{2}\right) - 2(0.135) = 2.71 \text{ m}$$

$$DLA = 0.4 \text{ (Clause 3.8.4.5.3, CSA S6:19)}$$

APPENDIX A: DETAILED DESIGN CHECK OF SELECT NS BRIDGE DECKS

Self-weight Dead Load

$$w_{sw} = h \gamma_c = (0.225)(24) = 5.40 \frac{kN}{m}$$

$$M_{D_{sw}}^+ = \frac{w_{sw} l^2}{16} = \frac{(5.40)(3.157)^2}{16} = 3.36 \text{ kN} - m/m$$

$$M_{D_{sw}}^- = \frac{w_{sw} l^2}{11} = \frac{(5.40)(3.157)^2}{11} = 4.89 \text{ kN} - m/m$$

Wearing Surface Dead Load

$$w_{ws} = h_{ws} \gamma_{ws} = (0.080)(23.5) = 1.88 \frac{kN}{m}$$

$$M_{D_{ws}}^+ = \frac{w_{ws} l^2}{16} = \frac{(1.88)(3.157)^2}{16} = 1.17 \text{ kN} - m/m$$

$$M_{D_{ws}}^- = \frac{w_{ws} l^2}{11} = \frac{(1.88)(3.157)^2}{11} = 1.70 \text{ kN} - m/m$$

Live Load

$$M_{TL} = \frac{0.8(S_e + 0.6) P}{10} = \frac{0.8(2.71 + 0.6) P}{10} = 23.15 \text{ kN} - m/m$$

$$M_{TL,DLA} = M_{TL}(1 + DLA) = (23.15)(1 + (0.4)) = 32.41 \text{ kN} - m/m$$

$$\begin{aligned} M_{LL,DLA} &= \left(\frac{120}{S_e^{0.5}} \% < 67\% \right) * M_{TL,DLA} = \left(\frac{120}{2.71^{0.5}} \% = 73 \not< 67\% \right) * 32.41 = 67\% * 32.41 \\ &= 21.71 \text{ kN} - m/m \end{aligned}$$

APPENDIX A: DETAILED DESIGN CHECK OF SELECT NS BRIDGE DECKS

Load Combination (Table 3.1, 3.2 & 3.3, CSA S6:19)

$$\text{ULS Combination 1} = 1.2 M_{D_{sw}} + 1.5 M_{D_{sw}} + 1.7 M_L$$

$$\text{Positive Transverse Moment} = 1.2(3.36) + 1.5(1.17) + 1.7(32.41) = 61 \text{ kN} - \text{m/m}$$

$$\text{Negative Transverse Moment} = 1.2(4.89) + 1.5(1.70) + 1.7(32.41) = 64 \text{ kN} - \text{m/m}$$

$$\text{Positive Longitudinal Moment} = 1.2(3.36) + 1.5(1.17) + 1.7(21.71) = 43 \text{ kN} - \text{m/m}$$

Exterior Spans

$$l_e = 1.93 \text{ m}$$

$$S_p = l_e - \left(\frac{w_t}{2}\right) - f_t = 1.93 - \left(\frac{0.180}{2}\right) - 0.135 = 1.705 \text{ m}$$

Self-weight Dead Load

$$M_{D_{sw,cant}}^- = \frac{w_{sw} l_e^2}{11} = \frac{(5.40)(1.93)^2}{11} = 1.83 \text{ kN} - \text{m/m}$$

Wearing Surface Dead Load

$$M_{D_{ws,cant}}^- = \frac{w_{ws} l_e^2}{11} = \frac{(1.88)(1.93)^2}{11} = 0.64 \text{ kN} - \text{m/m}$$

Live Load

$r_t = 1.0$, for uniform deck thickness

$$S_p = 1.705 \text{ m}$$

Using interpolation on Table 5.15 of CSA S6:19, $M_y = 47.10 \text{ kN} - \text{m/m}$.

APPENDIX A: DETAILED DESIGN CHECK OF SELECT NS BRIDGE DECKS

Load Combination (Table 3.1, 3.2 & 3.3, CSA S6:19)

$$\text{ULS Combination 1} = 1.2 M_{D_{sw,cant}} + 1.5 M_{D_{sw,cant}} + 1.7 M_y$$

$$\text{Negative Transverse Moment} = 1.2(1.83) + 1.5(0.64) + 1.7(47.10) = 83 \text{ kN} - \text{m/m}$$

Barrier Load (Clause 3.8.8.1, CSA S6:19)

Test level = TL-4

Barrier width, $b_w = 425 \text{ mm}$

$$S_p = 1.705 \text{ m}$$

From Table 3.7, CSAS6-19:

Transverse load, $P_t = 100 \text{ kN}$

Longitudinal load, $P_l = 30 \text{ kN}$

Vertical load, $P_v = 30 \text{ kN}$

From Figure 12.1, CSA S6:19:

Height to P_t , $h_{tt} = 700 \text{ mm}$

Length of P_t , $h_t = 1050 \text{ mm}$

Length of P_v , $h_v = 5500 \text{ mm}$

Using a 1H:2V Load Distribution for the barrier loads:

$$h_{t,r} = 1.05 + 2 \left(\frac{0.7}{2} \right) = 1.75 \text{ m}$$

$$h_{v,r} = 5.5 + 2 \left(\frac{1.5}{2} \right) = 7 \text{ m}$$

$$M_{Lb,t} = \left(\frac{P_t}{h_{t,r}} \right) (h_{tt}) = \left(\frac{100}{1.75} \right) (0.7) = 40 \text{ kN} - \text{m/m}$$

$$M_{Lb,v} = \left(\frac{P_l}{h_{v,r}} \right) \left(S_p - \left(\frac{b_w}{2} \right) \right) = \left(\frac{30}{7} \right) \left(1.71 - \left(\frac{0.425}{2} \right) \right) = 6.42 \text{ kN} - \text{m/m}$$

APPENDIX A: DETAILED DESIGN CHECK OF SELECT NS BRIDGE DECKS

$$M_{Lb} = M_{Lb,t} + M_{Lb,v} = 40 + 6.42 = 46.42 \text{ kN} - \text{m/m}$$

Recall,

$$M_{D_{sw,cant}}^- = 1.83 \text{ kN} - \text{m/m}$$

$$M_{D_{ws,cant}}^- = 0.64 \text{ kN} - \text{m/m}$$

Then using ULS Combination 1,

$$M_{f,b} = 1.2(1.83) + 1.5(0.64) + 1.7(46.42) = 82.07 \text{ kN} - \text{m/m}$$

Resistances (Clause 8.8 & Clause 16.8, CSA S6:19)

Positive Transverse Bending (BLL)

Bar spacing, $s = 200 \text{ mm}$

$$d_{bar} = 19.1 \text{ mm}$$

$$d = h - d_{c_{bot}} - \frac{d_{bar}}{2} = 225 - 30 - \frac{19.1}{2} = 185.5 \text{ mm}$$

$$A_{frp} = \frac{A_{bar} b}{s} = \frac{(285)(1000)}{200} = 1425 \text{ mm}^2$$

$$\rho_{frp} = \frac{A_{frp}}{b d} = \frac{1425}{(1000)(185.5)} = 0.007682$$

Using Equation 6.6 from ISIS Design Manual No. 3, 2007:

$$\rho_{bal} = \frac{\alpha_1 \beta_1 \phi_c f'_c \left(\frac{\varepsilon_{cu}}{\varepsilon_{cu} + \varepsilon_{frpu}} \right)}{\phi_{frp} f_{frpu}}$$

$$\rho_{bal} = \frac{(0.78)(0.86)(0.75)(45)}{(0.65)(1105)} \left(\frac{0.0035}{0.0035 + 0.017823} \right) = 0.00518$$

$\rho_{frp} > \rho_{bal} \therefore$ Section is Over-reinforced

APPENDIX A: DETAILED DESIGN CHECK OF SELECT NS BRIDGE DECKS

Using Equation 6.9 from ISIS Design Manual No. 3, 2007:

$$f_{frp} = 0.5 E_{frpu} \varepsilon_{cu} \left(\left(1 + \frac{4 \alpha_1 \beta_1 \phi_c f'_c}{\rho_{frp} \phi_{frp} E_{frpu} \varepsilon_{cu}} \right)^{\frac{1}{2}} - 1 \right)$$

$$f_{frp} = 0.5 (62,000)(0.0035) \left(\left(1 + \frac{4 (0.78)(0.86)(0.75)(45)}{(0.00768)(0.65)(62,000)(0.0035)} \right)^{\frac{1}{2}} - 1 \right) = 889 \text{ MPa}$$

$$\varepsilon_{frp} = \frac{f_{frp}}{E_{frpu}} = \frac{889}{62,000} = 0.01434$$

$$c = \left(\frac{\varepsilon_{cu}}{\varepsilon_{cu} + \varepsilon_{frp}} \right) d = \left(\frac{0.0035}{0.0035 + 0.01434} \right) (185.5) = 36.40 \text{ mm}$$

$$\begin{aligned} M_r &= \phi_{frp} A_{frp} f_{frp} \left(d - \frac{\beta_1 c}{2} \right) = (0.65)(1425)(889) \left(185.5 - \frac{(0.86)(36.40)}{2} \right) \\ &= 140 \text{ kN} - \text{m/m} \end{aligned}$$

Negative Transverse Bending (TUL)

Bar spacing, $s = 250 \text{ mm}$

$$d_{bar} = 15.9 \text{ mm}$$

$$d = h - d_{ctop} - \frac{d_{bar}}{2} = 225 - 50 - \frac{15.9}{2} = 167.1 \text{ mm}$$

$$A_{frp} = \frac{A_{bar} b}{s} = \frac{(197.9)(1000)}{250} = 791.6 \text{ mm}^2$$

$$\rho_{frp} = \frac{A_{frp}}{b d} = \frac{791.6}{(1000)(167.1)} = 0.00474$$

Using Equation 6.6 from ISIS Design Manual No. 3, 2007:

$$\rho_{bal} = \frac{\alpha_1 \beta_1 \phi_c f'_c}{\phi_{frp} f_{frpu}} \left(\frac{c_u}{\varepsilon_{cu} + \varepsilon_{frpu}} \right)$$

APPENDIX A: DETAILED DESIGN CHECK OF SELECT NS BRIDGE DECKS

$$\rho_{bal} = \frac{(0.78)(0.86)(0.75)(45)}{(0.65)(1184)} \left(\frac{0.0035}{0.0035 + 0.019097} \right) = 0.00456$$

$\rho_{frp} > \rho_{bal} \therefore$ Section is Over-reinforced

Using Equation 6.9 from ISIS Design Manual No. 3, 2007:

$$f_{frp} = 0.5 E_{frpu} \varepsilon_{cu} \left(\left(1 + \frac{4 \alpha_1 \beta_1 \phi_c f'_c}{\rho_{frp} \phi_{frp} E_{frpu} \varepsilon_{cu}} \right)^{\frac{1}{2}} - 1 \right)$$

$$f_{frp} = 0.5(62,000)(0.0035) \left(\left(1 + \frac{4 (0.78)(0.86)(0.75)(45)}{(0.00474)(0.65)(62,000)(0.0035)} \right)^{\frac{1}{2}} - 1 \right) = 1159 \text{ MPa}$$

$$\varepsilon_{frp} = \frac{f_{frp}}{E_{frpu}} = \frac{1159}{62,000} = 0.01869$$

$$c = \left(\frac{\varepsilon_{cu}}{\varepsilon_{cu} + \varepsilon_{frp}} \right) d = \left(\frac{0.0035}{0.0035 + 0.01869} \right) (167.1) = 26.36 \text{ mm}$$

$$\begin{aligned} M_r &= \phi_{frp} A_{frp} f_{frp} \left(d - \frac{\beta_1 c}{2} \right) = (0.65)(791.6)(1159) \left(167.1 - \frac{(0.86)(26.36)}{2} \right) \\ &= 93 \text{ kN} - \text{m/m} \end{aligned}$$

Positive Longitudinal Bending BUL)

Bar spacing, $s = 248 \text{ mm}$

$d_{bar} = 15.9 \text{ mm}$

$$d = h - d_{cbot} - d_{bar,BLL} - \frac{d_{bar}}{2} = 225 - 30 - 19.1 - \frac{15.9}{2} = 168 \text{ mm}$$

$$A_{frp} = \frac{A_{bar} b}{s} = \frac{(197.9)(1000)}{248} = 797.98 \text{ mm}^2$$

$$\rho_{frp} = \frac{A_{frp}}{b d} = \frac{797.98}{(1000)(168)} = 0.00475$$

APPENDIX A: DETAILED DESIGN CHECK OF SELECT NS BRIDGE DECKS

Using Equation 6.6 from ISIS Design Manual No. 3, 2007:

$$\rho_{bal} = \frac{\alpha_1 \beta_1 \phi_c f'_c \left(\frac{\varepsilon_{cu}}{\varepsilon_{cu} + \varepsilon_{frpu}} \right)}{\phi_{frp} f_{frpu}}$$

$$\rho_{bal} = \frac{(0.78)(0.86)(0.75)(45)}{(0.65)(1184)} \left(\frac{0.0035}{0.0035 + 0.019097} \right) = 0.00456$$

$\rho_{frp} > \rho_{bal} \therefore$ Section is Over-reinforced

Using Equation 6.9 from ISIS Design Manual No. 3, 2007:

$$f_{frp} = 0.5 E_{frpu} \varepsilon_{cu} \left(\left(1 + \frac{4 \alpha_1 \beta_1 \phi_c f'_c}{\rho_{frp} \phi_{frp} E_{frpu} \varepsilon_{cu}} \right)^{\frac{1}{2}} - 1 \right)$$

$$f_{frp} = 0.5(62,000)(0.0035) \left(\left(1 + \frac{4 (0.78)(0.86)(0.75)(45)}{(0.00475)(0.65)(62,000)(0.0035)} \right)^{\frac{1}{2}} - 1 \right) = 1158 \text{ MPa}$$

$$\varepsilon_{frp} = \frac{f_{frp}}{E_{frpu}} = \frac{1158}{62,000} = 0.01868$$

$$c = \left(\frac{\varepsilon_{cu}}{\varepsilon_{cu} + \varepsilon_{frp}} \right) d = \left(\frac{0.0035}{0.0035 + 0.01868} \right) (168) = 26.52 \text{ mm}$$

$$M_r = \phi_{frp} A_{frp} f_{frp} \left(d - \frac{\beta_1 c}{2} \right) = (0.65)(797.98)(1159) \left(168 - \frac{(0.86)(26.52)}{2} \right)$$

$$= 94 \text{ kN} - \text{m/m}$$

Negative Transverse Bending (TUL) – Cantilever portions

Bar spacing, $s = 125 \text{ mm}$

$d_{bar} = 15.9 \text{ mm}$

APPENDIX A: DETAILED DESIGN CHECK OF SELECT NS BRIDGE DECKS

$$d = h - d_{c_{top}} - \frac{d_{bar}}{2} = 225 - 50 - \frac{15.9}{2} = 167.1 \text{ mm}$$

$$A_{frp} = \frac{A_{bar} b}{s} = \frac{(197.9)(1000)}{125} = 1583.2 \text{ mm}^2$$

$$\rho_{frp} = \frac{A_{frp}}{b d} = \frac{1583.2}{(1000)(167.1)} = 0.00947$$

Using Equation 6.6 from ISIS Design Manual No. 3, 2007:

$$\rho_{bal} = \frac{\alpha_1 \beta_1 \phi_c f'_c \left(\frac{\varepsilon_{cu}}{\varepsilon_{cu} + \varepsilon_{frpu}} \right)}{\phi_{frp} f_{frpu}}$$

$$\rho_{bal} = \frac{(0.78)(0.86)(0.75)(45)}{(0.65)(1184)} \left(\frac{0.0035}{0.0035 + 0.019097} \right) = 0.00456$$

$\rho_{frp} > \rho_{bal} \therefore$ Section is Over-reinforced

Using Equation 6.9 from ISIS Design Manual No. 3, 2007:

$$f_{frp} = 0.5 E_{frpu} \varepsilon_{cu} \left(\left(1 + \frac{4 \alpha_1 \beta_1 \phi_c f'_c}{\rho_{frp} \phi_{frp} E_{frpu} \varepsilon_{cu}} \right)^{\frac{1}{2}} - 1 \right)$$

$$f_{frp} = 0.5(62,000)(0.0035) \left(\left(1 + \frac{4 (0.78)(0.86)(0.75)(45)}{(0.00947)(0.65)(62,000)(0.0035)} \right)^{\frac{1}{2}} - 1 \right) = 791 \text{ MPa}$$

$$\varepsilon_{frp} = \frac{f_{frp}}{E_{frpu}} = \frac{1159}{62,000} = 0.01276$$

$$c = \left(\frac{\varepsilon_{cu}}{\varepsilon_{cu} + \varepsilon_{frp}} \right) d = \left(\frac{0.0035}{0.0035 + 0.01276} \right) (167.1) = 35.96 \text{ mm}$$

$$M_r = \phi_{frp} A_{frp} f_{frp} \left(d - \frac{\beta_1 c}{2} \right) = (0.65)(1583.2)(791) \left(167.1 - \frac{(0.86)(35.96)}{2} \right)$$

$$= 123 \text{ kN} - \text{m/m}$$

APPENDIX A: DETAILED DESIGN CHECK OF SELECT NS BRIDGE DECKS

$$f_{cr} = 0.4\sqrt{f'_c} = 0.4\sqrt{45} = 2.68 \text{ MPa}$$

Using Clause 8.8.4.4 from CSA S6:19:

$$M_{cr} = \frac{f_{cr}I}{y_t} = \frac{\left((2.68 * 10^6) \frac{(1)(0.225)^3}{12} \right)}{\frac{0.225}{2}} = 22.61 \text{ kN} - \text{m/m}$$

Checking Clause 16.8.2.2:

$$M_r \text{ for all sections} > 1.5 M_{cr} = 33.91 \text{ kN} - \text{m/m}$$

Cracking (Clause 16.8.2.3, CSA S6:19)

Check if $\varepsilon_{frp} > 0.0015$ and if $w_{cr} \leq 0.7 \text{ mm}$

$$w_{cr} = 2 \frac{f_{frp}}{E_{frp}} \frac{h_2}{h_1} k_b \sqrt{d_c^2 + (s/2)^2}$$

$$k_b = 0.8$$

Crack width: Positive Transverse Bending Direction

SLS Combination 1:

$$M_s = 1.0 M_{D_{sw}}^+ + 1.0 M_{D_{ws}}^+ + 0.9 M_{TL} = 1(3.36) + 1(1.17) + 0.9(23.15) = 25 \text{ kN} - \text{m/m}$$

Using Equations 7.1 to 7.5 from ISIS Design Manual No. 3, 2007:

$$E_c = 4500\sqrt{f'_c} = 4500\sqrt{45} = 30,187 \text{ MPa}$$

$$n_{frp} = \frac{E_{frp}}{E_c} = \frac{62,000}{30,187} = 2.05$$

$$\rho_{frp} = 0.00768$$

APPENDIX A: DETAILED DESIGN CHECK OF SELECT NS BRIDGE DECKS

$$k = \sqrt{(\rho_{frp} n_{frp})^2 + 2\rho_{frp} n_{frp} - \rho_{frp} n_{frp}}$$

$$= \sqrt{((0.00768)(2.05))^2 + 2(0.00768)(2.05) - (0.00768)(2.05)} = 0.163$$

$$j = 1 - \frac{k}{3} = 1 - \frac{0.163}{3} = 0.946 \text{ MPa}$$

$$f_{frp} = \frac{M_s}{A_{frp} j d} = \frac{25 \times 10^6}{(1425)(0.946)(185.5)} = 100 \text{ MPa}$$

$$f_{allowable} = 0.3 (f_{frpu}) = 0.3(1105) = 331.5 \text{ MPa}$$

$$f_{frp} = 100 \text{ MPa} < f_{allowable} = 331.5 \text{ MPa} \therefore f_{frp} = 100 \text{ MPa}$$

$$\varepsilon_{frp} = \frac{f_{frp}}{E_{frp}} = \frac{100}{62,000} = 0.00163$$

$$\therefore \varepsilon_{frp} > 0.0015$$

$$h_1 = d - kd = 185.5 - (0.163)(185.5) = 155.32 \text{ mm}$$

$$h_2 = h - kd = 225 - (0.163)(185.5) = 194.95 \text{ mm}$$

$$d_c = h - d = 225 - 185.5 = 39.5 \text{ mm}$$

$$w_{cr} = 2 \frac{f_{frp} h_2}{E_{frp} h_1} k_b \sqrt{d_c^2 + (s/2)^2} = 2 \frac{(100)(194.95)}{(62,000)(155.32)} (0.8) \sqrt{(39.5)^2 + \left(\frac{200}{2}\right)^2}$$

$$= 0.35 \text{ mm}$$

$$w_{cr} = 0.35 \text{ mm} < 0.7 \text{ mm}$$

Crack width: Negative Transverse Bending Direction

SLS Combination 1:

$$M_s = 1.0 M_{D_{sw}}^- + 1.0 M_{D_{ws}}^- + 0.9 M_{TL} = 1(4.89) + 1(1.70) + 0.9(23.15) = 27 \text{ kN} - \text{m/m}$$

APPENDIX A: DETAILED DESIGN CHECK OF SELECT NS BRIDGE DECKS

Using Equations 7.1 to 7.5 from ISIS Design Manual No. 3, 2007:

$$E_c = 4500\sqrt{f'_c} = 4500\sqrt{45} = 30,187 \text{ MPa}$$

$$n_{frp} = \frac{E_{frp}}{E_c} = \frac{62,000}{30,187} = 2.05$$

$$\rho_{frp} = 0.00474$$

$$k = \sqrt{(\rho_{frp}n_{frp})^2 + 2\rho_{frp}n_{frp} - \rho_{frp}n_{frp}}$$

$$= \sqrt{((0.00474)(2.05))^2 + 2(0.00474)(2.05) - (0.00474)(2.05)} = 0.130$$

$$j = 1 - \frac{k}{3} = 1 - \frac{0.130}{3} = 0.957 \text{ MPa}$$

$$f_{frp} = \frac{M_s}{A_{frp}jd} = \frac{25 \times 10^6}{(791.73)(0.957)(167.1)} = 217 \text{ MPa}$$

$$f_{allowable} = 0.3(f_{frpu}) = 0.3(1184) = 355.2 \text{ MPa}$$

$$f_{frp} = 217 \text{ MPa} < f_{allowable} = 355.2 \text{ MPa} \therefore f_{frp} = 217 \text{ MPa}$$

$$\varepsilon_{frp} = \frac{f_{frp}}{E_{frp}} = \frac{217}{62,000} = 0.0035$$

$$\therefore \varepsilon_{frp} > 0.0015$$

$$h_1 = d - kd = 167.1 - (0.130)(167.1) = 145.32 \text{ mm}$$

$$h_2 = h - kd = 225 - (0.130)(167.1) = 203.26 \text{ mm}$$

$$d_c = h - d = 225 - 167.1 = 57.94 \text{ mm}$$

$$w_{cr} = 2 \frac{f_{frp} h_2}{E_{frp} h_1} k_b \sqrt{d_c^2 + (s/2)^2} = 2 \frac{(217)(203.26)}{(62,000)(145.32)} (0.8) \sqrt{(57.94)^2 + \left(\frac{250}{2}\right)^2} = 1.08 \text{ m}$$

$$w_{cr} = 1.08 \text{ mm} \not\leq 0.7 \text{ mm}$$

Crack width: Positive Longitudinal Bending Direction

APPENDIX A: DETAILED DESIGN CHECK OF SELECT NS BRIDGE DECKS

SLS Combination 1:

$$M_s = 1.0 M_{D_{sw}}^+ + 1.0 M_{D_{ws}}^+ + 0.9 M_{LL} = 1(3.36) + 1(1.17) + 0.9(15.51) = 18 \text{ kN} - \text{m/m}$$

Using Equations 7.1 to 7.5 from ISIS Design Manual No. 3, 2007:

$$E_c = 4500\sqrt{f'_c} = 4500\sqrt{45} = 30,187 \text{ MPa}$$

$$n_{frp} = \frac{E_{frp}}{E_c} = \frac{62,000}{30,187} = 2.05$$

$$\rho_{frp} = 0.00475$$

$$k = \sqrt{(\rho_{frp}n_{frp})^2 + 2\rho_{frp}n_{frp} - \rho_{frp}n_{frp}}$$

$$= \sqrt{((0.00475)(2.05))^2 + 2(0.00475)(2.05) - (0.00475)(2.05)} = 0.130$$

$$j = 1 - \frac{k}{3} = 1 - \frac{0.130}{3} = 0.957 \text{ MPa}$$

$$f_{frp} = \frac{M_s}{A_{frp}jd} = \frac{18 \times 10^6}{(798.12)(0.957)(168)} = 144 \text{ MPa}$$

$$f_{allowable} = 0.3 (f_{frpu}) = 0.3(1184) = 355.2 \text{ MPa}$$

$$f_{frp} = 144 \text{ MPa} < f_{allowable} = 355.2 \text{ MPa} \therefore f_{frp} = 144 \text{ MPa}$$

$$\varepsilon_{frp} = \frac{f_{frp}}{E_{frp}} = \frac{144}{62,000} = 0.0023$$

$$\therefore \varepsilon_{frp} > 0.0015$$

$$h_1 = d - kd = 168 - (0.130)(168) = 146.12 \text{ mm}$$

$$h_2 = h - kd = 225 - (0.130)(168) = 203.11 \text{ mm}$$

$$d_c = h - d = 225 - 168 = 57 \text{ mm}$$

APPENDIX A: DETAILED DESIGN CHECK OF SELECT NS BRIDGE DECKS

$$w_{cr} = 2 \frac{f_{frp} h_2}{E_{frp} h_1} k_b \sqrt{d_c^2 + (s/2)^2} = 2 \frac{(144)(203.11)}{(62,000)(146.12)} (0.8) \sqrt{(57)^2 + \left(\frac{248}{2}\right)^2} = 0.71 \text{ mm}$$

$$w_{cr} = 0.71 \text{ mm} \leq 0.7 \text{ mm}$$

Crack width: Negative Transverse Bending Direction - Cantilever

SLS Combination 1:

$$\begin{aligned} M_s &= 1.0 M_{D_{sw,cant}}^- + 1.0 M_{D_{ws,cant}}^- + 0.9 M_y = 1(1.83) + 1(0.64) + 0.9(47.10) \\ &= 45 \text{ kN} - \text{m/m} \end{aligned}$$

Using Equations 7.1 to 7.5 from ISIS Design Manual No. 3, 2007:

$$E_c = 4500 \sqrt{f'_c} = 4500 \sqrt{45} = 30,187 \text{ MPa}$$

$$n_{frp} = \frac{E_{frp}}{E_c} = \frac{62,000}{30,187} = 2.05$$

$$\rho_{frp} = 0.00948$$

$$\begin{aligned} k &= \sqrt{(\rho_{frp} n_{frp})^2 + 2\rho_{frp} n_{frp} - \rho_{frp} n_{frp}} \\ &= \sqrt{((0.00948)(2.05))^2 + 2(0.00948)(2.05) - (0.00948)(2.05)} = 0.179 \end{aligned}$$

$$j = 1 - \frac{k}{3} = 1 - \frac{0.179}{3} = 0.940 \text{ MPa}$$

$$f_{frp} = \frac{M_s}{A_{frp} j d} = \frac{45 \times 10^6}{(1583.46)(0.940)(167.1)} = 180 \text{ MPa}$$

$$f_{allowable} = 0.3 (f_{frpu}) = 0.3(1184) = 355.2 \text{ MPa}$$

$$f_{frp} = 180 \text{ MPa} < f_{allowable} = 355.2 \text{ MPa} \therefore f_{frp} = 180 \text{ MPa}$$

APPENDIX A: DETAILED DESIGN CHECK OF SELECT NS BRIDGE DECKS

$$\varepsilon_{frp} = \frac{f_{frp}}{E_{frp}} = \frac{180}{62,000} = 0.0029$$

$$\therefore \varepsilon_{frp} > 0.0015$$

$$h_1 = d - kd = 167.1 - (0.179)(167.1) = 137.19 \text{ mm}$$

$$h_2 = h - kd = 225 - (0.179)(167.1) = 195.13 \text{ mm}$$

$$d_c = h - d = 225 - 167.1 = 57.94 \text{ mm}$$

$$w_{cr} = 2 \frac{f_{frp}}{E_{frp}} \frac{h_2}{h_1} k_b \sqrt{d_c^2 + (s/2)^2} = 2 \frac{(180)(195.13)}{(62,000)(137.19)} (0.8) \sqrt{(57.94)^2 + \left(\frac{125}{2}\right)^2}$$

$$= 0.56 \text{ mm}$$

$$w_{cr} = 0.56 \text{ mm} < 0.7 \text{ mm}$$

Utilization Ratios (U.R.) = M_r/M_f

Positive Transverse Bending, Interior = $61/140 = 0.44$

Negative Transverse Bending, Interior = $64/93 = 0.68$

Positive Longitudinal Bending, Interior = $43/94 = 0.45$

Negative Transverse Bending, Exterior = $83/123 = 0.67$

Negative Transverse Bending, Exterior Barrier Load = $82/123 = 0.67$

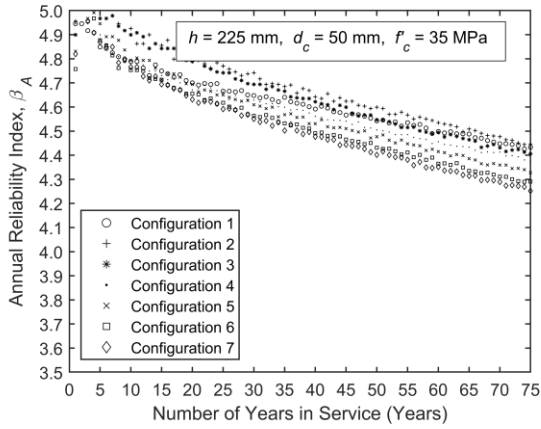
Crack width: Positive Transverse, Interior = $0.35/0.7 = 0.5$

Crack width: Negative Transverse, Interior = $1.08/0.7 = 1.54$

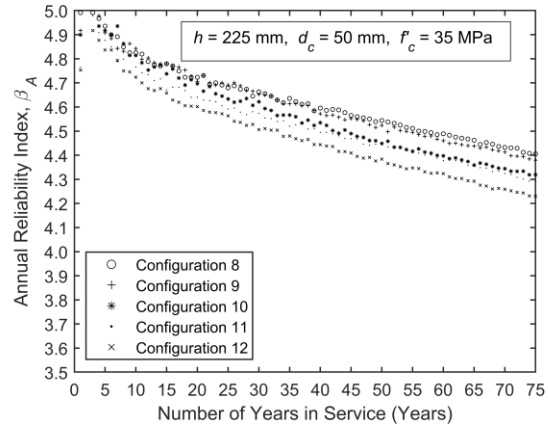
Crack width: Positive Longitudinal, Interior = $0.71/0.7 = 1.01$

Crack width: Negative Transverse, Exterior = $0.56/0.7 = 0.81$

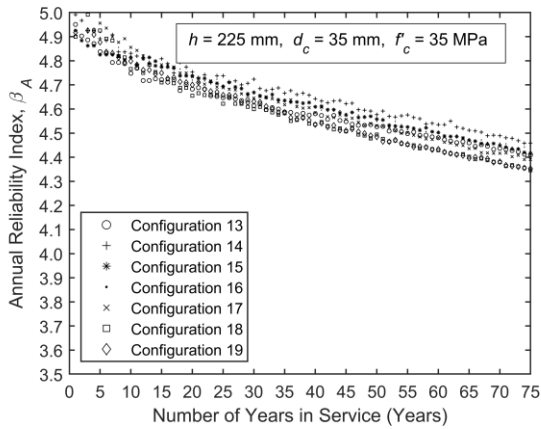
APPENDIX B: ANNUAL RELIABILITY INDEX FOR CONFIGURATIONS IN PARAMETRIC ANALYSIS



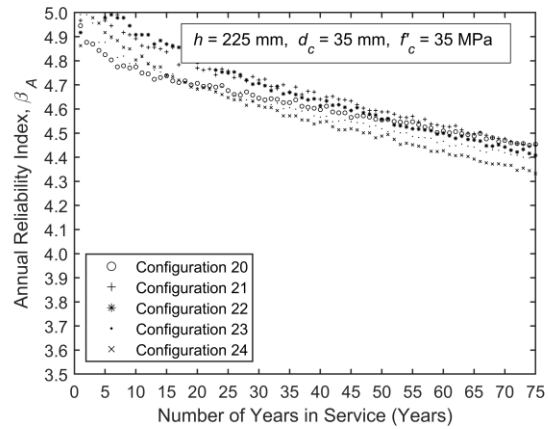
(a) Analysis 1



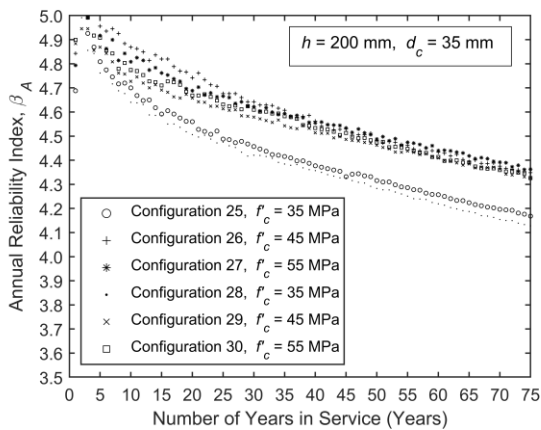
(b) Analysis 2



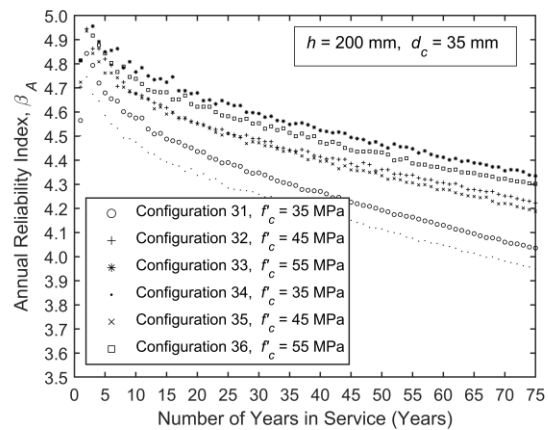
(c) Analysis 3



(d) Analysis 4



(e) Analysis 5



(f) Analysis 6